The Hong Kong Polytechnic University

Department of Electrical Engineering

Magnetic Levitation Based on Switched Reluctance Actuator

Sun Zhen Gang

A thesis submitted in partial fulfillment of the requirements for the degree of Doctor of Philosophy

August, 2010

CERTIFICATE OF ORIGINALITY

I hereby declare that this thesis is my own work and that, to the best of my knowledge and belief, it reproduces no material previously published or written, nor material that has been accepted for the award of any other degree or diploma, except where due acknowledge has been made in the text.

____ (Signed)

Sun Zhen Gang (Name of student)

Abstract

For a high performance mechatronic system, magnetic levitation has many advantages. It is contact-free, and it can eliminate many mechanical components e.g., gears, guide, ball bearings, etc. On the operation side, magnetic levitation can reduce the mechanical alignment cost, the wear and tear, and maintenance cost. Therefore, investigations into contact-free mechatronic systems have been actively performed by worldwide researchers.

Switched reluctance actuator is an electrical device in which the output force is produced by the tendency of its magnetic circuit to minimize the reluctance of excited winding. Switched reluctance actuator has the merits of simple structure, low cost and high reliability. Hence, the magnetic levitation system based on switched reluctance principle could be a potential candidate for mechatronic carrier systems.

The magnetic levitation system based on switched reluctance actuator is hard to control due to high inertia and inherent nonlinear flux characteristics. For a multipoint levitation system, the coupling behavior will complicate the control algorithm of this multiple-input and multiple-output system.

The ultimate objective of this project is to investigate and propose an effective control scheme for the multiple-input and multiple-output magnetic levitation system by using switched reluctance actuators.

To achieve this target, the first step is to investigate and develop the magnetic levitation actuator and to explore the magnetic performance characteristics of this actuator. The principles of operation of the proposed magnetic levitation system with switched reluctance actuator are reviewed. Magnetic circuit analysis model, three-dimensional finite element analysis model and experimental implementation

are applied to analyze electromagnetic force. The accuracy of the magnetic circuit analysis model is developed and further improved.

Following the establishment of the switched reluctance magnetic levitation actuator, the next task is to model the magnetic levitation system. Both the single-input and single-output magnetic levitation system and the proposed multiple-input and multiple-output magnetic levitation system are modeled. These modeling reveal the open loop instability and coupling behavior of the proposed system. To simplify the control scheme of the overall system, a two-time scale method is implemented, and the magnetic levitation system can be divided into two reduced-order subsystems, electrical model and mechanical motion model.

On basis of the reduced-order model, a sliding mode controller is approached for the single-input and single-output magnetic levitation system. The stability and the system characteristics of the controller are both analyzed. An observer based the sliding mode controller is developed to against disturbances and to improve the system performance.

Finally, a control algorithm for the multiple-input and multiple-output magnetic levitation system is proposed. The coupling system is decoupled into three individually controllable subsystems by mathematical transformation. Following that, the sliding mode controller approached in single-input and single-output magnetic levitation system can be applied to these subsystems. This project has demonstrated that, through proper actuator design and control, multipoint magnetic levitation based on switched reluctance actuators could be an alternative to the present existing magnetic levitation methods.

Publications arising from the project

Journal papers

[1] N. C. Cheung, S. W. Zhao, W. C. Gan, Z. G. Sun, and S. C. Kwok, "A Novel Solar Tracking System Design based on Linear Switched Reluctance Motor," *Control Theory and Applications*, vol. 25, No 2, Apr. 2008.

[2] S. W. Zhao, N. C. Cheung, W. C. Gan, and Z. G. Sun, "A Novel Flux Linkage Measurement Method for Linear Switched Reluctance Motors", *IEEE Trans. Instrumentation and Measurement*, vol. 58, no. 10, pp. 3569-3575, 2009.

[3] Z. G. Sun, N. C. Cheung, S. W. Zhao, and W. C. Gan, "Application of Disturbance Observer Based Sliding Mode Control for Magnetic Levitation Systems", *Proceedings of the Institution of Mechanical Engineers Part C: Journal of Mechanical Engineering Science*, vol. 224, no. 8, pp. 1635-1644, Aug. 2010.

[4] Z. G. Sun, N. C. Cheung, S. W. Zhao, and W. C. Gan, "Magnetic Analysis of Switched Reluctance Actuators in Levitated Linear Transporters", *IEEE Trans. on Vehicular Technology*, vol. 59, no. 9, pp. 4280-4288, Nov. 2010.

[5] Z. G. Sun, N. C. Cheung, S. W. Zhao, and Y. Lu, "Sliding Mode Control for Decoupled MIMO Magnetic Levitation Systems Based on Switched Reluctance Actuators", *IEEE Trans. on Industrial Electronics*, submitted.

Conference proceedings

[1] N. C. Cheung, S. W. Zhao, W. C. Gan, Z. G. Sun, and S. C. Kwok, "A Novel Solar Tracking System Design Based on Linear Switched Reluctance Motor", *Symposium on Use of Control and Power Electronics in New Energy Generation*, Guangzhou, China, 25-29 Nov. 2007.

[2] Z. G. Sun, N. C. Cheung, J. F. Pan, S. W. Zhao, and W. C. Gan, "Design and Simulation of a Magnetic Levitated Switched Reluctance Linear Actuator System for High Precision Application", *2008 IEEE International Symposium on Industrial Electronics (ISIE2008)*, pp. 624-629, Cambridge, UK, 30 Jun.-2 Jul. 2008.

[3] S. W. Zhao, N. C. Cheung, Y. Lu, W. C. Gan, and Z. G. Sun, "Linear Switched Reluctance Motor Based Position Tracking System", *The 13th International Power Electronics and Motion Control Conference (EPE-PEMC2008)*, pp. 1221-1224, Poznan, Poland, 1-3 Sept. 2008.

[4] Z. G. Sun, N. C. Cheung, S. W. Zhao, and W. C. Gan, "Integral Sliding Mode Control with Integral Switching Gain for Magnetic Levitation Apparatus", *The 3rd International Conference on Power Electronics Systems and Applications (PESA2009)*, Hong Kong, 20-22 May 2009.

[5] N. C. Cheung, Z. G. Sun, S. W. Zhao, and W. C. Gan, "Design and Simulation of a Testing Fixture for Planar Magnetic levitation system Control Using Switched Reluctance Actuator", *The 3rd International Conference on Power Electronics Systems and Applications (PESA2009)*, Hong Kong, 20-22 May 2009.

[6] Y. Lu, K.W.E. Cheng, K. W. Chan, Z. G. Sun, and S. W. Zhao, "Development of a Commercial Induction Cooker", *The 3rd International Conference on*

Power Electronics Systems and Applications (PESA2009), Hong Kong, 20-22 May 2009.

[7] Z. G. Sun, N. C. Cheung, S. W. Zhao, Y. Lu and Z. H. Shi, "Design and Simulation of a Linear Switched Reluctance Generator for Wave Energy Conversion", *The 4th International Conference on Power Electronics Systems and Applications (PESA2011)*, Hong Kong, 8-10 Jun. 2011.

[8] S. W. Zhao, N. C. Cheung, C. K. Lee, X. Y. Yang, and Z. G. Sun, "Survey of Modeling Methods for Flux Linkage of Switched Reluctance Motor", *The 4th International Conference on Power Electronics Systems and Applications (PESA2011)*, Hong Kong, 8-10 Jun. 2011.

Acknowledgements

First of all, I would like to express my sincere gratitude and appreciation to my supervisor, Dr. Norbert C. Cheung. He has always been supportive and encouraging throughout my research period. His academic guidance is extremely useful and beneficial. Without him, it would be impossible for me to fulfill my goal of pursuing for a PhD degree.

Secondly, I would like to thank Prof. Ma Xiaoqian, my master study supervisor in South China University of Technology, Guangzhou, China. It was his spiritual guidance that encouraged me to engage in research work.

I must also thank Dr. Zhao Shiwei, a post doctor of the Hong Kong Polytechnic University. He has selflessly taught me the essential control theories. His valuable suggestions and remarks are also very helpful.

I have to thank all my valuable friends and colleagues, especially Mr. Jones W. W. Chan, who has assisted me in the fabrication of the experimental setup. Their help are highly appreciated.

I would like to give my special thanks to the University Grants Council for support of this research work through project code: PolyU 5141/05E.

Lastly, I would like to deeply thank my parents, my wife, Du Xiaohui, and my family for their full support during my study.

Table of Contents

List of Figures

List of Tables

List of Acronyms

AC	Alternate Current
AD	Analog to Digital
AI	Artificial Intelligence
DA	Digital to Analog
DC	Direct Current
DO	Disturbance Observer
DSP	Digital Signal Processor
EMF	Electromotive Force
FEA	Finite Element Analysis
FL	Fuzzy Logic
ISA	Industry Standard Architecture
LED	Light Emitting Diode
LSRM	Linear Switched Reluctance Motor
LVDT	Linear Variable Differential Transducer
MCA	Magnetic Circuit Analysis
MIMO	Multiple-Input and Multiple-Output
MMF	Magnetomotive Force
PCI	Peripheral Component Interconnect
PD	Proportional-Differential
PID	Proportional-Integral-Differential
PM	Permanent Magnet
PWM	Pulse Width Modulation
RTI	Real-time Interface

RTW	Real-time Workshop
SISO	Single-Input and Single-Output
SMC	Sliding Mode Control
SRA	Switched Reluctance Actuator
VSS	Variable Structure Systems
VSC	Variable Structure Control

List of Symbols

a	side length of the equilateral triangle plane, *mm*
A	cross section areas, m^2
B	flux density, *T*
c	constant gain
d	tooth depth, *mm*
e_v	induced voltage, *V*
f_d	disturbance force, *N*
f_j	electromagnetic forces, *N*
f_z	electromagnetic force, *N*
F_m	magnetomotive force, *A*
g	acceleration of gravity, m/s^2
h	tooth height, *mm*
H	magnetic field intensity, *A/m*
i	current, *A*
I_{xx}	moments of inertia rotating about X axis, kg/m^2
I_{yy}	moments of inertia rotating about Y axis, kg/m^2
I_{zz}	moments of inertia rotating about Z axis, kg/m^2
J_s	source current density, A/S^2
K_{in}	constant gain
K_o	constant observer gain
K_{out}	constant gain
l	flux path length, *mm*
l_l	flux path length of levitator, *mm*

l_s	flux path length of stator, *mm*
L	inductance, *H*
M	mass, *kg*
N	number of turns
p	constant gain
P	air-gap permeance, *b/AW*
R	reluctance, *AW/b*
R_c	winding resistance, Ω
R_g	air-gap reluctance, *AW/b*
T	sample time, *s*
T_x	torques rotating about X axis, *Nm*
T_y	torques rotating about Y axis, *Nm*
T_z	torques rotating about Z axis, *Nm*
v	voltage, *V*
W_c	co-energy, *J*
W_e	input electrical energy, *J*
W_f	stored energy, *J*
W_m	mechanical energy, *J*
W_{tp}	width of tooth, *mm*
z	displacement along Z axis, *mm*
λ	flux linkage, *Vs*
Φ	flux, *Wb*
μ_s	magnetic permeability of stator, *H/m*
μ_l	magnetic permeability of levitator, *H/m*
μ_0	magnetic permeability of air-gap, *H/m*

ϕ	Euler angle with respect to X axis, *rad*
θ	Euler angle with respect to Y axis, *rad*
ψ	Euler angle with respect to Z axis, *rad*
ω_x	angular velocities rotating about X axis, rad/s
ω_y	angular velocities rotating about Y axis, rad/s
ω_z	angular velocities rotating about Z axis, rad/s
ε	constant gain
η	constant gain
Δ	constant gain

Chapter 1

Introduction

This thesis investigates the possibility of implementing a magnetic levitation system using Switched Reluctance Actuators (SRAs). An SRA consists of a moving translator and a stator, the attraction force from these two components will be used to levitate the translator.

The investigation includes all aspects of SRA for magnetic levitation, it consists of the structure, the magnetic characteristics and the performance analysis, the modeling, and the controller design of a Multiple-Input and Multiple-Output (MIMO) magnetic levitation system.

In this chapter, the significance and objectives of the research are addressed first. Then, the overall arrangement of the thesis is introduced. The contributions arising from this research are summarized in the final chapter.

1.1 Significance and objectives of the research

In many advance manufacturing processes, the working environment will affect the quality of the final product. Conventional transportation systems (e.g., belt-type conveyors or articulated robots) generate dusts and pollution due to the mechanical wear or lubrication contamination, are inadequate to satisfy the clean-room environmental demands. Magnetic levitated system has the advantage of being contact-free; therefore, it can solve the pollution problem. Moreover, magnetic levitation system has a simple mechanical structure, it can eliminate the mechanical components (e.g., gears, guide, ball bearings etc.), reduce the mechanical alignment and maintenance cost. Hence, contact-free type motion systems have been actively pursued by worldwide researchers.

Presently, a few forms of magnetic levitation motion systems exist; these magnetic levitation technologies use (i) permanent magnets [1], (ii) superconducting magnets [2], (iii) eddy current induced in a conductor [3], (iv) a current carrying conductor in a magnetic field [4], and (v) electromagnets [5]. Among those magnetic levitation schemes, the manufacturing costs of motors using permanent magnets and superconducting magnets are expensive, and the levitation force produced from current carrying conductor in a magnetic field is small. In addition, permanent magnets have temperature dependent characteristics [6], and the employment of high temperature superconductors in the motors creates manufacturing and maintenance problems. The electromagnets method could be targeted for industrial automation transportation systems.

Linear SRA is an electrical actuator with a very simple structure. Its attraction force is produced by the tendency of its moving translator to minimize the reluctance of the excited winding. As a type of electromagnetic levitation systems, without permanent magnet material, an SRA has the merits of simple construction, low cost and high reliability [7]-[8]. Besides, the switched reluctance actuator is free from the partial or complete demagnetization problems occurred in permanent magnet actuators, although resistance of coils could produce temperature problems in switched reluctance actuator, these problems in switched reluctance actuator are no worse than in the other actuator types. Moreover, the driving power converter of switched reluctance actuator has an independent circuit for each phase, which provides the great advantages of inherent fault tolerance and the potential of high reliability. A SRM can be a potential candidate for high reliability magnetic levitated motion system [9].

On the other hand, there are three main challenges in magnetic levitation system based on the SRA.

i) Firstly, owing to the inherent nonlinear flux characteristics, SRA has high force ripple and its modeling is complex. These make the SRA difficult for high precision magnetic levitation control.

ii) Secondly, magnetic levitation system is contact-free and it has a relatively high inertia due to the absence of friction damping. High inertia can worsen the force ripple of the SRA, hence high precision levitation position control is hard to implement.

iii) Finally, the levitated transporter requires multipoint levitation, and each levitation point is not decoupled from the others. Therefore, a form of MIMO control needs to be approached.

The objective of this research is to tackle the above mentioned problems, in order to make SRA based magnetic levitation system widely acceptable to industry. The research work includes the modeling and the controller design of the magnetic levitation system.

i) The first effort is to analyze and establish the magnetic circuit characteristics of magnetic levitation system with SRA, so as to obtain the relationship within force, current and position.

ii) The second goal is to design an effective robust controller for the Single-Input and Single-Output (SISO) magnetic levitation system.

iii) Based on the experience gained from the SISO magnetic levitation system, the final stage is to propose a suitable controller for MIMO magnetic levitation system.

1.2 Previous literature review

In recent years, magnetic levitation technologies have been successfully implemented in many engineering applications, including micro-robotic manipulator system, bearingless motors and maglev trains [10]-[12]. However, there are few publications on magnetic levitation system using SRA. To further investigate the design and application on magnetic levitation system and SRA, the following sections will explore the literatures related to (i) magnetic and force analysis of SRA, (ii) control algorithms of SISO magnetic levitation system, and (iii) control issues about MIMO magnetic levitation system.

1.2.1 Magnetic and force analysis of SRA

In order to validate the design of the magnetic levitated actuator, a comprehensive levitation force analysis of the SRA is required. Two techniques could generally be used to analyze the electromagnetic force. These two techniques are Magnetic Circuit Analysis (MCA) method [13]-[18] and Finite Element Analysis (FEA) method [19]-[25]. MCA is simple and efficient in computation, but its accuracy is highly dependent on the choice of magnetic flux paths. FEA is accurate in calculation by spatial discretization, but it is computational intensive and time consuming [15].

For the MCA, the method for analytical estimation of the permeance of flux paths is discussed in [13], and the flux paths models of several type structures of high permeability material are built and analyzed. The permeance model and the reluctance force between tooth-structures of motors are developed in [14]. In this paper, three different translator position regions are considered to evaluate the permeance through the air-gap during the motion of the translator. On the basis of the above flux paths models, numerous permeance models and their corresponding

MCA methods are developed and employed in the design and analysis of different structures of switched reluctance motors. In [15], four different translator position regions are used to calculate the permeance in the air-gap of a Linear Switched Reluctance Motor (LSRM). In [16], permeance models in five different translator position regions are built to evaluate the propulsion force of a double-sided, double-translator LSRM. In [17], inductances and flux linkages for three identified rotor position regions of rotary SRM are computed to verify the design of motor. A high speed magnetic circuit network is approached as the calculation tool for electromechanical actuators design [18], this method is effective in solving the problem within a very short time.

On the other hand, the FEA method is a widely accepted method in the design and analysis of electromechanical devices. In [19], different physical sizes of SRMs are compared by using a 2-dimensional (2D) FEA model. In [20], the flux linkage and force of an electromechanical valve actuator are simulated by 3-dimensional (3D) FEA model. A 3D FEA model of rotary SRMs is developed to simulate the motor in many different rotor positions in [21]. The force and torque computation of SRMs are compared by a 2D FEA model and a 3D FEA model in [22], and the results show that the accuracy of the 3D model is better than that of the 2D model. The FEA method based on Maxwell stress is used to predict the electromagnetic vibration in [23]. The FEA method on the basis of virtual work principle is presented to solve the electromagnetic force in [24]. In [25], the above two FEA methods – Maxwell stress method and virtual work method are proposed for electromagnetic torque computation, and merits of each method are concluded.

In this research, both the MCA and FEA are used to obtain the characteristics of the SRA.

1.2.2 Control algorithms of SISO magnetic levitation system

A Single-Input and Single-Output (SISO) magnetic suspension system was designed in [26], and the Proportional-Derivative (PD) control was adopted to levitate the metallic ball, but the detailed system performances of the magnetic suspension system were not analytically examined. Feedback linearization control of the magnetic levitation system has been applied by numerous researches because of the inherent nonlinearities of the system [27]-[28]. The findings in [27] revealed that the feedback linearization method was superior to the classical Proportional-Integral-Derivative (PID) control in a large air-gap magnetic levitation system. However, the disturbance of the system was not taken into account in the paper. While the disturbance was considered in [28], the experimental results indicated that there were static errors due to the magnetic levitation mass perturbation. In [29], an adaptive nonlinear control composed of feedback linearization method was introduced, and the experimental results reflected its robustness to system parameters uncertainties. However, adaptive control is computational intensive and time consuming. In this literature the disturbance was also not taken into consideration.

Sliding Mode Control (SMC) is applied widely in electro-mechanical systems [30]-[32]. It is efficient to control complicated high-order dynamic plants operating under uncertainty conditions [33]. Due to the above merits, SMC is one of the effective candidates for the magnetic levitation system. The purposes of [34]-[35] were to replace linear sliding surface by the nonlinear one, as a result, the desired performances of the magnetic levitation systems were improved. In [36], the sliding mode equivalence control with exponential reaching law was adopted to a magnetic levitation system. Although the simulation results show that the response air-gap could follow the command under the assumption of disturbances, there was no real-time implementation to prove the results.

For improving the system performance, some hybrid controllers, including SMC are applied on the magnetic levitation systems. For instance, the integral sliding mode controller with grey forecast was proposed in [37], a combination of SMC and radial basis function network was employed to design the controller in [38]. Although experimental results suggest the effectiveness of these methods, the algorithms are complicated and time consuming.

In this project, an SMC with disturbance observer is schemed for an SISO magnetic levitation system. This control algorithm can guarantee the robustness of the system no matter how uncertainties or external disturbance.

1.2.3 Control issues about MIMO magnetic levitation system

Magnetic levitation systems are well known for the nonlinear dynamic characteristics and open loop instability. In addition, the MIMO magnetic levitation system using switched reluctance actuators has the addition difficulty of coupling elements due to the interaction effect of different electromagnetic forces. Therefore, the position control for this MIMO magnetic levitation system presents a challenging problem. Multivariable controller for MIMO magnetic levitation systems is possible, but the stability of the system could be easily affected by parameter uncertainties and disturbances due to the complexity of the controller.

From the viewpoint of decoupling control, a more simple control method is to employ torsion springs to introduce flexibility in levitation platform [39], therefore the mechanical structure of the MIMO system is separated into several single output systems, and levitation of each magnet can be controlled independently. This method is feasible, but it defeats the purpose of completely contactless between moving surfaces. An alternative controller design scheme is on the basis of the tight association between a magnet and its nearest transducer, each magnet is individually controlled by using the nearest transducer as feedback signals [40]. This method dose not consider the cross coupling, and it is hard to have good tracking performance. Additionally, it can not guarantee robust stability against disturbances. The MIMO magnetic levitation system has at least 3 degrees-of-freedom (DOF), vertical motion, roll rotation and pitch rotation. The concept of independent control of each DOF for the MIMO magnetic levitation system is mentioned in [41]. However, the detailed decoupling transformation is not addressed. In [42], multiphase permanent magnets are used to the generate suspension forces, and a *dq* frame is employed to decouple the forces, then three DOF of levitation are controlled individually.

On the control side, the conventional Proportional- Integral -Derivative (PID) controller [43]-[45] and its transformation, the Proportional-Integral (PI) controller [46] or the Proportional- Derivative (PD) controller [47]-[48] are used in magnetic levitation systems due to its simplicity and usefulness. The lead-lag compensator [42], [49] is also an alternative for magnetic levitation systems, and the electrical voltage or current is typically used as the control signal. Sliding Mode Control (SMC) is applied widely in electro-mechanical systems, and it is efficient to control complicated high-order dynamic plants operating under uncertainty conditions [33]. This merit makes SMC be one of the effective candidates for the magnetic levitation system, and SMC is performed better than PID control in the nonlinear magnetic levitation systems [50].

In this research, the mathematical modeling of the proposed MIMO magnetic levitation system based on SRA is conducted, following that, the system is decoupled by mathematics transformation, and an SMC is adopted for the decoupled subsystems to guarantee the stability of the magnetic levitation system.

1.3 Organization of the thesis

The thesis is organized as follows:

Chapter 1 elaborates the significance and objectives of the research. Previous work related to the research is thoroughly reviewed and structure of the thesis is presented.

In chapter 2, the structure of the magnetic levitated switched reluctance actuator is depicted firstly. Then, the basic operation and electromechanical energy conversion principles are introduced. After that, the magnetic and force characteristics of the proposed magnetic levitated switched reluctance actuator are analyzed by using MCA and FEA methods. Next an improved MCA method is proposed to better the accuracy of results. Finally, experiment tests are also implemented to verify the effectiveness of these methods.

In chapter 3, the mathematical models for both an SISO magnetic levitation system and an MIMO magnetic levitation system are established. These models form the base for simulation and controller design. A two-time scale scheme is proposed to simplify the control modeling.

The main objective of chapter 4 is to design a suitable controller for a single point magnetic levitation system. A sliding mode controller together with a simple and effective observer is proposed. The system is very effective in uncertainty and disturbance rejections. Both the simulation results and experimental results confirm the validity of the robust controller.

Chapter 5 discusses the control algorithm of an MIMO magnetic levitation system. The MIMO magnetic levitation system is more complex than SISO magnetic levitation system because of inter-points couplings. A mathematics decoupling method using inverse matrix is applied; thereby the sliding mode controller designed in chapter 4 can be used for the decoupled modeling. The feasibility of the control algorithm is proved by simulation results and experimental results.

The main results and achievements of the thesis are summarized in the last chapter. Some remaining issues within the context of the thesis for future research are also suggested.

Chapter 2

Structure and Performance Analysis of Magnetic Levitated Switched Reluctance Actuator

This chapter focuses on the structure of the magnetic levitation system, its operation principle and its performance analysis. These are the fundamentals of magnetic levitation system modeling and controller design.

2.1 Construction of magnetic levitation system based on SRA

According to the location of phase coils, SRA for magnetic levitation system can be classified as two types: i) passive-stator active-levitator, and ii) active-stator passive-levitator. Passive-stator active-levitator means that the coils are wound on the levitator; the levitation part of SRA, while active-stator passive-levitator has the coils wound on the stator, the stationary part of SRA. In this project, active-stator passive-levitator type is employed for magnetic levitation system to avoid the turbulence of windings on levitation plane. The proposed MIMO magnetic levitation system is shown in figure 2.1. Figure 2.2 shows the schematic diagram of the MIMO magnetic levitation system.

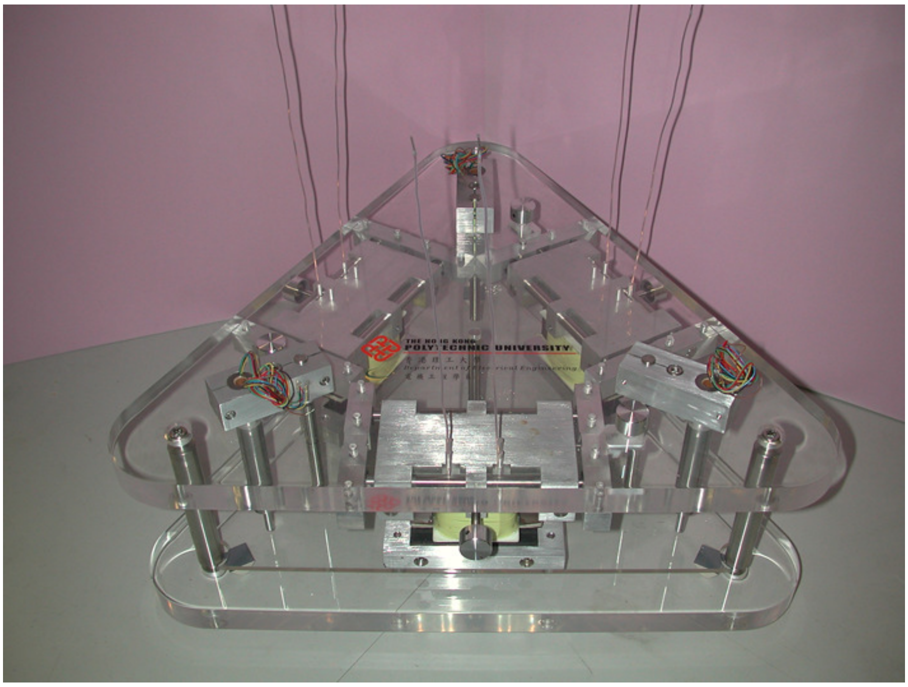

Fig. 2.1 Photo of the proposed MIMO magnetic levitation system

The MIMO magnetic levitation system is driven by three levitation coils, one on each center side of the equilateral triangular platform. The reason why three coils are used is because that a plane can be decided by three points at least, and the total experimental cost can be low (e.g. it needs no more than three position sensors and three servo amplifiers). From the viewpoint of control algorithm, if the levitation plane is supposed to be three degrees of freedom system in a Cartesian coordinates, i.e., translational movement along Z axis, roll movement along X axis and pitch movement along Y axis, whether three or four levitation actuators are used, the controlled system both can be described by three variables: displacement for translational movement and Euler angles for roll and pitch movements. Actually, the levitation plane can be rectangular and four coils are used to levitation. The control algorithm discussed in this thesis is feasible whatever three or four coils are employed.

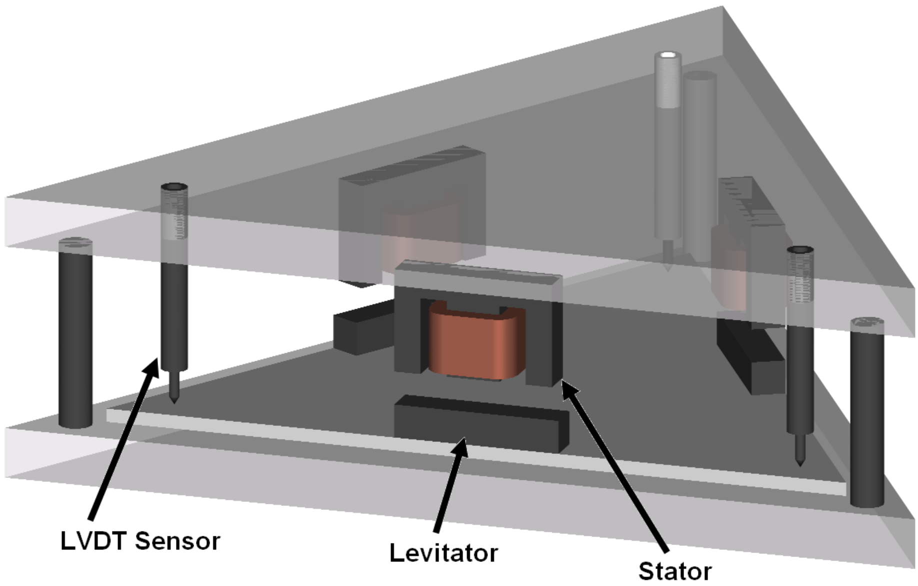

Fig. 2.2 Schematic diagram of the proposed MIMO magnetic levitation system

Figure 2.3 shows one pair of levitation coils and figure 2.4 shows the schematic of single levitation coil. The stators and levitators are both made from 0.5mm laminated silicon steel plates. In linear theory, the eddy current component of core losses increases in proportion to $B^2f_s^2$, in which B is flux density and f_s is switching frequency, so the core losses increase rapidly with high frequencies. In principle, this core losses problem can be solved by decreasing the lamination thickness to keep the eddy current in the “resistance-limited” condition, but in practice there is a limit set on the lamination thickness due to the manufacturing cost, the fragility of individual lamination and the reduction in the stacking factor [51]. The thinnest lamination of silicon steel plate adopted for actuator is 0.35mm while 0.5mm thickness is also common used considering the above thickness limitations.

Three E type cores with windings are the stators, and three I type cores without windings are the levitators. The stators are installed in the top plane; the levitators are fixed onto a levitated plane below the stators. Each pair of stator and levitator can be adjusted to align by tuning the corresponding knobs. The fixing setup for stator and levitator are both fabricated with aluminum and the levitation plane is manufactured with transparent plastic, these materials result in two advantages: i) weight and inertia of the levitation plane are low, ii) the magnetic circuit is decoupled because the relative magnetic permeability of aluminum and plastic are almost the same as air.

Three Linear Variable Differential Transducer (LVDT) position sensors are installed in each corner of the equilateral triangular top plane, and they are used to observe the vertical motion profile of the equilateral triangular levitation plane and to provide the position feedback. The core of LVDT is very light, and it dose not touch with the house of LVDT, so the core of LVDT will not affect the mechanical behavior of the levitation plate.

Normally, for an electromechanical system, the system efficiency is the ratio of mechanical energy to input electrical energy, but it is hard to calculate the efficiency for the proposed magnetic levitation system. When the levitation system is at steady state, the levitation platform is theoretically unmovable. As a result, there is no mechanical energy. On the other hand, the proposed magnetic levitation system based on switched reluctance could be used in linear automation carrier system, then, the efficiency of the linear motion system could be decided. Furthermore, the experimental setup of the proposed MIMO magnetic levitation system is not a commercial product and efficiency is not the focus in this research. The experimental setup is mainly used to validate the effectiveness of control algorithm approached for this MIMO magnetic levitation system.

The parameters of the magnetic levitation system are listed in table 2.1.

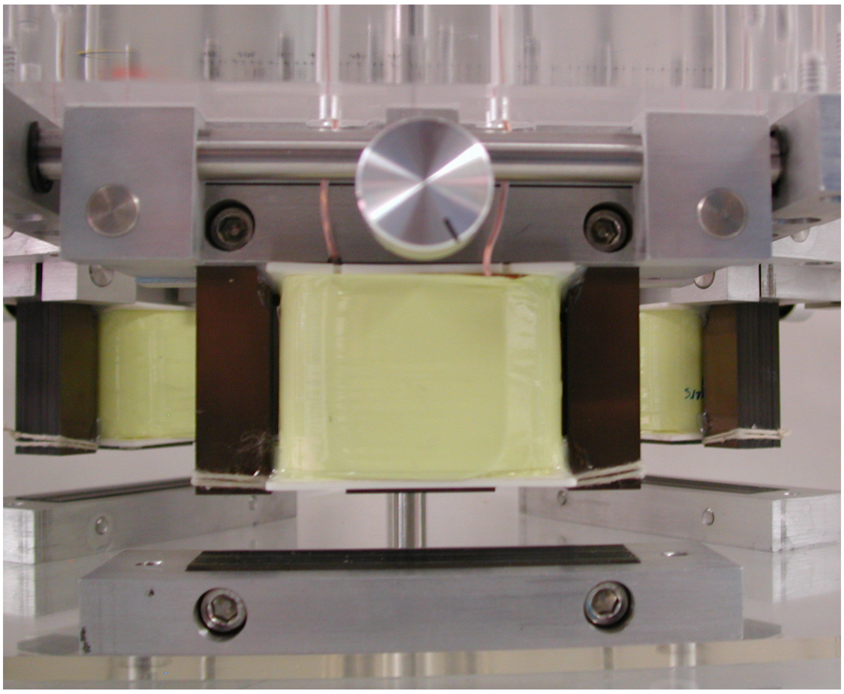

Fig. 2.3 The stator and levitator

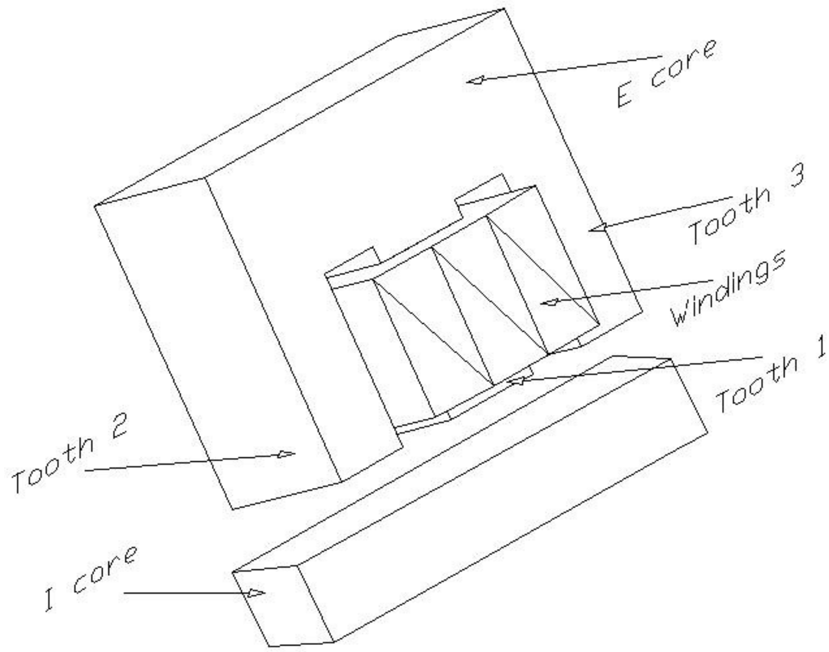

Fig. 2.4 Schematic of single levitation coil model of the proposed system

	Definition	Value
Stator	Width of teeth 2 and 3 separately	16mm
	Width of tooth 1	32mm
	Teeth height	47mm
	Teeth depth	20mm
	Width between teeth 1 and 2	16mm
	Width between teeth 1 and 3	16mm
	Yoke height	16mm
	Number of coil turns	407
Levitator	Levitator depth	20mm
	Levitator height	20mm
Levitation platform	Side length of equilateral triangular	448mm
	Mass of levitation platform	1.7kg

Table 2.1 Parameters of the proposed MIMO magnetic levitation system

2.2 Principles of operation

A switched reluctance actuator produces its electromagnetic force by the tendency of its moving part to come to the position where the maximum magnetic flux of the magnetic circuit occurs [51]. For the proposed SRA, when the stator is excited, the levitator will move to a location to minimize the overall reluctance. Hence, electromagnetic attractive force will be created between the stator and levitator. If the electromagnetic force is large enough, the levitation platform will be levitated.

To analyze the operation further, the magnetic paths and the electromechanical energy conversion need to be explored.

2.2.1 Reluctance calculation

As mentioned above, at the instance of excitation, the magnetic paths between the stator and the levitator drive the levitator to move for minimum reluctance. Although the exact value of reluctance is difficult to predict, an approximate estimation is adequate to design the actuator.

A solenoid, which is a simplified form of SRA, is used to explain the minimum reluctance tendency and reluctance calculation. Figure 2.5 shows the schematic of the solenoid. The solenoid has N turns. When coil is connected to an electrical energy source, the exciting current i sets up a flux Φ. Assuming that the flux density is substantially uniform throughout the cross section of the core and the mean circumference of the core can be adopted as the magnetic path length, the magnetic circuit of the solenoid can be given by Ampere's circuital law as equation (2.1)

$$F_m = Ni = l_s H_s + l_l H_l + 2zH_g \tag{2.1}$$

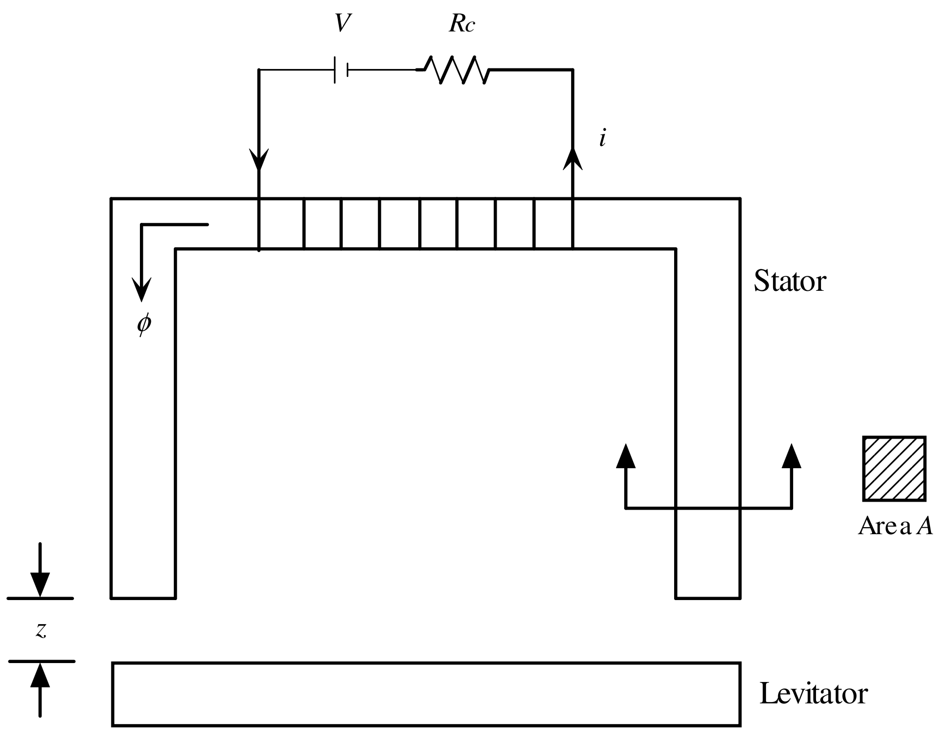

Fig. 2.5 Schematic of solenoid

Where the quantity $F_m = Ni$ is called the Magnetomotive Force (MMF), l_s and l_l denote the magnetic path lengths of stator and levitator respectively, z denotes the air-gap, and H_s, H_l and H_g are the magnetic field intensities in the stator, levitator and air-gap separately. In the close magnetic circuit, there are two equal air-gaps.

Considering the flux density B equation (2.2) and (2.3)

$$B = \frac{\Phi}{A} \tag{2.2}$$

$$B = \mu H \tag{2.3}$$

Equation (2.1) can be rewritten as equation (2.4) assuming that no flux leakage occurs in the magnetic circuit

$$Ni = l_s \frac{\Phi}{\mu_s A_s} + l_l \frac{\Phi}{\mu_l A_l} + 2z \frac{\Phi}{\mu_0 A_g} \tag{2.4}$$

Where Φ denotes the flux, μ_s, μ_l and μ_0 denote the magnetic permeability of the stator, levitator and air-gap respectively, A_s, A_l and A_g are the effective cross section areas of the stator, levitator and air-gap separately.

As shown in equation (2.5), reluctance R is the ratio of MMF to flux

$$R = \frac{Ni}{\Phi} \tag{2.5}$$

Combining equation (2.4) and (2.5) gives

$$R = \frac{l_s}{\mu_s A_s} + \frac{l_l}{\mu_l A_l} + 2\frac{z}{\mu_0 A_g} \tag{2.6}$$

Equation (2.6) shows that there are three part reluctances in the magnetic circuit, i.e. reluctances in stator, levitator and air-gap. If the magnetic circuit is not saturation, the reluctance in the air-gap is the main reluctance of the magnetic circuit because the magnetic permeability of stator and levitator is much larger than that of air-gap. Therefore, the tendency to obtain minimum reluctance needs to decrease the air-gap, and the electromagnetic attractive force between stator and levitator will increase.

2.2.2 Electromechanical energy conversion

The law of energy conservation is one of the fundamental elements to explain the various observed phenomena. It plays an important role in the study of electromechanical and electromagnetic systems. Experimental evidence reveals that energy stored in magnetic field or electric field will completely or partly convert into other forms when the field is destroyed or changed [52]. From a macroscopic viewpoint, the law of electromechanical energy conservation is a simple and powerful tool to analyze electromagnetic force produced in the proposed SRA.

In order to convert energy from electrical to mechanical form in an electromechanical device, the necessary conditions are: i) there must be more than one component capable of storing energy, and ii) the stored energy of this component needs to be a function of the displacement variable [53].

The proposed SRA can store energy in stator, levitator and air-gap, and this energy will be varied by changing the air-gap displacement. Hence, it is possible for energy conversion to take place in SRA.

The solenoid shown in figure 2.5 can be used to explain the force production through the law of electromechanical energy conversion. The voltage e_v induced in the exciting coil during the period of flux changing and its value is determined by Faraday's law

$$e_v = \frac{d\lambda}{dt} = \frac{d(N\Phi)}{dt} = N\frac{d\Phi}{dt} \tag{2.7}$$

Where λ is the flux linkage associated with the coil.

The stored energy due to the magnetic field variation is represented by W_f

$$W_f = \int_0^{\lambda_1} i d\lambda = \int_0^{\Phi_1} F_m d\Phi \tag{2.8}$$

Figure 2.6 shows the flux vs. MMF curve or magnetization curve for a particular position and equation (2.8) is graphically represented by the horizontally shaped portion in figure 2.6.

From this graph, co-energy W_c is defined by equation (2.9), is a compliment term to compute the electromagnetic force.

$$W_c = \int_0^{i_1} \lambda di = \int_0^{F_{m1}} \Phi dF_m = \Phi F_m - W_f \tag{2.9}$$

To have the force production, the excitation current is increased to make the levitator move towards the stator, and the air-gap is changed. The magnetization curves shown in figure 2.7 are plotted for two values of air-gap, z_1 and z_2, where $z_1 > z_2$.

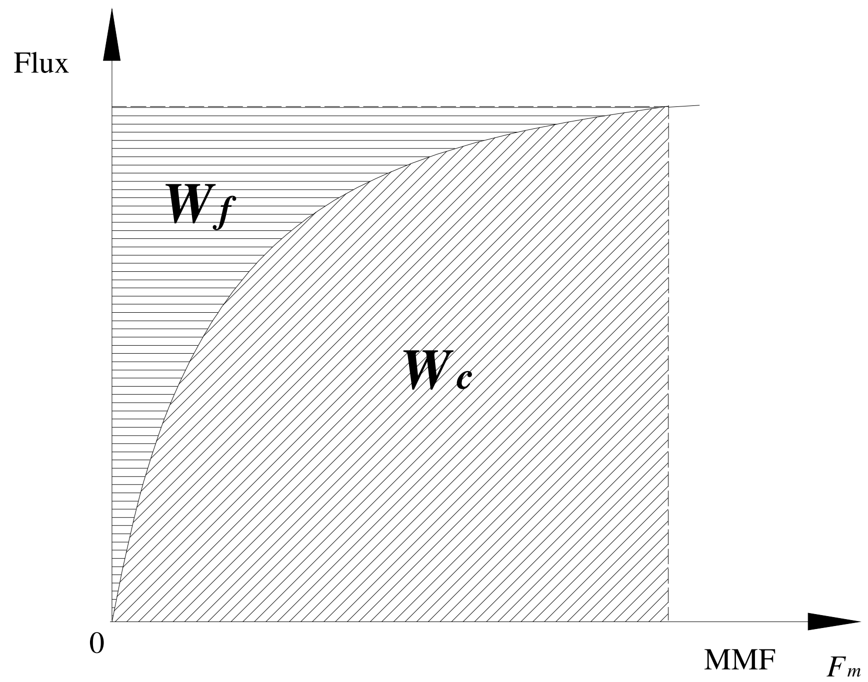

Fig. 2.6 Stored energy and co-energy

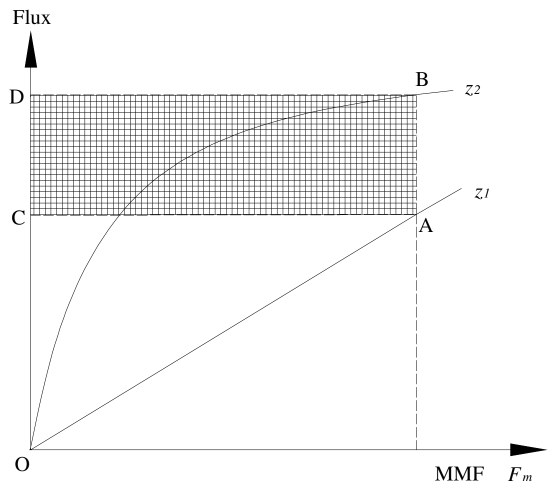

Fig. 2.7(a) Input electrical energy

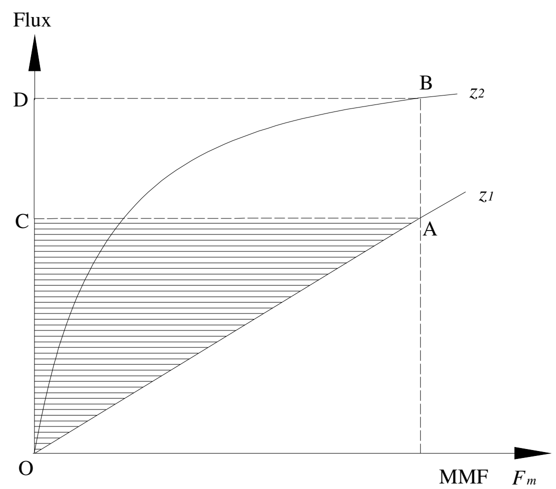

Fig. 2.7(b) Stored energy in z_1

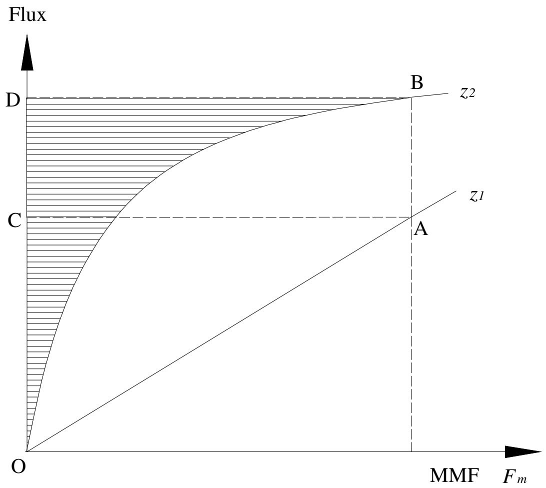

Fig. 2.7(c) Stored energy in z_2

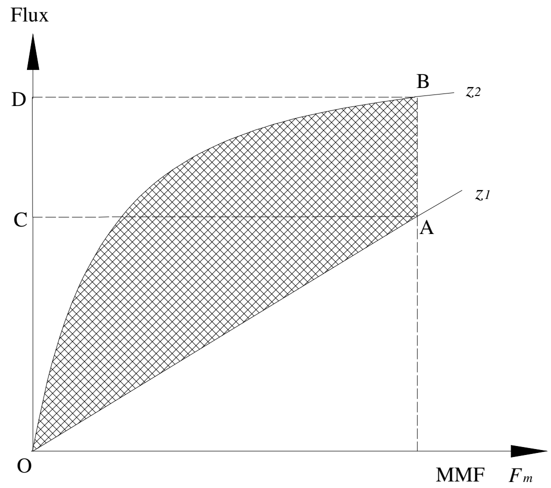

Fig. 2.7(d) Mechanical work

In agreement with the law of conservation of energy, the input electrical energy W_e is equal to the sum of the stored energy W_f, energy converted into mechanical work W_m and the loss energy W_l. Equation (2.10) gives the incremental form of conservation of energy

$$dW_e = dW_f + dW_m + dW_l \tag{2.10}$$

Due to the low resistance of the exciting coil and the low hysteresis loss of silicon steel, the dW_l term can be deleted to simplify the calculation as equation (2.11)

$$dW_e = dW_f + dW_m \tag{2.11}$$

Assuming that the MMF is a constant when air-gap varies from z_1 to z_2, figure 2.7 can be employed to depict conservation of electromechanical energy conversion conveniently. The various energy accords with the shade areas shown in figure 2.7.

$$dW_e = area(DCABD) \tag{2.12}$$

$$dW_f = W_f \Big|_{z=z_2} - W_f \Big|_{z=z_1} = area(OBDO) - area(OACO) \tag{2.13}$$

$$\begin{aligned} dW_m &= dW_e - dW_f \\ &= area(DCABD) - area(OBDO) + area(OACO) = area(OABO) \end{aligned} \tag{2.14}$$

It can be seen from figure 2.7 that the area (*OABO*) is the incremental co-energy dW_c. Hence, the electromagnetic force f_z conducted from the incremental mechanical work done can be expressed as

$$f_z\Big|_{i=constant} = \frac{dW_m}{dz} = \frac{dW_c}{dz} = \frac{d\int_0^i \lambda di}{dz} = \frac{d\int_0^{F_m} \Phi dF_m}{dz} \tag{2.15}$$

In addition, if the inductance L varies with air-gap linearly for a given current, the electromagnetic force can be represented as

$$f_z\Big|_{i=constant} = \frac{dW_c}{dz} = \frac{d\int_0^i \lambda di}{dz} = \frac{d\int_0^i L(z) i di}{dz} = \frac{1}{2}\frac{dL(z)}{dz} i^2 \tag{2.16}$$

2.3 Magnetic characteristics and levitation force analysis

In this section, the magnetic characteristics and levitation force of the proposed SRA are discussed through the principles of operation mentioned above.

2.3.1 Review of analysis methods

Equation (2.15) can be used to analyze electromagnetic force in the proposed switched reluctance actuator. To carry out this implementation, the relationship between flux and MMF needs to be found out. There are three techniques to solve this problem. The three techniques are actual flux measurement, Magnetic Circuit Analysis (MCA) and Finite Element Analysis (FEA).

2.3.1.1 Actual flux measurement method

Both the direct method and indirect methods can be implemented to measure flux. Direct method of determining flux is to apply a magnetic flux sensor to measure the flux inside the actuator [54], this method is not normally selected because of expensive, inconvenience installation and limited measurement range of the sensor [55]. The indirect methods are to obtain flux by processing the voltage and current data of the coil. In contrast to the direct method, the indirect methods are used widely due to cheap, simplification and easy implementation [55]-[64]. There are a few indirect methods available; it includes the search coil method [56]-[57], the step voltage method [55], [58]-[63] and the Alternate Current (AC) voltage source with online winding resistance estimation method [64].

The basic principle of search coil method is to calculate flux in a phase winding through integrating the induced Electromotive Force (EMF) in the search coil [56]-[57]. Therefore, a search coil is mounted on the phase winding, which is excited by an AC voltage source. Though this method is accurate, the difficult setup of the search coil limits its application.

The step voltage method is to obtain flux in a phase winding by using the phase voltage and current when the phase winding is energized by a step voltage. Digital integrator [55], [58]-[61] and analog integrator [62]-[63] can both be employed in this method. This method does not have the installation problem. However, the measurement accuracy relies on the characteristics of winding resistor and the experimental conditions, (e.g. temperature).

The AC voltage source with online winding resistance estimation method is to estimate winding resistance online according to the extreme value of current under an AC voltage excitation [64]. Then, the flux is computed from the relative voltage and current data of winding. This method is accurate and easy to implement.

2.3.1.2 Magnetic circuit analysis method

MCA is an analytical method for the estimation of flux in a magnetic circuit. It can be used to design an actuator with a simple structure based on its plain computing procedure. The basic postulate of MCA is to find the magnetic paths in the actuator and to use Ampere’s circuital law to solve the flux estimation problem.

The method for analytical estimation of the permeance of flux paths is discussed in [13], and the flux paths models of several type structures of high permeability material are built and analyzed. The permeance model and the reluctance force between tooth-structures of motors are developed in [14], three different translator position regions are considered to evaluate the permeance through the air-gap during the motion of the translator. On the basis of the above flux paths models, numerous permeance models and their corresponding MCA methods are developed and employed in the design and analysis of different structures of switched reluctance motors. In [15], four different translator position regions are used to calculate the permeance in the air-gap of a Linear Switched Reluctance Motor (LSRM). In [16], permeance models in five different translator position regions are built to evaluate the propulsion force of a double-sided, double-translator LSRM. In [17], inductances and flux linkages for three identified rotor position regions of rotary SRM are computed to verify the design of motor. A high speed magnetic circuit network is approached as the calculation tool for electromechanical actuators design [18], this method is effective in solving the problem within a very short time.

2.3.1.3 Finite element analysis method

In contrast to the MCA method, the FEA method has a higher accuracy and precision. On the other hand, it is more complex and time consuming. In [19], different physical sizes of SRMs are compared by using a 2-dimensional (2D) FEA model. In [20], the flux linkage and force of an electromechanical valve actuator are simulated by 3-dimensional (3D) FEA model. A 3D FEA model of rotary SRMs is developed to simulate the motor in many different rotor positions in [21]. The force and torque computation of SRMs are compared by a 2D FEA model and a 3D FEA model in [22], and the results show that accuracy of 3D model is better than that of 2D model. The FEA method based on Maxwell stress is used to predict the electromagnetic vibration in [23]. The FEA method on the basis of virtual work principle is presented to solve the electromagnetic force in [24]. In [25], the above two FEA methods – Maxwell stress method and virtual work method are proposed for electromagnetic torque computation, and merits of each method are concluded.

2.3.1.4 Analysis method for the proposed SRA

In this thesis, one of the objectives is to investigate the characteristics of electromagnetic force vs. current and air-gap. Therefore, the force is measured directly at different currents and air-gaps. At the same time, the MCA model and the 3D FEA model are used to analyze magnetic levitation force behavior. The simulated results are compared with the actual measurement of the prototype hardware to validate the accuracy of the actuator estimation.

2.3.2 Equivalent magnetic circuit approach

It has been seen in figure 2.1 that there are three levitation coils with the same dimensions. Therefore, the analysis of one coil is sufficient for the analysis of the actuator. The coil includes stator and levitator. For force measurement convenient, MCA modal and FEA model are utilized to design a different dimension of stator and levitator as shown in figure 2.8, and the specifications of the actuator are listed in table 2.2.

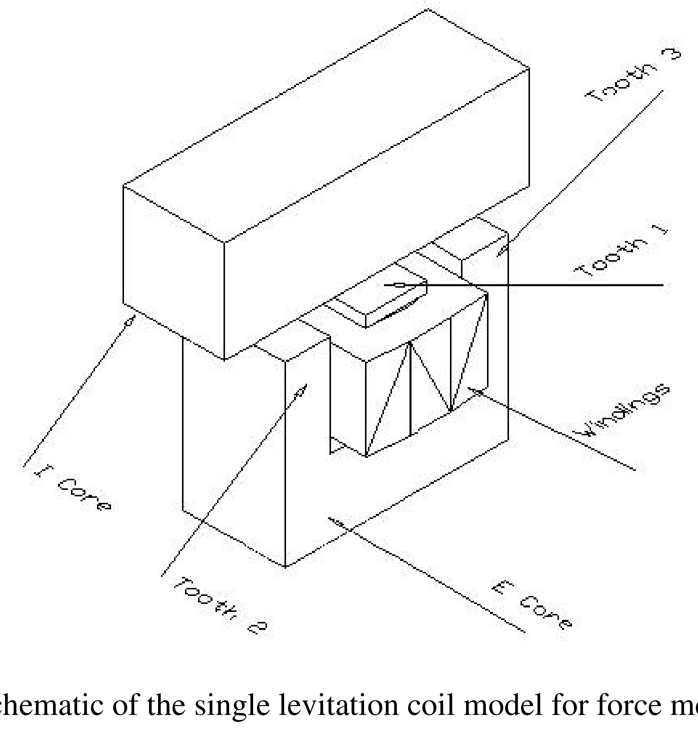

Fig. 2.8 Schematic of the single levitation coil model for force measurement

Symbol	Definition	Value
W_{tp2}, W_{tp3}	Width of teeth 2 and 3 separately	9mm
W_{tp1}	Width of tooth 1	12mm
h	Teeth height	20mm
d	Teeth depth	20mm
W_{12}	Width between teeth 1 and 2	9mm
W_{13}	Width between teeth 1 and 3	9mm
l_{yh}	Yoke height	15mm
D	Track depth	20mm
H_{th}	Track height	20mm
N	Number of coil turns	30

Table 2.2 Parameters of the single levitation coil for force measurement

2.3.2.1 The magnetic circuit analysis modeling

Figure 2.9 shows the magnetic equivalent circuit diagram of the single levitation coil. This diagram is corresponding to figure 2.8.

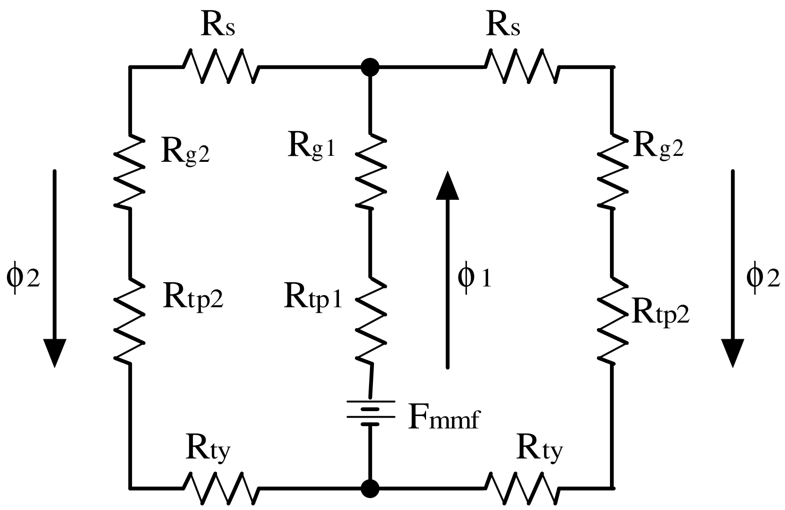

Fig. 2.9 Magnetic equivalent circuit diagram

In each close loop magnetic circuit shown in figure 2.9, the reluctances of I-core track, air-gap between tooth 1 and track, air-gap between tooth 2 and track, pole of tooth 1, pole of tooth 2, and yoke between tooth 1 and tooth 2 are denoted as R_s, R_{g1}, R_{g2}, R_{tp1}, R_{tp2}, and R_{ty}, respectively.

2.3.2.2 Levitation force

The MMF equation can be written as

$$F_{mmf} = Ni = \Phi_1 R_{g1} + \Phi_2 R_{g2} + H_s l_s + H_{tp1} l_{tp1} + H_{tp2} l_{tp2} + H_{ty} l_{ty} \tag{2.17}$$

Where F_{mmf} denotes the total MMF source, N denotes the number of coil turns, i denotes the exciting current, Φ denotes the flux, R_g denotes the air-gap reluctance and $R_g = 1/P$, P is the air-gap permeance, H denotes the magnetic field intensity, l denotes the flux path length.

Table 2.2 shows that width between adjacent teeth is 9mm, while the air-gap doesn't exceed 2mm. Therefore, the flux due to leakage between adjacent teeth is small and the leakage flux could be neglected, then, the flux $\Phi_1 = 2\Phi_2$ because of the symmetry of the E core.

The flux density B is given by equation (2.2).

The magnetic field intensity H can be obtained from the B-H characteristics curve of silicon steel as shown in figure 2.10.

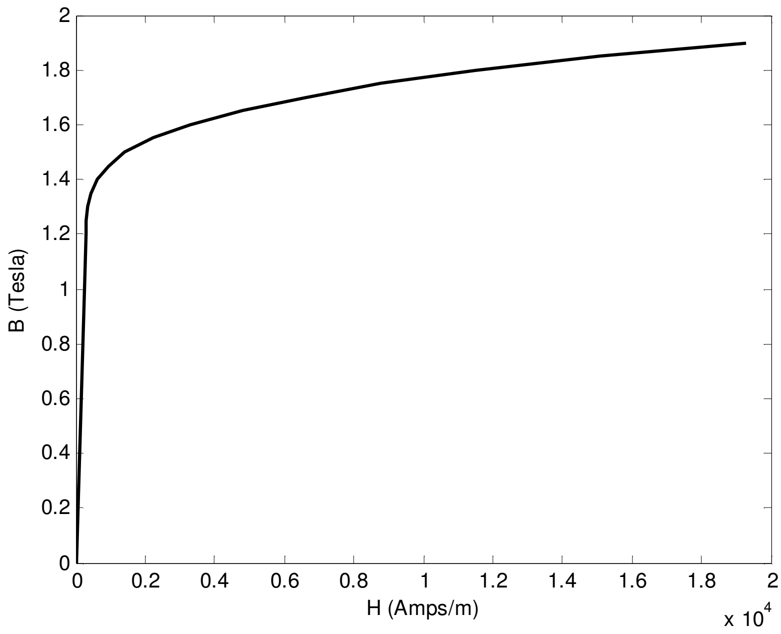

Fig. 2.10 B-H characteristic curve of silicon steel

Due to the nonlinearity of B-H characteristics, iterative procedure is adopted to calculate the flux Φ. A bisection root-finding algorithm [15] is introduced by assuming that an arbitrary initial value of Φ. However, the value of flux density B is limited in the B-H characteristics curve, hence the initial value Φ cannot be arbitrary large, otherwise the interpolation calculation will be difficult. Assume that the total F_{mmf} is used up in the air-gap. Then the extreme value of the flux can be gotten from equation (2.17) by omitting $\sum Hl$. Therefore the initial maximum value of the flux Φ_1 can be supposed as:

$$\Phi_{1\max} \le \Phi_{ext} = \frac{2Ni}{2R_{g1} + R_{g2}} \tag{2.18}$$

The error between the right hand side and the left hand side of equation (2.17) can be used to test for convergence. The flow chart for the iterative procedure is shown in figure 2.11, and the suggested value for error in iterative procedure is $\varepsilon = 0.0001$.

Then, the levitation force can be calculated by using equation (2.15).

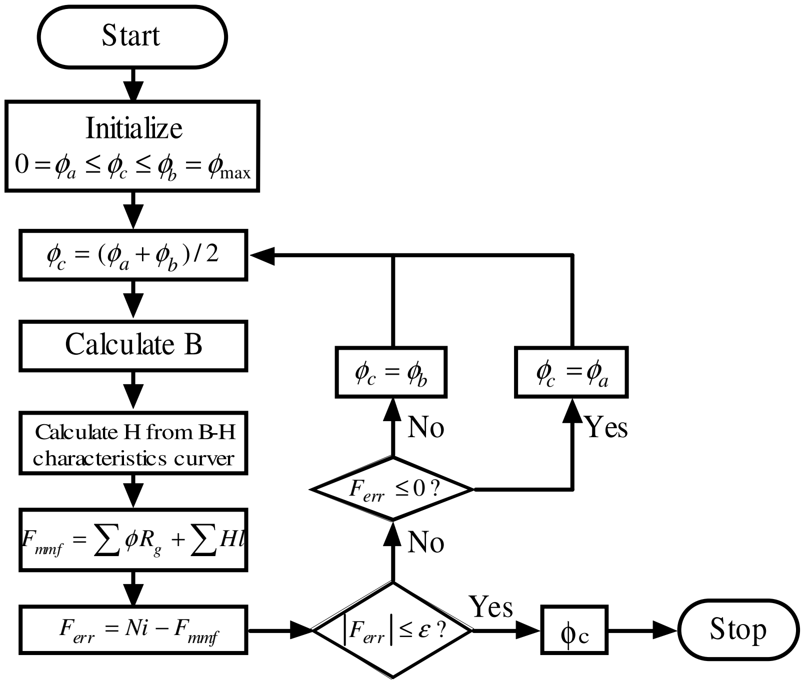

Fig. 2.11 Flow chart of iterative procedure for calculating the flux

2.3.2.3 Air-gap permeance

Once the air-gap permeance is known, the iterative solution gives the value of flux; therefore the levitation force can be deduced from equation (2.15). The air-gap permeance can be determined by selecting suitable flux paths. In this paper, the air-gap permeance model is based on [15]. The air-gap has seven different types of flux paths to estimate air-gap permeance, as shown in figure 2.12.

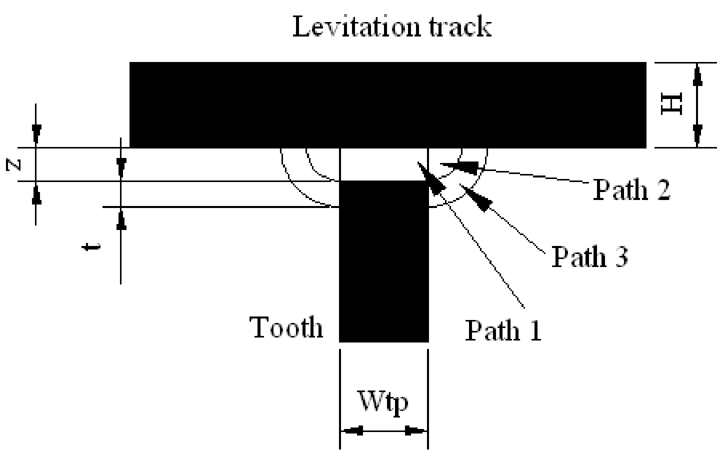

(a) Front view

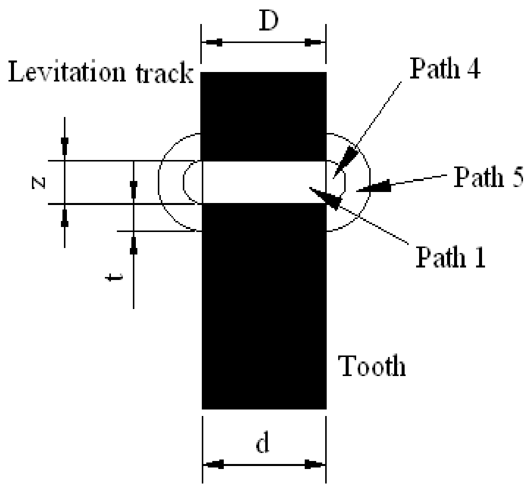

(b) Side view

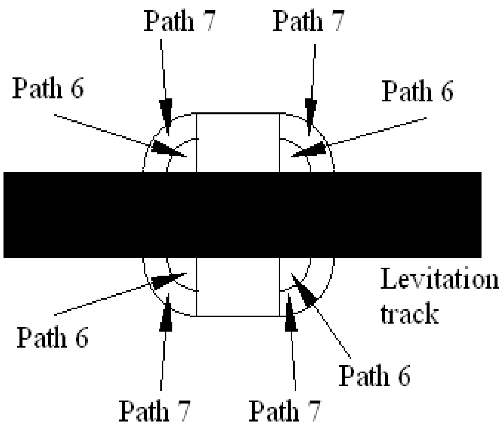

(c) Top view

Fig. 2.12 Seven flux paths within air-gap

The derived air-gap permeances are given in the following corresponding to each flux path:

Path 1 is the basic parallelepiped geometry,

$$P_{j1} = \mu_0 \frac{W_{tpj} d}{z} \tag{2.19}$$

Path 2 is quarter-circular cylinder geometry,

$$P_{j2} = \mu_0 \frac{\frac{1}{4}\pi z^2 d \Big/ 1.211z}{1.211z} = 0.535\mu_0 d \tag{2.20}$$

Path 3 is quarter annulus geometry,

$$P_{j3} = \int_z^{z+t} \mu_0 \frac{d}{\pi r/2} dr = 0.637\mu_0 d \ln\left(1 + \frac{t}{z}\right) \tag{2.21}$$

Path 4 is semicircular cylinder geometry,

$$P_{j4} = \mu_0 \frac{\frac{1}{2}\pi\left(\frac{z}{2}\right)^2 W_{tpj} \Big/ 1.211z}{1.211z} = 0.268\mu_0 W_{tpj} \tag{2.22}$$

Path 5 is half annulus geometry,

$$P_{j5} = \int_{z/2}^{t+z/2} \mu_0 \frac{W_{tpj}}{\pi r} dr = 0.318\mu_0 W_{tpj} \ln\left(1 + \frac{2t}{z}\right) \tag{2.23}$$

Path 6 is spherical quadrant geometry,

$$P_{j6} = \mu_0 \frac{\frac{1}{8}\times\frac{4}{3}\pi z^3 \Big/ 1.311z}{1.311z} = 0.304\mu_0 z \tag{2.24}$$

Path 7 is spherical shell quadrant geometry,

$$P_{j7} = \mu_0 \frac{1}{2} \frac{\pi/2(z + t/2)t}{\pi/2(z + t/2)} = 0.5\mu_0 t \tag{2.25}$$

Where j = 1 or 2, denotes the tooth 1 and tooth 2 respectively, μ_0 is the permeability of air, W_{tp} is the width of tooth, d is the tooth depth, h is the tooth height, $t = h/12$.

The flux of each path can be calculated by the combination of (2.17) and (2.19)-(2.25). Then the levitation forces are obtained by using equation (2.15). Fig. 2.13 shows MCA force-current-position 3D chart.

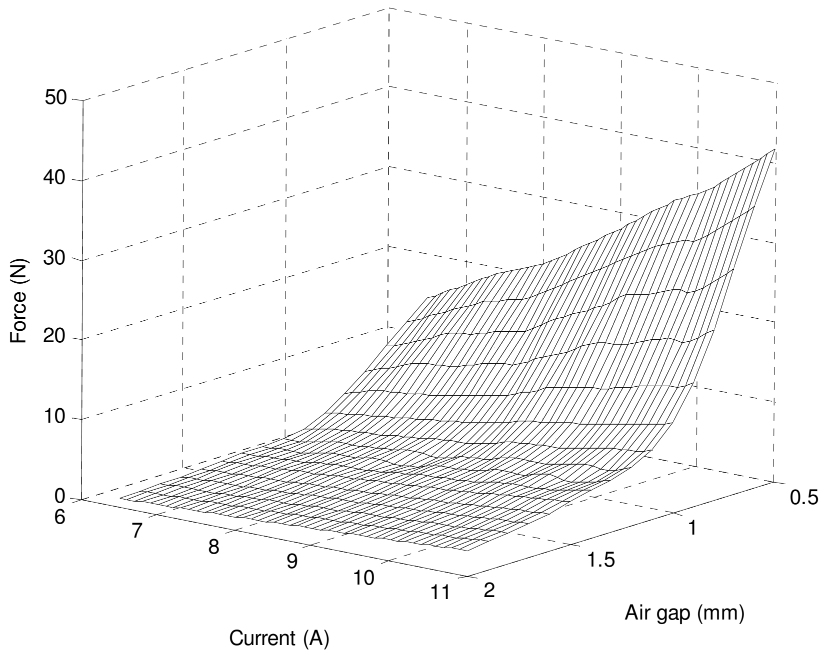

Fig. 2.13 MCA force-current-position 3D chart

2.3.3 Finite element analysis modeling

In general, FEA provides more accurate results than the magnetic equivalent circuit approach since it considers a large number of flux paths compared to the MCA method. In order to fully characterize the proposed levitation system and verify the accuracy of the analytical MCA method, a 3D FEA models are built by using the MEGA software. This software can be used to model any device which can be described in terms of Maxwell's Equations. The use of 3D finite elements by MEGA software in switched reluctance motor and other electrical machines design have been discussed in [65, 66].

Fig. 2.14 shows the 3D FEA model and figure 2.15 shows the cross section of 3D meshes. The 3D model is built by extruding a base plane (X-Z plane) along its perpendicular axis (Y axis). A base is first constructed in the X-Z plane as a 2D framework of nodes and elements. This structure consists of triangles and quadrilaterals with each edge defined by two nodes. The field distribution is the key factor that affects the distribution of finite elements. When the rate of change of field is greater, the elements should be more refined otherwise the estimations at these nodes will not be accurate. After the 2D model is set up, 3D mesh can be created level by level from the base plane. The model contains sufficient detail to define all the changes that occur along the Y axis direction to form a series of similar spaced planes having the similar discretization. The type of "race track" winding is chosen from a variety of coils in the software library. The winding is "wound" on the levitation tooth and current distribution is uniform over the entire coil cross sectional space. Though meshing is not needed for winding, it should be embedded as reduced scalar elements. The region where the finite elements reside this winding should be represented as a "reduced scalar potential" ϕ. The magnetic field due to the source current is derived form Biot-Savart Law [65]:

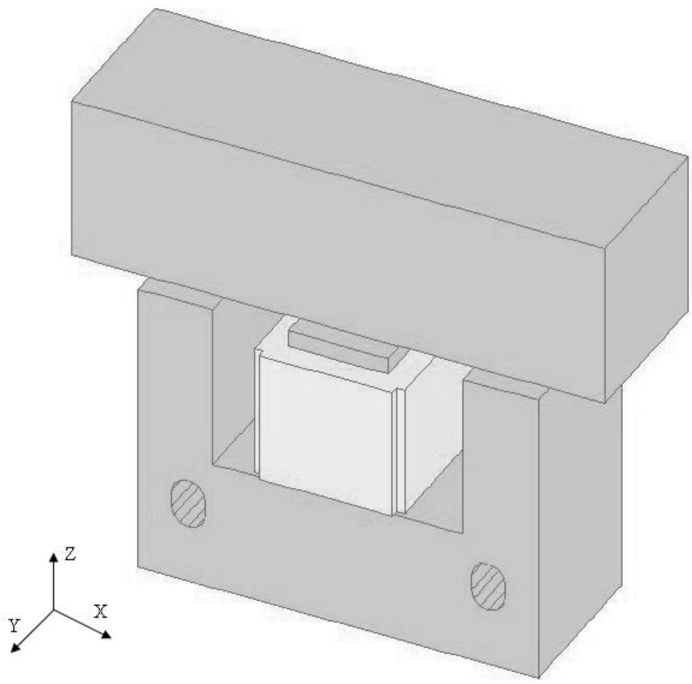

Fig. 2.14 3D FEA model

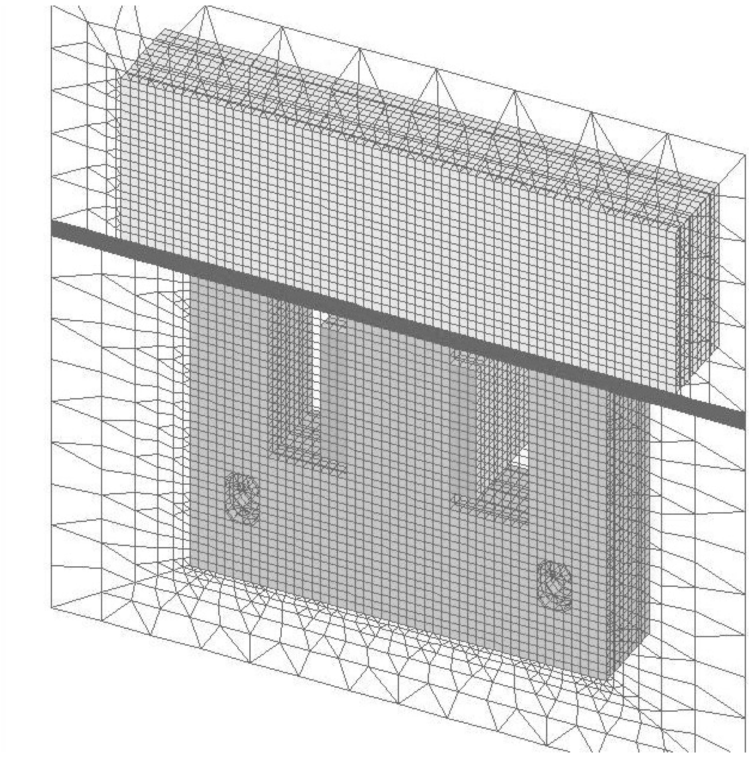

Fig. 2.15 Cross section of 3D meshes

$$H_s = -\frac{1}{4\pi}\int_v J_s \times \nabla\left(\frac{1}{r}\right) dV_m \tag{2.26}$$

Where r is the distance between the current source point where the field is calculated, J_s is source current density and V_m is the current carrying volume.

The actual field is the sum of source field H_s and the gradient of ϕ:

$$H = -\nabla\phi + H_s \tag{2.27}$$

After 3D model is meshed and the winding is defined, normal flux or tangential flux boundary conditions can be set for planes of symmetry. The next step is to calculate the solutions.

It can be seen from figure 2.15 that the number of nodes in air-gap is very large, which means that the elements in air-gap are very fine. These meshes are based on the following criterion: the air-gap predominantly determines the flux distribution, as most of the MMF. Hence the magnetic energy is applied to the air-gap as long as the core is not saturated. This will guarantee the accuracy of the FEA model.

After modifying the air-gap and the exciting currents, the levitation forces for various exciting currents and air-gap can be obtained. The simulation takes into account of the cases that air-gap positions change from 0.5mm to 2mm; and exciting currents change from 6.5A to 11A. The flux contours are shown in figure 2.16. Note that values of numeric bar in each figure are different. Values in figure 2.16(a) (z=0.5mm, i=6.5A) are lower than those in figure 2.16(b) (z=0.5mm, i=11A), but higher than those in figure 2.16(c) (z=2mm, i=6.5A); Values in figure 2.16(d) (z=2mm, i=11A) are lower than those in figure 2.16(b) (z=0.5mm, i=11A), but higher than those in figure 2.16(c) (z=2mm, i=6.5A).

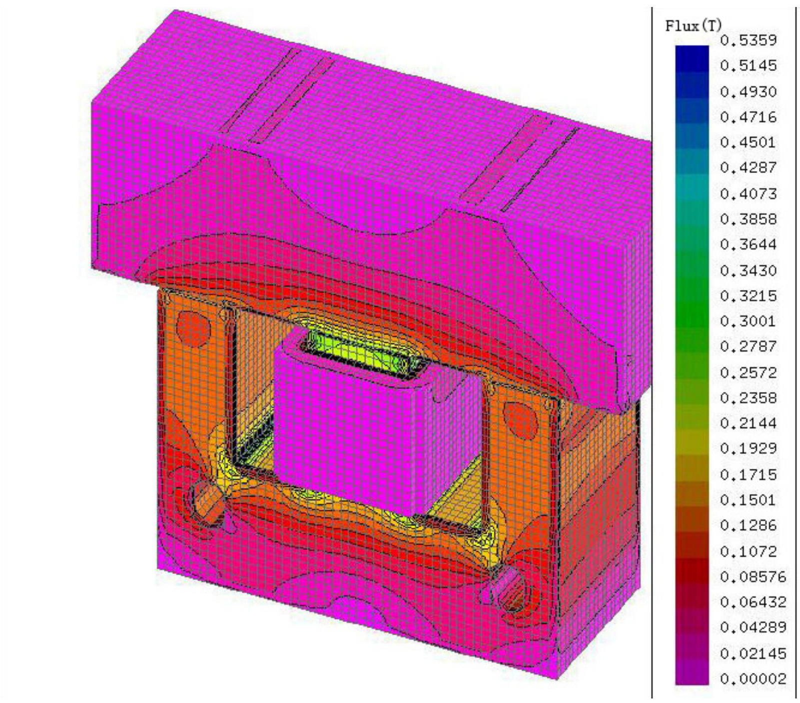

Fig. 2.16(a) Flux contours: z=0.5mm, i=6.5A

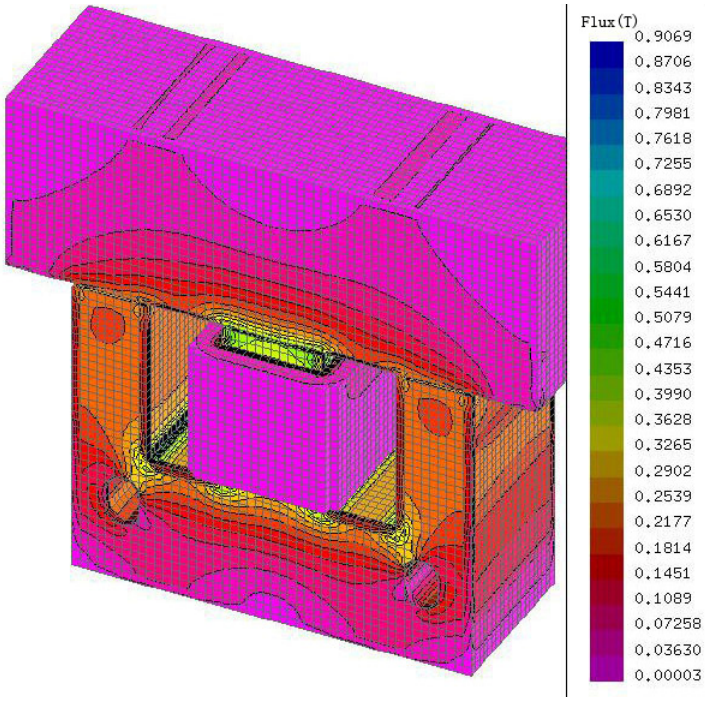

Fig. 2.16(b) Flux contours: z=0.5mm, i=11A

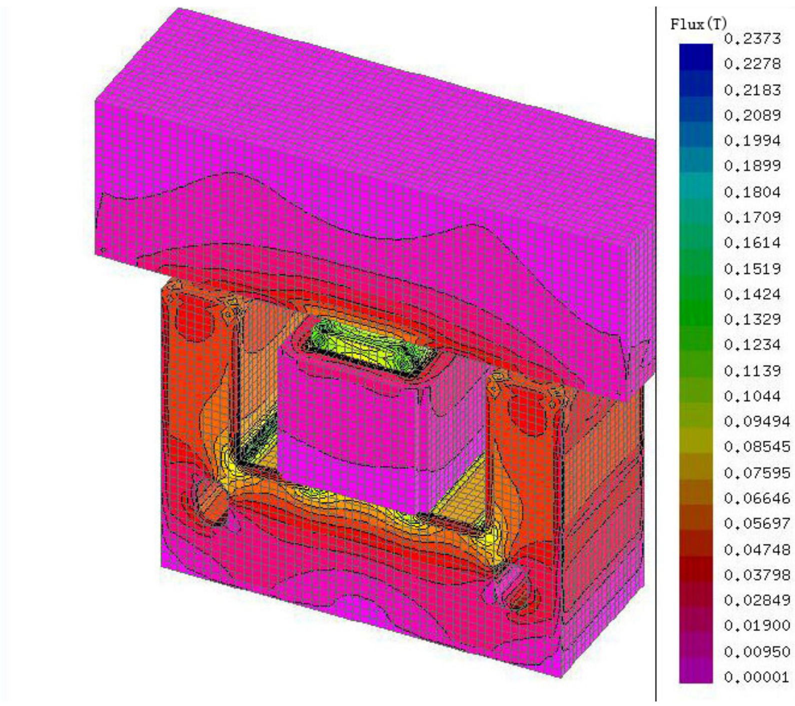

Fig. 2.16(c) Flux contours: z=2mm, i=6.5A

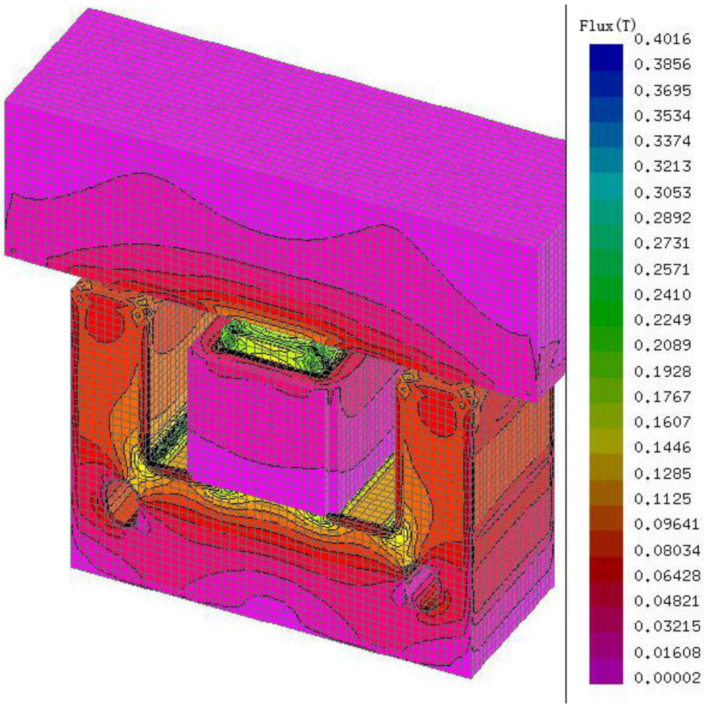

Fig. 2.16(d) Flux contours: z=2mm, i=11A

By comparing the flux contours figure 2.16(a) (z=0.5mm, i=6.5A) with figure 2.16(b) (z=0.5mm, i=11A), or comparing figure 2.16(c) (z=2mm, i=6.5A) with figure 2.16(d) (z=2mm, i=11A), the results show that the higher exciting current, the relatively higher levels of flux. By comparing the flux contours figure 2.16(a) (z=0.5mm, i=6.5A) with figure 2.16(c) (z=2mm, i=6.5A), or comparing figure 2.16(b) (z=0.5mm, i=115A) with figure 2.16(d) (z=2mm, i=11A), the results show that the larger air-gap position, the higher reluctance flux paths, and hence relatively lower levels of flux. All those results accord with the MMF equation (2.17), which indicates that the function between the flux Φ and the exciting current i is monotone increasing, and the function between the flux Φ and the air-gap reluctance R_g is monotone decreasing.

Figure 2.17 shows FEA force-current-position 3D chart. As is shown in figure 2.13 and figure 2.17, the force variation trend of the FEA model is similar to that of MCA model.

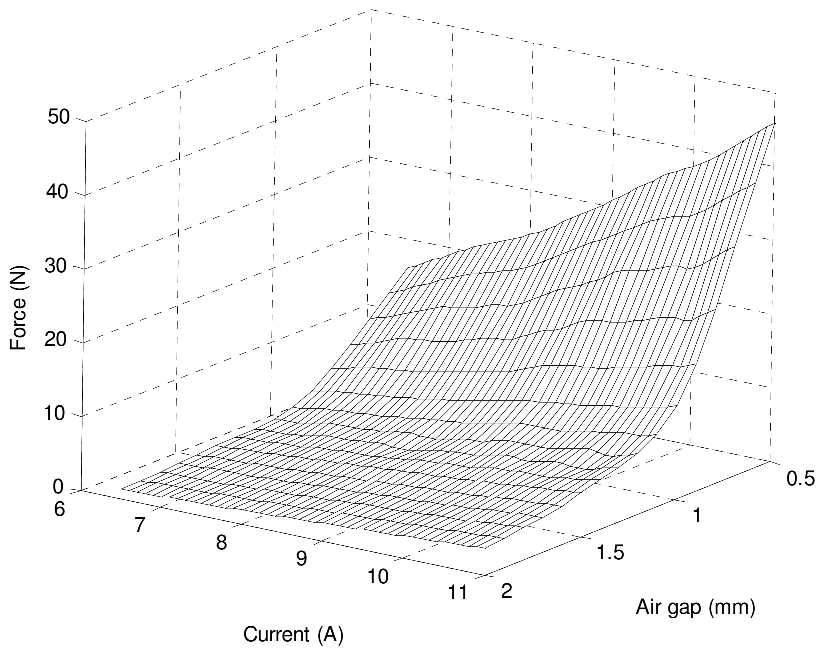

Fig. 2.17 FEA force-current-position 3D chart

2.3.4 Force measurement and results analysis

The block diagram of the force measurement experimental setup is shown in figure 2.18. A dSPACE board, plugged into an Industry Standard Architecture (ISA) bus of a computer, executes all the control functions. The current drive is implemented by an analog amplifier driver.

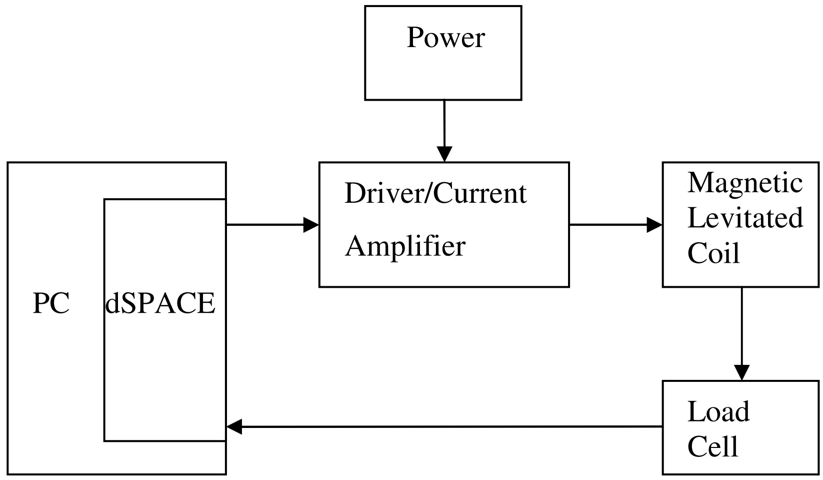

Fig. 2.18 The block diagram of experimental setup for force measurement

The force measurement installation is shown in figure 2.19. The installation consists of two rounded poles embedded in base of the structure, one supporting pole which can be moved up and down, and one connector. The installation is fixed on the body of the motor. The levitation coil is fixed on the connector and it is limited to move in the vertical direction by the two round poles. The air-gap can be changed by adjusting the supporting pole's position. A Load Cell is fixed onto the supporting pole and the connector to measure the levitation force. The levitation force profile is measured at different current excitation levels and air-gaps and it is shown in figure 2.20.

The same force variation trend can be found from the MCA model, the FEA model and the experimental model, as shown in figure 2.13, figure 2.17 and figure 2.20, respectively. Levitation force comparison is illustrated in figure 2.21.

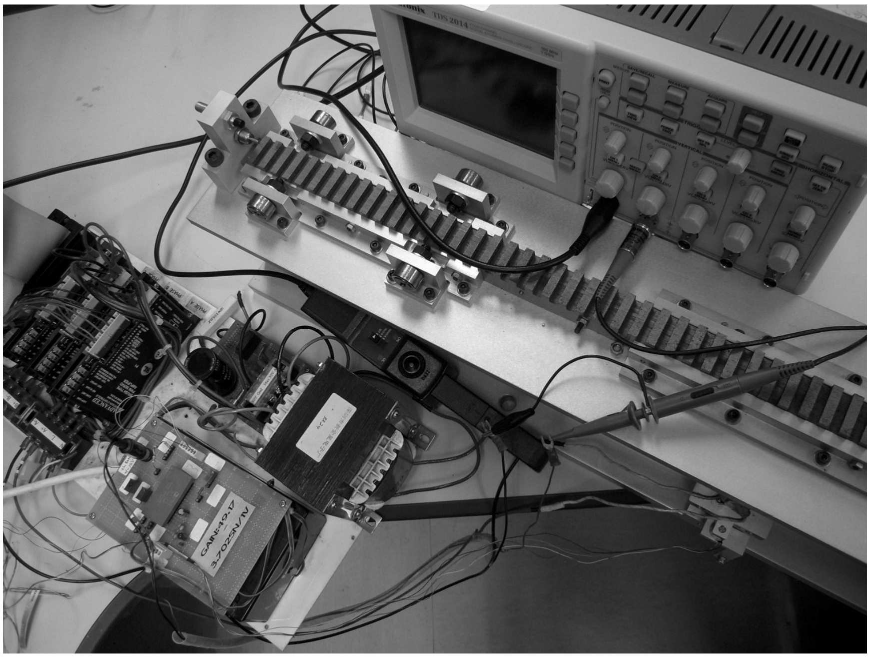

(a)

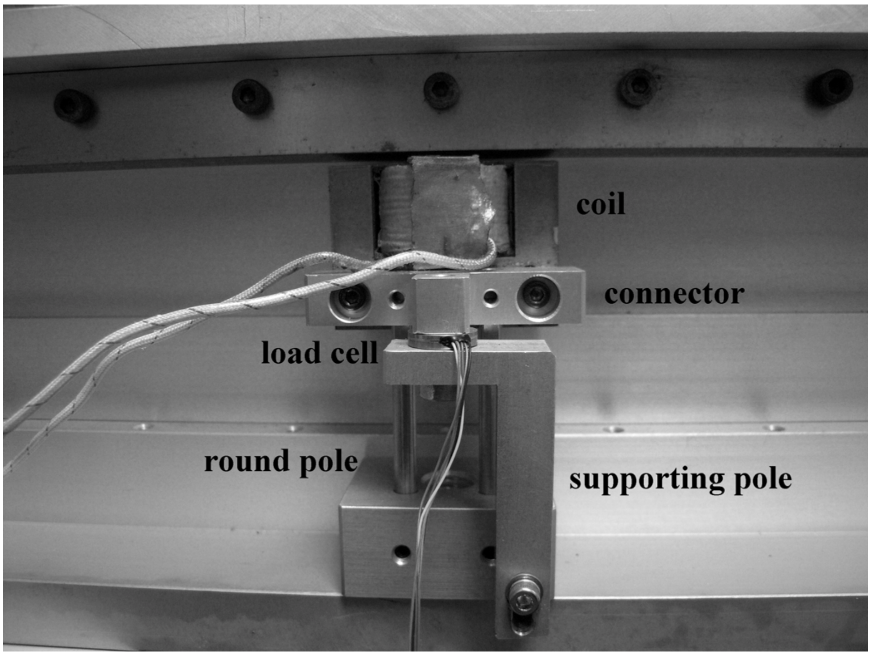

(b)

Fig. 2.19 Force measurement installation

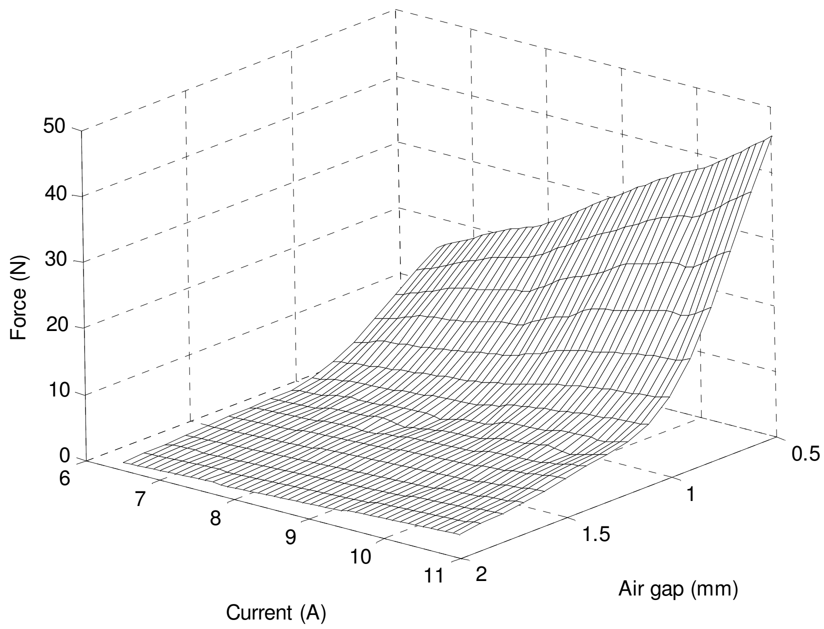

Fig. 2.20 Experimental force-current-position 3D chart

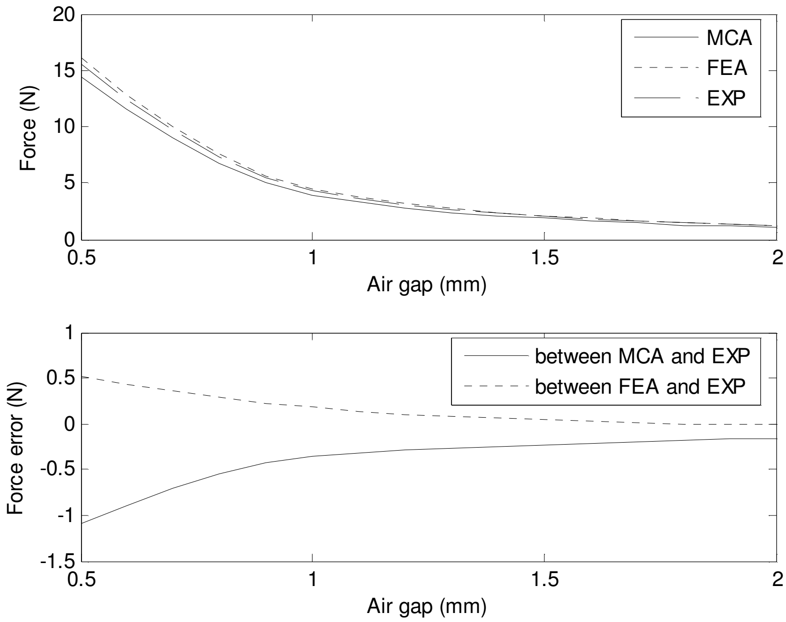

Fig. 2.21 Force comparison with *i*=6.5A

According to figure 2.21, the nonlinear characteristics of the levitation force are demonstrated. It can be seen that the levitation force increase abruptly when air-gap is less than 1 mm. This suggests that higher efficient levitation force can be obtained by restricting the air-gap within a small distance.

Figure 2.21 and table 2.3 give the force comparison and the force error when the exciting current is 6.5A. As shown in figure 2.21, the estimated force from the FEA model is a little bit larger than the measured force, the estimated force from the MCA model is slightly less than the measured force, and the force error between the FEA model and the experiment is less than that between the MCA model and the experimental measurement. As shown in table 2.3, when air-gap is 0.5mm, the error between FEA and experiment is 3.61% while the error between MCA and experiment is 6.58%; when air-gap is 2mm, the error between FEA and experiment is 2.46% while the error between MCA and experiment is 9.84%. For reasons of simply and rapid calculation, there are only seven main flux paths considered in the MCA model. While FEA method simulates the levitation system by mesh discretization, there are much more paths considered in FEA model. As a result, the total flux and the levitation force computed from the MCA model is less than that from the FEA model. There are two possible explanations for the force error between FEA model and experiment. One reason is that there is energy loss in the measurement. Another reason is due to the small mechanical friction that exists though the smooth rounded poles. Consequently the measured force is a little less than the estimated force from FEA model.

Air-gap	MCA	FEA	EXP	Improved MCA (IMCA)	MCA /EXP	FEA /EXP	IMCA /EXP
0.5mm	14.48 N	16.06 N	15.50 N	15.03 N	6.58%	3.61%	3.03%
1mm	3.92 N	4.41 N	4.26 N	4.07 N	7.98%	3.52%	4.46%
1.5mm	1.89 N	2.11 N	2.07 N	1.99 N	8.70%	1.93%	3.86%
2mm	1.10 N	1.25 N	1.22 N	1.26 N	9.84%	2.46%	3.28%

Table 2.3 Force values and relative errors when i=6.5A

2.3.5 Improved equivalent magnetic circuit approach

Table 2.3 also reveals that the FEA model is more accurate than the MCA model, and the errors between the MCA model and the experiment tend to large when the air-gap enlarges. Noting that the air-gap is not a fixed value, from figure 2.16, the 3D FEA flux contours simulation, we find that the configuration of flux path in air-gap changes with the increase of air-gap. Therefore, the parameter t in MCA model could be supposed to be adjustable according to the air-gap. Assuming $\alpha = kz / h$, where k is a constant gain, let $t = h\alpha / 12$, then, the parameter t will change adhere to air-gap, and the MCA model is improved on the basis of 3D FEA model. The force value and error of the improved MCA model are listed in table 3 when the current is 6.5A. When air-gap is 0.5mm, the force error is meliorated from 6.58% to 3.03% after using the improved MCA model; when air-gap is 2 mm, the force error is meliorated from 9.84% to 3.28%. It can be seen from table 3 that the result of improved MCA model is very close to that of FEA model.

Although FEA model is an accurate simulation tool, the slow executive time is a great disadvantage to FEA model. MCA calculation is implemented by MATLAB software, according to a fixed air-gap and a given current, the force computing time is about 3 seconds, and forces with different air-gaps and currents can be calculated conveniently by changing the numerical values of air-gap and current. In contrast to the MCA model estimation, with a fixed air-gap and a given current, the force calculating time for the 3D FEA model is more than 1 minute owing to the large number of nodes calculation. Moreover, it needs additional time to execute the model and mesh generation. In the process of operating the FEA software, the meshing time is relative to user's skill, and it is especially time consuming for some local regions which need mesh refinement, (e.g. the air-gap region). Generally, the total calculating time for the 3D FEA model including meshing time is around 20 minutes. Furthermore, the space of air-gap needs to be meshed again if the air-gap is changed, then it will be even more time consuming for a 3D FEA model.

As a result, the MCA method can be used in the first stage of design process to obtain a coarse size and variables of actuator, and this analytic design approach can be refined with FEMA to improve the accuracy of the performance prediction in the final design stage.

From the comparisons between MCA, FEA and experiment, it can be seen that results of the improved MCA are very close to those of FEA, and both are in close approximation to those of the experimental values. These agreements demonstrate the effectiveness of simulation models for the design of the proposed magnetic levitated actuator.

2.3.6 Analytic levitation force of the proposed magnetic levitation system with SRA

The improved MCA method is employed to calculate the relationship among electromagnetic force, current and air-gap for the proposed magnetic levitation system with SRA. The specifications of the SRA are shown in table 2.1. Figure 2.22 shows the levitation force profile at different current excitation levels and air-gaps while figure 2.23 describes current profile at different levitation forces and air-gaps. Those data can be used to construct a look-up table for the control system.

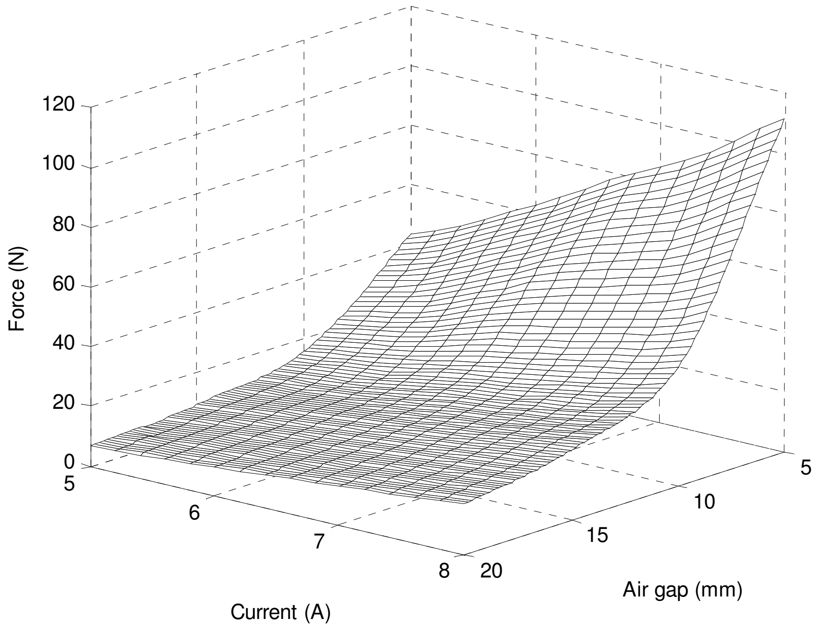

Fig. 2.22 Force-current-position 3D chart of the proposed system

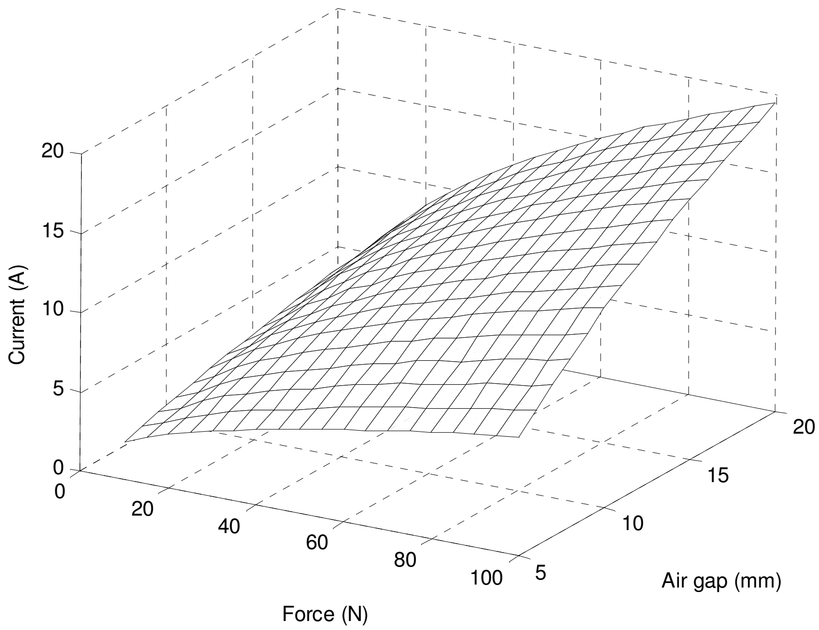

Fig. 2.23 Current-force-position 3D chart of the proposed system

2.4 Summary

A novel magnetic levitated switched reluctance actuator system is proposed in this chapter. The magnetic levitated system is composed of three magnetic levitation coils. No permanent magnet is required in the proposed actuator, so the total cost is lower than permanent magnet actuators. Moreover, the proposed actuator can operate in harsh environmental conditions, such as high temperature and high humidity.

The principles of operation of the proposed magnetic levitation system with SRA are reviewed. Magnetic circuit theory and electromechanical energy conversion theory are employed to investigate the behavior of SRA.

To analyze electromagnetic levitation force, law of electromechanical energy conversion is employed. Hence, the methods to procure flux are surveyed. Those methods are actual flux measurement method, magnetic circuit analysis method and finite element analysis method. In this thesis, both the MCA model and the three-dimensional FEA model are applied to analyze the force of the levitation coils. Corresponding force measurements are also performed. The MCA method can be used to quickly calculate the approximate electromagnetic force, and the accuracy of the MCA model is improved on the basis of the FEA model. The results of improved MCA model are very close to that of the FEA model. Both methods' results agree with the measurement results; this verifies the feasibility of the two simulation models. These results provide useful information for the mechanical structure design of the Magnetic Levitated SRA.

Chapter 3

Modeling of magnetic levitated switched reluctance actuator

In this chapter, a mathematical model of the proposed magnetic levitated switched reluctance actuator is built for the purposes of performance analysis, simulation and controller design. For these purposes, this chapter will investigate the flux modeling method firstly. Then, the dynamic modeling of an SISO magnetic levitation system is constructed. Based on the knowledge of the SISO magnetic levitation system, the dynamic modeling of the proposed MIMO magnetic levitation system is formed. Finally, a two-time scale analysis of magnetic levitation system is represented.

3.1 Review of flux modeling methods

Modeling of the flux linkage of SRAs plays important role on model construction. Many flux modeling methods for switched reluctance actuator have been proposed in the past years. A commonly used method is to construct a look-up table to store the entire flux data [67]-[68]. This look-up table model is direct and simple, and its precision depends on the storage capacity of flux data. If numerous data are needed, it requires large memory capability and lengthy computing time. Piecewise polynomial approximation is another simple method to build flux model for switched reluctance actuator [69]-[74]. This method separates flux characteristics into several parts with a few different linear polynomials [69]-[71] or nonlinear polynomials [72]-[74]. The precision of this method relies on the reasonableness of separation and accuracy of polynomial fitting. A large number of data will enlarge the memory capability and lengthen the computing time.

Trigonometric function approximation is a two dimensional curve family to approach flux characteristics. The method comes from the fact that flux could be function of position and phase current by using Fourier series [75]-[76]. The rotor position is regarded as the variable of the Fourier series and the least squares estimator is adopted to solve the coefficients of the series, which are function of phase current. This method is accurate, but the solution of trigonometric function needs much time. Another two dimensional curve family approximation is exponential function [77]-[79]. The flux is expressed as the exponential function of current and position. This method is also computation complex and time consuming. In recent years, Artificial Intelligence (AI) approximation method is proposed to model the nonlinear flux behavior. It has the advantage of the elimination of the exact mathematical model [80]-[81]. This method is as precise as the trigonometric function approximation method. The disadvantage of this method is the large amount of data generated during the training of the artificial intelligence model and this is a time consuming process.

3.2 Dynamic model for an SISO magnetic levitation system

The proposed magnetic levitation system with SRA has levitation coils located on each side of the equilateral triangular platform, and all the three levitation coils need to be controlled. The rigid framework of the levitation plane creates the coupling forces between the three levitation coils. Therefore, for levitation position control of the plane, the proposed magnetic levitation system with SRA presents an MIMO system coupling problem. On the other hand, the single levitation coil is an SISO control system, and this system has no coupling problem. Although the SISO system is much simpler than the MIMO system, the SISO magnetic levitation system could still be a concerned issue owing to its nonlinear flux characteristics and high inertia. To analyze the MIMO magnetic levitation system step by step, the SISO magnetic levitation system would be explored firstly.

The dynamic model for an SISO magnetic levitation drive system includes the electromagnetic characteristics of winding, the mechanical motion of levitator and the interaction factor between all these parts. To obtain the general dynamic model of the SISO magnetic levitation system, the Kirchhoff's law, the principles of electromechanical energy conversion and the Newton's law are used as a theoretic base.

3.2.1 Electrical model

According to the Kirchhoff's circuit law, the voltage balancing equation of an SISO magnetic levitation system can be expressed as

$$v = R_c i + \frac{d\lambda}{dt} \tag{3.1}$$

Where v denotes the terminal voltage on electromagnet, i denotes the excitation current, R_c denotes circuit internal resistance and λ denotes the flux linkage. On the right hand of equation (3.1), $R_c i$ denotes the voltage drop on circuit internal resistance, $\frac{d\lambda}{dt}$ is referred as back EMF.

Equation (3.1) can be rewritten as (3.2) because flux linkage λ is a function of current i and air-gap z.

$$v = R_c i + \frac{d\lambda}{di}\frac{di}{dt} + \frac{d\lambda}{dz}\frac{dz}{dt} \tag{3.2}$$

Equation (3.2) can be expanded to (3.3) due to $\lambda = Li$

$$v = R_c i + L\frac{di}{dt} + i\frac{dL}{di}\frac{di}{dt} + \frac{d\lambda}{dz}\frac{dz}{dt} = R_c i + L_i\frac{di}{dt} + \frac{d\lambda}{dz}\frac{dz}{dt} \tag{3.3}$$

Where L denotes the coil inductance and $L_i = L + i\frac{dL}{dt}$ denotes the incremental inductance. In equation (3.3), $L\frac{di}{dt}$ term is the voltage drop of coil inductance, $i\frac{dL}{di}\frac{di}{dt}$ term is the voltage relative to flux linkage saturation, and $\frac{d\lambda}{dz}\frac{dz}{dt}$ term is the effect of mechanical motion of levitator to voltage and is referred as the motional EMF.

3.2.2 Electromagnetic force model

As mentioned in section 2.2.2, electromagnetic force model is derived from principle of electromechanical energy conversion and given by equation (2.15).

$$f_z\Big|_{i=constant} = \frac{dW_m}{dz} = \frac{dW_c}{dz} = \frac{d\int_0^i \lambda di}{dz} = \frac{d\int_0^{F_m} \Phi dF_m}{dz} \tag{2.15}$$

The precise solution for electromagnetic force from equation (2.15) takes time owing to the intricate relationship between flux linkage and current. If assuming the flux linkage has linear characteristics, an approximated electromagnetic force model can be simplified as equation (2.16).

$$f_z \big|_{i=constant} = \frac{dW_c}{dz} = \frac{d\int_0^i \lambda di}{dz} = \frac{d\int_0^i L(z) i di}{dz} = \frac{1}{2}\frac{dL(z)}{dz} i^2 \qquad (2.16)$$

3.2.3 Mechanical motion model

The mechanical motion model can be conducted from Newton's law

$$M\frac{d^2 z}{dt^2} = f_z + Mg \qquad (3.4)$$

Where M denotes the mass of levitator, f_z denotes the electromagnetic force and g is the acceleration of gravity, g=9.81m/s^2. As the results shown in equation (3.4), there is no friction relative term $\frac{dz}{dt}$ because of the magnetic levitation.

Suppose the system variables $x_1 = z$, $x_2 = \frac{dz}{dt}$ and $x_3 = i$, the dynamic model of the SISO magnetic levitation drive system can be delineated by using the state space equations as follows

$$\begin{cases} \dfrac{dx_1}{dt} = x_2 \\ \dfrac{dx_2}{dt} = \dfrac{f_z}{M} + g \\ \dfrac{dx_3}{dt} = \dfrac{1}{L_i}(v - \dfrac{d\lambda}{dz} x_2 - R_c x_3) \end{cases} \qquad (3.5)$$

The above equation will form the dynamic model of an SISO magnetic levitation system.

3.3 Dynamic model for the proposed MIMO magnetic levitation system

Similar to the SISO magnetic levitation system, the kinetics characteristics of the MIMO magnetic levitation system can also be represented by electrical model, electromagnetic force model and mechanical motion model. However, owing to the multiple degrees of freedom, the model of the MIMO magnetic levitation system is more complicated than that of the SISO magnetic levitation system. The severe coupling behaviors between the three coils result in the difficulty to extend the analysis of the SISO magnetic levitation system to the MIMO magnetic levitation system.

3.3.1 Electrical model

The voltage equilibrium equation for the three coils is given by

$$v_j = R_{cj} i_j + \frac{d\lambda_j}{dt} \tag{3.6}$$

Where j=1, 2, 3 denotes each coil. Same as the SISO magnetic levitation system, the expansion equation can be described as

$$v_j = R_{cj} i_j + L_j \frac{di_j}{dt} + i_j \frac{dL_j}{di_j}\frac{di_j}{dt} + \frac{d\lambda_j}{dz_j}\frac{dz_j}{dt} = R_{cj} i_j + L_{ij}\frac{di_j}{dt} + \frac{d\lambda_j}{dz_j}\frac{dz_j}{dt} \tag{3.7}$$

3.3.2 Electromagnetic force model

The electromagnetic force equation for the three coils can be expressed as

$$f_{z_j}\Big|_{i_j = constant} = \frac{dW_{mj}}{dz_j} = \frac{dW_{cj}}{dz_j} = \frac{d\int_0^{i_j}\lambda_j di_j}{dz_j} = \frac{d\int_0^{F_{mj}}\Phi_j dF_{m_j}}{dz_j} \tag{3.8}$$

Assuming the flux linkage has linear characteristics, the simplified model is

$$f_{z_j}\Big|_{i_j=\text{constant}} = \frac{1}{2}\frac{dL_j}{dz_j} i_j^{\,2} \tag{3.9}$$

3.3.3 Mechanical motion model

The levitation plane is a rigid body. In a Cartesian coordinates, the system has six degrees of freedom, three translational motions and three rotational motions, which is shown is figure 3.1. The mechanical motion equations of the proposed MIMO magnetic levitation system can be conducted from the postulates of linear and angular momentum. Generally six second order nonlinear differential equations are received and variables interact in these equations.

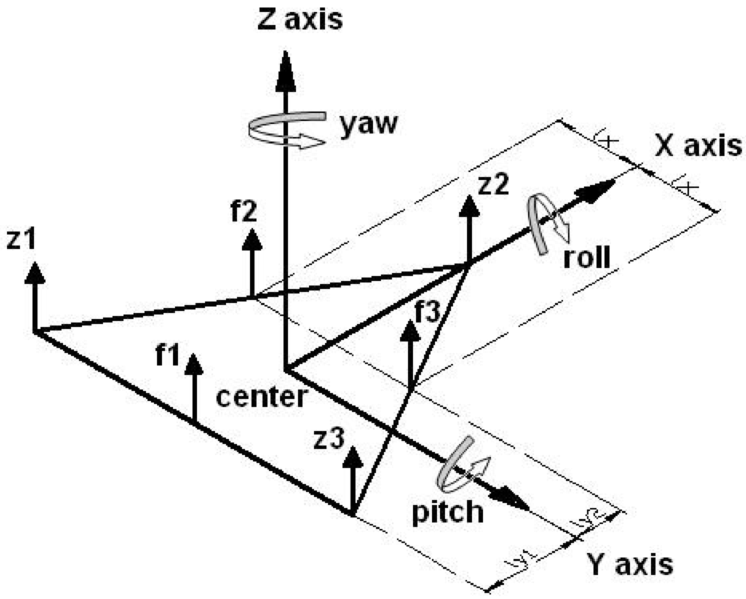

Fig. 3.1 Schematic of the motion model

Due to the uniform of the equilateral triangle form of levitation plane and the symmetry location of the three levitators, the center of mass of the levitation plane could be assumed to coincident with the center of geometry of the levitation plane. The principle of linear momentum results in linear motion equations as follows

$$\begin{cases} M\ddot{x} = F_x \\ M\ddot{y} = F_y \\ M\ddot{z} = F_z \end{cases} \tag{3.10}$$

Where M denotes the total mass of the levitation plane, x, y and z are the displacement along the X axis, Y axis and Z axis, F_x, F_y and F_z are the resultant forces performing along the X axis, Y axis and Z axis.

The doctrine of angular momentum results in torque equations in rotational coordinates. Using appropriate Euler's angles, the torque equations are

$$\begin{cases} T_x = I_{xx}\dot{\omega}_x + (I_{zz} - I_{yy})\omega_y\omega_z \\ T_y = I_{yy}\dot{\omega}_y + (I_{xx} - I_{zz})\omega_z\omega_x \\ T_z = I_{zz}\dot{\omega}_z + (I_{yy} - I_{xx})\omega_x\omega_y \end{cases} \tag{3.11}$$

Where T_x, T_y and T_z are torques rotating about X axis, Y axis and Z axis, I_{xx}, I_{yy} and I_{zz} are moments of inertia rotating about X axis , Y axis and Z axis respectively, ω_x, ω_y and ω_z are the angular velocities rotating about X axis , Y axis and Z axis separately. The angular velocities in terms of Euler angles are

$$\begin{cases} \omega_x = \dot{\phi} + \dot{\psi}\sin\theta \\ \omega_y = \dot{\theta}\cos\phi - \dot{\psi}\sin\phi\cos\theta \\ \omega_z = \dot{\theta}\sin\theta + \dot{\psi}\cos\phi\cos\theta \end{cases} \tag{3.12}$$

Where ϕ, θ and ψ are Euler angles with respect to X axis, Y axis and Z axis separately.

For small angles, the sine and cosine of angles and the differentials of angles could be approximately depicted as, for instant, $\sin\theta = \theta$, $\cos\theta = 1$, $\frac{d(\sin\theta)}{dt} = \frac{d\theta}{dt} = \dot{\theta}$ and $\frac{d(\cos\theta)}{dt} = -\sin\theta\frac{d\theta}{dt} = -\dot{\theta}\sin\theta = -\dot{\theta}\theta$. Hence, the angular accelerations can be represented by

$$
\begin{cases}
\dot{\omega}_x = \ddot{\phi} + (\ddot{\psi}\theta + \dot{\psi}\dot{\theta}) \\
\dot{\omega}_y = \ddot{\theta} + (\dot{\psi}\dot{\theta}\phi\theta - \dot{\theta}\dot{\phi}\phi - \ddot{\psi}\phi - \dot{\psi}\dot{\phi}) \\
\dot{\omega}_z = \ddot{\psi} + (\ddot{\theta}\phi + \dot{\theta}\dot{\phi} - \dot{\psi}\dot{\phi}\phi - \dot{\psi}\dot{\theta}\theta)
\end{cases}
\tag{3.13}
$$

On the right hand of equation (3.13), comparing to the first term, the angle accelerations of roll (X axis), pitch (Y axis) and yaw (Z axis), the terms in brackets could be negligible for small angular motions. Therefore, the equations can be simplified as

$$
\begin{cases}
\dot{\omega}_x = \ddot{\phi} \\
\dot{\omega}_y = \ddot{\theta} \\
\dot{\omega}_z = \ddot{\psi}
\end{cases}
\tag{3.14}
$$

Also, the resulting equations for rotational motions and torques can be simplified as

$$
\begin{cases}
T_x = I_{xx}\ddot{\phi} \\
T_y = I_{yy}\ddot{\theta} \\
T_z = I_{zz}\ddot{\psi}
\end{cases}
\tag{3.15}
$$

Equations (3.10) and (3.15) give the mechanical linear motions and rotational motions of the proposed MIMO magnetic levitation system with switched reluctance actuator. Although the system has six degrees of freedom, movement of the levitation plane can be restricted in particular directions. Owing to the unique magnetic circuit structure of the SRA, the stators and the levitators will move automatic alignment. Hence, the translational movement along X axis and Y axis, and the yawing movement around Z axis can be reasonable ignored. The simplified motion equations about the mass center of the levitation plane are

$$
\begin{cases}
F_z = M\ddot{z} \\
T_x = I_{xx}\ddot{\phi} \\
T_y = I_{yy}\ddot{\theta}
\end{cases}
\tag{3.16}
$$

As shown in figure 3.1, as derived from the three coils, the three electromagnetic levitation forces lead to the force and torque expressions are:

$$\begin{cases} F_z = f_1 + f_2 + f_3 - Mg \\ T_x = (f_2 - f_3) l_x \\ T_y = (f_2 + f_3) l_{y2} - f_1 l_{y1} \end{cases} \tag{3.17}$$

Where f_j (j=1, 2 and 3) are electromagnetic forces generated by the three levitation coils, l_x is the arm of f_2 and f_3 according to X axis, l_{y1} is the arm of f_1 according to Y axis, and l_{y2} is the arm of f_2 and f_3 according to Y axis. The arms of force are

$$\begin{cases} l_x = \dfrac{a}{4} \\ l_{y1} = \dfrac{\sqrt{3}a}{6} \\ l_{y2} = \dfrac{\sqrt{3}a}{12} \end{cases} \tag{3.18}$$

Where a is the side length of the equilateral triangle.

It can also seen from figure 3.1, the three levitation positions z_1, z_2 and z_3 can lead to the displacement and angles of the levitation plane.

$$\begin{cases} z = (z_1 + z_2 + z_3)/3 \\ \phi = (z_1 - z_3)/a \\ \theta = (2z_2 - z_1 - z_3)/(\sqrt{3}a) \end{cases} \tag{3.19}$$

If the three positions are measured by transducers as the feedback signals, the mechanical motion equations of the proposed MIMO magnetic levitation system consist of equations (3.16), (3.17) and (3.19).

These equations are the model of the MIMO magnetic levitation system based on switched reluctance actuator, and it can be seen that the three electromagnetic levitation forces are coupled with the three air-gaps. Therefore, the control of this MIMO magnetic levitation system is a big challenging.

3.4 Two-time scale analysis of magnetic levitation system

The kinetic characteristics of magnetic levitation drive system include the electromagnetic behavior of winding and the mechanical motion of levitator. The two-time scale analysis of magnetic levitation system is based on the fact that the order of response times of electrical behavior and mechanical motion are not the same. The bandwidth of current system is much higher than that of mechanical system, the experimental test conforms that the current loop bandwidth is in the order of several kHz while the output mechanical bandwidth is only in the order of ten Hz [82]. Therefore, a two-time scale method can be applied as the modeling analysis and the cascaded control of the electromechanical system [83]-[84]. The cascaded scheme means that the complete driving system is separated into fast subsystem and slow subsystem according to the two-time scale. Electrical system is the fast subsystem due to the rapid response while mechanical motion system is the slow subsystem because of the dilatory response. Figure 3.2 shows the cascaded control diagram of a magnetic levitation system.

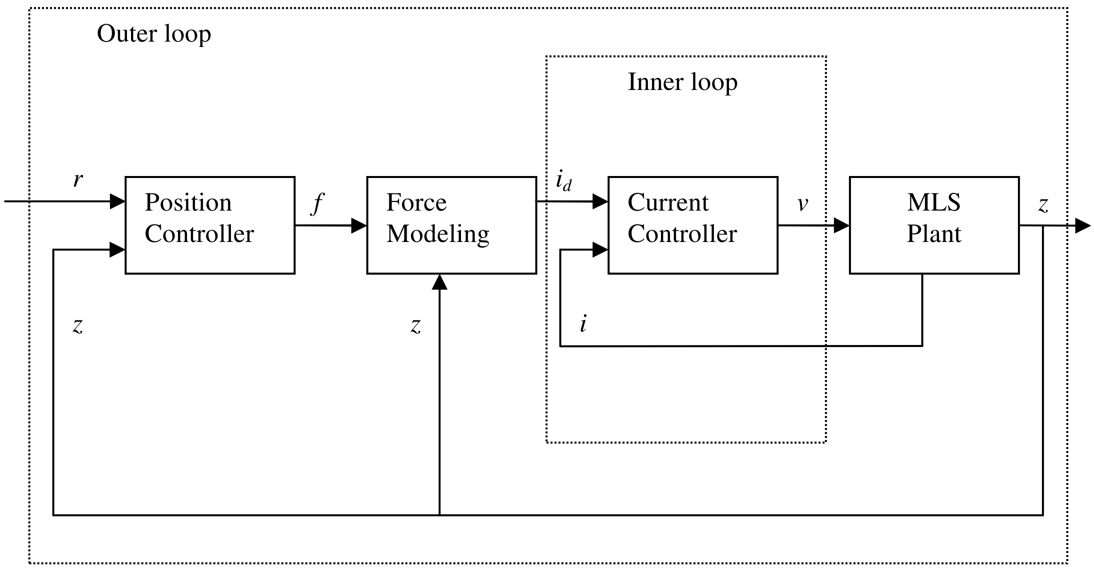

Fig. 3.2 The cascaded control diagram of a magnetic levitation system

It can be seen from figure 3.2 that inner loop control and outer loop control are cascaded for the magnetic levitation system. The inner loop for current control is a fast subsystem while the outer loop for position control is a slow subsystem. The variables of the slow subsystem are referred as the invariant approximation for the fast subsystem, and the stable value of fast subsystem could be adopted into the slow subsystem. In this case, the position variables of outer loop can be treated as constant for the inner loop control. Hence, the equation (3.3) for electrical model of magnetic levitation system can be simplified as

$$v = R_c i + L_i \frac{di}{dt} \tag{3.20}$$

Equation (3.20) is a first order differential equation, and a high gain controller such as the simple proportional controller can guarantee stability and speedy response of the electrical system [82], [85].

3.5 Summary

Firstly, the existing flux modeling methods for SRA have been reviewed. Then, the models for magnetic levitation system with SRA are established. To reveal the characteristics of magnetic levitation system completely, models for both the SISO magnetic levitation system and the MIMO magnetic levitation system are proposed. On the basis of the Kirchhoff's law, the principles of electromechanical energy conversion and the Newton's law, the electrical model, the electromagnetic force model and the mechanical motion model are developed. Following that the two-time scale method is implemented to simply the control of the whole driving system. Using this method, the complicated system can be divided into two reduced order subsystems, the fast subsystem for electrical model and the slow subsystem for mechanical motion model. This separation is applied to controller implementation.

Chapter 4

Sliding mode control for an SISO magnetic levitation system

A robust control algorithm for the position tracking of magnetic levitation systems is presented in this paper. The magnetic levitation systems are well known for the nonlinear dynamic characteristics and open loop instability. This triggers enormous interests in designing various controllers for the nonlinear dynamic systems. In addition, in the magnetic levitation automation transportation system, the variations of the load can be considered as disturbances to the system. The disturbances will deteriorate the dynamic performance of the system and even can give rise to the instability of the system. In this paper, a magnetic levitation system is first modeled by mathematical equations. Then, a sliding mode controller is proposed, with a simple but effective disturbance observer, to perform disturbance rejection. Both the simulation results and the experimental results verify the validity of the robust nonlinear controller.

4.1 Review of controller design for SISO magnetic levitation system

A magnetic suspension system was designed in [26], and the Proportional plus Derivative (PD) control was used to levitate the metallic ball, but the detailed system performance of the magnetic suspension system were not illuminated. Feedback linearization control of the magnetic levitation system has been applied by numerous researches [27]-[28]. The findings in [27] revealed that the feedback linearization method were superior to the classical PID control in a large air-gap of the magnetic levitation system. However, the disturbance of the system was not taken into account. While the disturbance was considered in [28], the experimental results indicated that there were static errors due to the magnetic levitation mass perturbation. In [29], an adaptive nonlinear control composed of feedback linearization method was introduced, and the experimental results reflected its robustness to system parameters uncertainties. However, adaptive control is computational intensive and time consuming, as well as the disturbance was also not taken into consideration.

Sliding Mode Control (SMC) is applied widely in electro-mechanical systems [30]-[32]. It is efficient to control complicated high-order dynamic plants operating under uncertainty conditions [33]. SMC focuses on two domains: selection of sliding surface and design of sliding control law. The sliding surface will decide the desirable behavior of the operating system. The sliding control law will force the system state trajectories move towards the sliding surface and stay on it.

Due to the above merits, SMC is one of the effective candidates for the magnetic levitation system. The purposes of [34]-[35] were to replace linear sliding surface by the nonlinear one, as a result, the desired performances of the magnetic levitation systems were boosted. In [36], the sliding mode equivalence control with exponential reaching law was adopted to a magnetic levitation system, although the simulation results show that the response air-gap could follow the command under the assumption of disturbances, there was no real-time implementation to prove the results.

For improving the system performance, some hybrid controllers including SMC are applied on the magnetic levitation systems. For instance, the integral sliding mode controller with grey forecast was proposed in [37], combination of SMC and radial basis function network was employed to design the controller in [38]. Although experimental results suggest the effectiveness of these methods, they have complicated algorithms and are computational intensive and time consuming.

4.2 Brief of sliding mode control

In control theory, Sliding Mode Control (SMC) is derived from the control schemes on Variable Structure Systems (VSS). It is a kind of the Variable Structure Control (VSC) scheme [86]. SMC is a nonlinear control method that alters the system dynamics by employing high frequency switching control. The discontinuous control law switches from one continuous structure to another continuous structure on the basis of the location in the state space. Multiple control structures are approached in order to force the trajectories of state space move toward a switching condition. The new type of system slides along the boundaries, and it is called sliding mode. The geometrical locus making up the boundaries is called the sliding surface [87].

Intuitively, SMC essentially employs infinite gain to push the trajectories of a kinetic system to slide along the constrained sliding mode subspace. Trajectory from this reduced-order sliding mode has a desirable property that it slides along the surface repeatedly until it reaches a desired equilibrium. The SMC is as simple as a switching between two states, e.g., "on"/"off", so the main advantage of SMC is its robustness, and SMC is an effective control plan for complicated high-order nonlinear dynamic plants operating under uncertainty conditions [33]. In additional, the control law is discontinuous, the sliding mode can be reached in finite time rather than asymptotic behavior.

Owing to the delay and other imperfections of actuators, the action from SMC can result in chattering problems. This may cause energy loss, plant damage, and excitation of unmodeled dynamics [88]. In contrast, continuous control design methods are not easily affected by those problems and can be compromised as a mimic to SMC.

There are two steps in the design of SMC. Firstly, the sliding surface needs to be chosen to represent the desired characteristics of system. Secondly, the switching control law should be found so that trajectory could arrive at the sliding surface and move along the sliding surface.

4.3 Sliding mode controller design for an SISO magnetic levitation system

Figure 4.1 shows the experimental setup of the magnetic levitation system, and the schematic diagram is given in figure 4.2. The experimental setup is only an example for the magnetic levitation system, and the control method discussed later could be applied to any other typical magnetic levitation system.

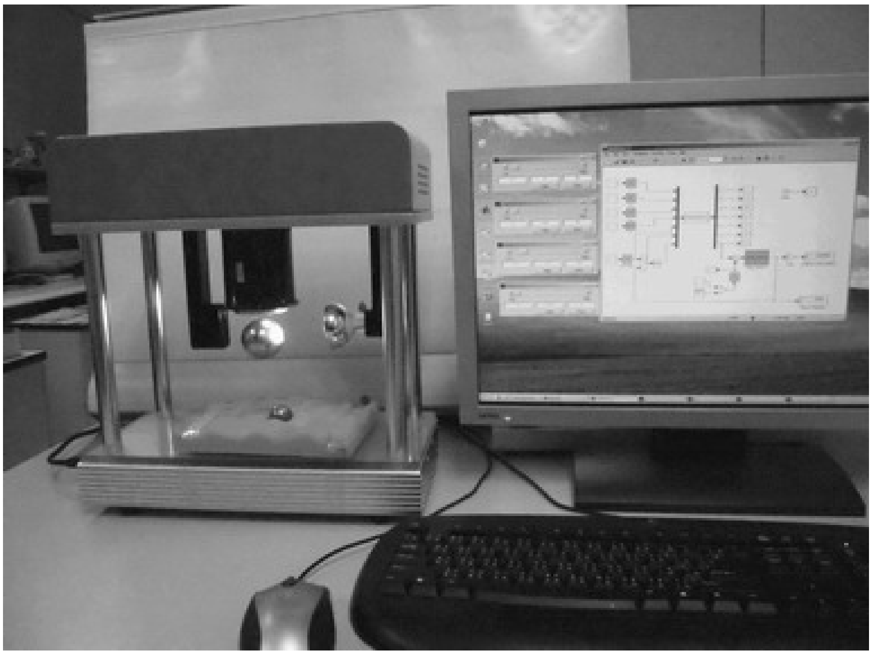

Fig. 4.1 Experimental setup of the SISO magnetic levitation system

The magnetic levitation system consists of an electromagnet, a steel ball, a light source, a position sensor, a data acquisition Analog to Digital/Digital to Analog (AD/DA) board, a control computer and a drive circuit. The steel ball can be suspended at the desired set point by the electromagnetic force, which can be adjusted by the input current. The feedback apparatus includes Light Emitting Diode (LED) light source and optoelectronic sensor. There is a slot in the light receiver panel to detect the light intensity, and it can be generated to relate voltage signals with the range from -10V to 0V. The output photo-voltage signals from optoelectronic sensor are transferred to controller through circuit's signal process and AD board data collection. By analyzing these data, the controller regulates the input current to implement on the electromagnet to match the levitation requirements. The above is the basic operational principle of this magnetic levitation system, and the system model is considered as follows.

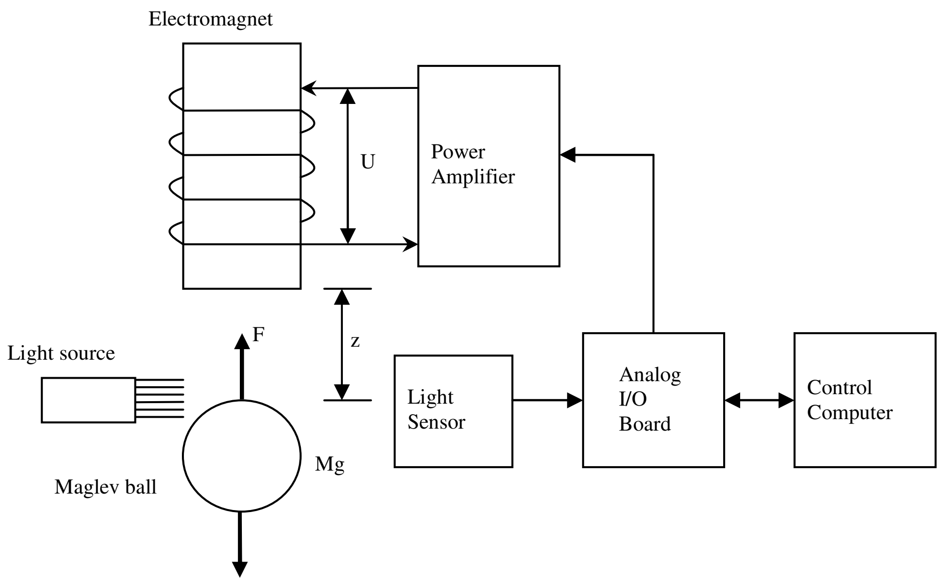

Fig. 4.2 Schematic diagram of the SISO magnetic levitation system

4.3.1 Mathematic equations of model

As mentioned above, the model of the magnetic levitation system can be divided into three parts: electrical model, electromagnetic force model and mechanical kinetics model. The electrical model and mechanical kinetics model are expressed by equation (3.3) and equation (3.4) individually. Therefore, the differential equation of mechanical kinetics model can be written as

$$M \frac{d^2 z(t)}{dt^2} = F(i, z) + Mg \tag{4.1}$$

Where M is the mass of the steel ball, z is the air-gap distance between the electromagnet and steel ball, F is the electromagnetic force, i is the current through the electromagnet, g is the gravitational acceleration.

The electromagnetic force model described by equation (2.16) can be further expanded. The electromagnetic co-energy W can be conducted from the Virtual Work

$$W(i,z) = \frac{1}{2} L(i,z) i^2 \tag{4.2}$$

Where L denotes the inductance of electromagnet coil.

The inductance L can be regarded as a function of z for this magnetic levitated ball system [89]:

$$L = L_1 + \frac{L_0}{1 + z/p} \tag{4.3}$$

Where $L_1 = L(\infty), L_0 = L(0) - L(\infty)$, p are positive constant coefficient. $L(\infty)$ is the inductance when the ball is removed, $L(0)$ is the inductance when the ball is in contact with the coil. The coefficients can be obtained from the experiment, which consists of determining the minimum current required to levitate the steel ball at various positions [90]-[91].

Hence, the electromagnetic force can be written as:

$$F(i,z) = \frac{\partial W(i,z)}{\partial z} = \frac{1}{2} \frac{\partial L}{\partial z} i^2 = -\frac{L_0 i^2}{2p(1 + z/p)^2} \tag{4.4}$$

The equation (4.4) reveals the nonlinear nature of the magnetic levitation system, since the electromagnetic force is a nonlinear function of the air-gap distance and current.

Owing to the two-time scale analysis method, the inner loop current control can be treated as a fast subsystem while the outer loop position control can be viewed as a slow subsystem. The current control is decided by the circuit driving system. Hence, the next step is to design the position controller.

4.3.2 Linearized model of the magnetic levitation system

The equation (4.4) can be rewritten by Taylor series expansion at the nominal operating point, when the error between the variation point and the nominal point is small:

$$F(i,z) = F(i_0, z_0) + K_i(i - i_0) + K_z(z - z_0) \tag{4.5}$$

$$K_i = \frac{\partial F(i,z)}{\partial i}\Big| i = i_0, z = z_0 \tag{4.6}$$

$$K_z = \frac{\partial F(i,z)}{\partial z}\Big| i = i_0, z = z_0 \tag{4.7}$$

Where z_0 is the desired air-gap distance, i_0 is the corresponding current with stability of the magnetic levitation system.

When the magnetic levitation system is stable, the electromagnetic force equals to gravity of the steel ball

$$F(i_0, z_0) + Mg = 0 \tag{4.8}$$

Then, the following equation can be conducted from equations (4.1), (4.4), (4.5) and (4.8):

$$\frac{d^2 z}{dt^2} = -\frac{2g}{i_0} i + \frac{2g}{z_0 + p} z + \frac{2gp}{z_0 + p} \tag{4.9}$$

4.3.3 Model of the controlled system

In this controlled system, the terminal voltage on electromagnet is defined as the input variation of system, the photo-voltage from the position sensor is defined as the output variation of system.

The current passes through the power amplifier to produce the input voltage. The power amplifier is approximate a proportional amplifier since the response of the circuit is very quickly. Hence, the mathematic function of input voltage and current can be written as:

$$u_{in} = K_{in} i \tag{4.10}$$

Where K_{in} is a constant value decided by the circuit.

The output voltage of position sensor can be experimentally measured at different air-gap distance. The collated data are least squares fitted to determine the function between output voltage and air-gap distance. Figure 4.3 shows the static state characteristic curve of the output voltage, and the mathematic function of output voltage and air-gap distance can be represented as:

$$u_{out} = K_{out}\left(z + z_{out}\right) \tag{4.11}$$

Where K_{out} and z_{out} are constant values determined by the least squares fit.

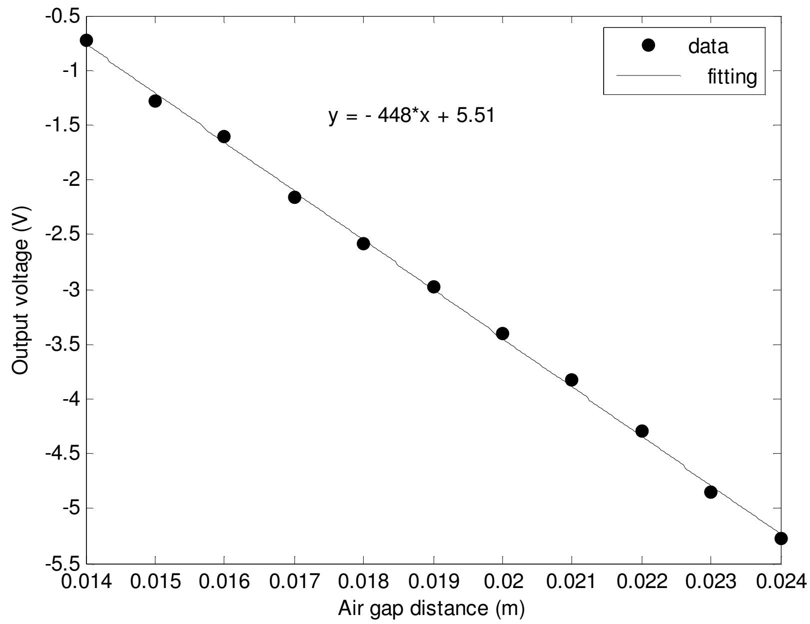

Fig. 4.3 Fitted static state characteristic curve of output voltage

Combination of equations (4.9)-(4.11) gives:

$$\frac{d^2u_{out}}{dt^2}+a_0u_{out}+l_0=b_0u_{in} \tag{4.12}$$

$$a_0=-\frac{2g}{z_0+p}$$

$$b_0=-\frac{2gK_{out}}{i_0K_{in}}$$

$$l_0=\frac{2gK_{out}}{z_0+p}\left(z_{out}-p\right)$$

As shown from the above equation, the system under control is a second-order time-invariant system, and it is unstable system in open loop configuration. Furthermore, the simplified and linearized model of the controlled system is different from the actual system to some degree. To guarantee a satisfied closed-loop performance, a robust and effective controller is necessary for this system.

The specifications and system parameters of the SISO magnetic levitation system are listed in Table 4.1.

Mass of the steel ball	0.11kg
Gravitational acceleration	$9.81ms^{-2}$
Reference air-gap distance at steady state	0.0235m
Reference current at steady state	0.92A
L_0	0.575H
p	0.00315m
K_{in}	$5.893VA^{-1}$
K_{out}	$-448Vm^{-1}$
a_0	$-736.2s^{-2}$
b_0	$1621.3s^{-2}$
l_0	$5095.8Vs^{-2}$

Table 4.1 Specifications and parameters of the SISO magnetic levitation system

4.3.4 The sliding mode controller

An SMC is proposed for this magnetic levitation system. The state space equations and the SMC method are depicted as follows.

4.3.4.1 State space equations

Figure 4.4 shows the control structure of the magnetic levitation system, r is the reference input, y is the output, e is the error between r and y, and $e=r-y$, u is the control law, f_d is the outside disturbance, and it satisfies:

$$\left|b_0 f_d\left(t\right)\right| \le \varepsilon \tag{4.13}$$

Where ε is a constant parameter, $\varepsilon>0$.

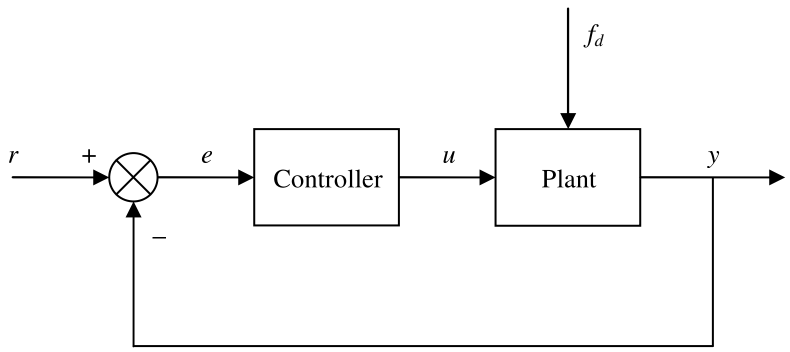

Fig. 4.4 Control structure of the SISO magnetic levitation system

The differential equation of the system shown in figure 4.4 can be conducted from equation (4.12) as follows

$$\frac{d^2}{dt^2}y(t)+a_0y(t)+l_0=b_0\left[u(t)+f_d(t)\right] \tag{4.14}$$

The system state-space equations are given by adopting error e as the state variation, suppose $x_1=e$, then

$$\begin{cases} \dfrac{dx_1(t)}{dt}=x_2(t) \\ \dfrac{dx_2(t)}{dt}=-a_0x_1(t)-b_0u(t)+F(t) \end{cases} \tag{4.15}$$

Where

$$F(t)=\frac{d^2}{dt^2}r(t)+a_0r(t)+l_0-b_0f_d(t) \tag{4.16}$$

4.3.4.2 Sliding mode control

An SMC is adopted for the magnetic levitation system. Firstly, the sliding surface is chosen. Secondly, a sliding control law is designed to force the system state trajectories toward the sliding surface and stay on it in small vicinity bound.

(a) Sliding surface

In a second-order time-invariant system, the sliding surface is a switching line in the phase space. This switching line can be represented by

$$S = cx_1 + x_2 \tag{4.17}$$

Where c>0 is a constant parameter. Therefore, its differential can be

$$\dot{S} = c\dot{x}_1 + \dot{x}_2 \tag{4.18}$$

(b) Sliding control law

The sliding control law is designed as shown in (4.19):

$$u = \frac{1}{b_0}\left[-a_0x_1 + cx_2 + \frac{d^2}{dt^2}r + a_0r + l_0 + \varepsilon sat\left(S\right) + \eta S\right] \tag{4.19}$$

Where η is constant parameter, η>0, and $sat(S)$ is saturation function:

$$sat\left(S\right) = \begin{cases} 1, & S > \Delta \\ S/\Delta, & \left|S\right| \le \Delta \\ -1, & S < -\Delta \end{cases} \tag{4.20}$$

Where Δ denotes a small vicinity of the origin to define the boundary layer, 0< Δ <1.

The saturation function can convert the discontinuous control into continuous control. The system state trajectories are bounded in a small vicinity of the switching line S=0, in place of the exactly ideal mode. Since the switching action is replaced by a continuous approximation, the chattering problem can be undermined.

(c) Stability analysis

Employing the positive definite Lyapunov function candidate:

$$V = \frac{1}{2}S^2 \tag{4.21}$$

Combining equations (4.15), (4.16) and (4.19):

$$\dot{x}_2 = -cx_2 - \varepsilon sat(S) - \eta S - b_0 f_d \tag{4.22}$$

Substituting equations (4.15) and (4.22) to (4.18):

$$\dot{S} = -\varepsilon sat(S) - \eta S - b_0 f_d \tag{4.23}$$

Hence,

$$\dot{V} = S\dot{S} = -\varepsilon sat(S)S - \eta S^2 - b_0 f_d S \tag{4.24}$$

Since the system behavior is not determined within the small vicinity, the system will be stable if the phase trajectory can converge into the small vicinity. For this purpose, the saturation function can be replaced by sign function, therefore

$$\begin{aligned}\dot{V} = S\dot{S} &= -\varepsilon|S| - \eta S^2 - b_0 f_d S \\ &\le -\varepsilon|S| - \eta S^2 + |b_0 f_d||S| \\ &\le -\eta S^2 - (\varepsilon - |b_0 f_d|)|S| \le 0 \end{aligned} \tag{4.25}$$

That verifies the system is stable.

(d) System characteristics analysis

To analyze the system characteristics, the following steps are taken:

It can be calculated from equation (4.23) that

$$\begin{cases} S = p_1 e^{-\eta t} - \dfrac{\varepsilon sign(S) + b_0 f_d}{\eta}, & S < -\Delta, S > \Delta \\ S = p_2 e^{-\left(\frac{\varepsilon}{\Delta}+\eta\right)t} - \dfrac{b_0 f_d \Delta}{\varepsilon + \eta\Delta}, & |S| \le \Delta \end{cases} \tag{4.26}$$

Where p_1 and p_2 are constant parameters.

Combination of equations (4.22) and (4.26) gives

$$\begin{cases} \dot{x}_2 = -cx_2 - \eta p_1 e^{-\eta t}, & S < -\Delta, S > \Delta \\ \dot{x}_2 = -cx_2 - \left(\dfrac{\varepsilon}{\Delta} + \eta\right) p_1 e^{-\left(\frac{\varepsilon}{\Delta}+\eta\right)t}, & |S| \le \Delta \end{cases} \tag{4.27}$$

$$\begin{cases} x_2 = p_3 e^{-ct} + \dfrac{\eta p_1}{\eta - c} e^{-\eta t}, & S < -\Delta, S > \Delta \\ x_2 = p_4 e^{-ct} + \dfrac{\left(\dfrac{\varepsilon}{\Delta} + \eta\right) p_2}{\dfrac{\varepsilon}{\Delta} + \eta - c} e^{-\left(\frac{\varepsilon}{\Delta}+\eta\right)t}, & |S| \le \Delta \end{cases} \tag{4.28}$$

Where p_3 and p_4 are constant parameters.

Then, from equations (4.17) and (4.27)

$$\begin{cases} x_1 = -\dfrac{p_1}{\eta - c} e^{-\eta t} - \dfrac{p_3}{c} e^{-ct} - \dfrac{\varepsilon sign(s) + b_0 f_d}{\eta}, & S < -\Delta, S > \Delta \\ x_1 = -\dfrac{p_2}{\dfrac{\varepsilon}{\Delta} + \eta - c} e^{-\left(\frac{\varepsilon}{\Delta}+\eta\right)t} - \dfrac{p_4}{c} e^{-ct} - \dfrac{b_0 f_d}{c\left(\dfrac{\varepsilon}{\Delta} + \eta\right)}, & |S| \le \Delta \end{cases} \tag{4.29}$$

From the above equations, we can draw the following conclusions:

i) The system dynamic characteristic is decided by η and c before the phase trajectory converge within the small vicinity; the system dynamic characteristic mainly follows ε and Δ within the small vicinity because ε/Δ is far larger than η and c.

ii) The system steady state characteristics have the following ideal conditions:

$$\lim_{t\to\infty} S = -\frac{b_0 f_d \Delta}{\varepsilon + \eta\Delta}$$

$$\lim_{t\to\infty} x_2 = 0$$

$$\lim_{t\to\infty} x_1 = -\frac{b_0 f_d \Delta}{c(\varepsilon + \eta\Delta)}$$

Although the system characteristics seem satisfying, the system performance could be affected by the external disturbance, and the results may not be satisfactory. In this case, the steady error will not tend towards zero if the system does not allow the gain to be high. On the other hand, if the system gain ε/Δ is too high, the switching frequency will also be high, and this can cause the chattering problem. According to equation (4.13), the value of ε may not be small; hence, the dynamics characteristics of system will be affected. Therefore a novel control law is needed to improve the system performance.

4.4 Disturbance Observer based sliding mode control

An asymptotic observer is designed to estimate the unknown disturbance, and the estimated disturbance is included in the novel control law to reduce the impact of the disturbance. Figure 4.5 shows the new control structure of the magnetic levitation system including observer.

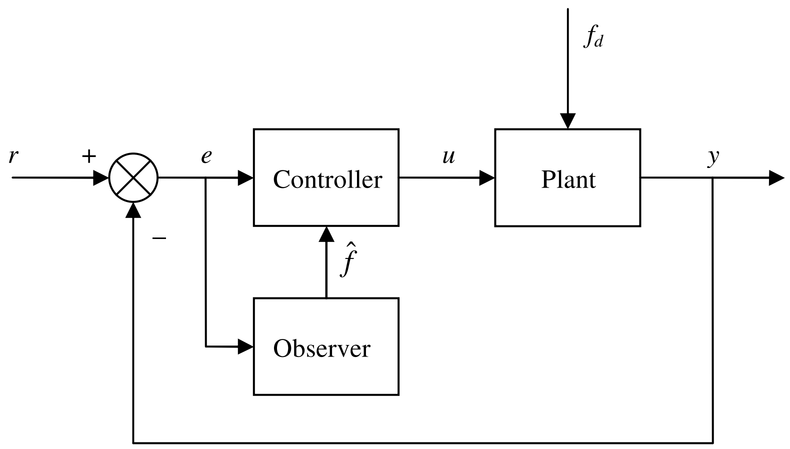

Fig. 4.5 The new control structure of the SISO magnetic levitation system

4.4.1 The disturbance observer

Construct an intermediate variable as below:

$$h = f_d + K_o x_2 \tag{4.30}$$

Where K_o is a constant observer gain. On the basis of the assumption that the disturbance f_d is a slow variation system, it is reasonable to impose that $\dot{f}_d = 0$, then:

$$\dot{h} = K_o \dot{x}_2 = K_o \left(-a_0 x_1 - b_0 u + \frac{d^2 r}{dt^2} + a_0 r + l_0 - b_0 f_d \right)$$

$$= K_o \left(-a_0 x_1 - b_0 u + \frac{d^2 r}{dt^2} + a_0 r + l_0 - b_0 h + b_0 K_o x_2 \right) \tag{4.31}$$

Then, design an observer for the intermediate variable h as follows:

$$\dot{\hat{h}} = K_o\left(-a_0x_1 - b_0u + \frac{d^2r}{dt^2} + a_0r + l_0 - b_0\hat{h} + b_0K_ox_2\right) \tag{4.32}$$

Where $\hat{h}$ denotes the estimated h.

The mismatch between equation (4.31) and (4.32) is given as:

$$\dot{\tilde{h}} = \dot{\hat{h}} - \dot{h} = -b_0K_o\left(\hat{h} - h\right) = -b_0K_o\tilde{h} \tag{4.33}$$

Where $\tilde{h}$ denotes the error between the estimated h and real h. Equation (4.33) reveals that $\tilde{h}$ tends to zero exponentially and the convergent rate varies with the choice of observer gain K_o.

The disturbance f_d can be estimated as:

$$\hat{f}_d = \hat{h} - K_ox_2 \tag{4.34}$$

Where $\hat{f}_d$ denotes the estimated f_d.

Combination of (4.30) and (4.34):

$$\tilde{f}_d = \hat{f}_d - f_d = \hat{h} - h = \tilde{h} \tag{4.35}$$

Where $\tilde{f}_d$ denotes the error between the estimated f_d and real f_d.

As a result, $\hat{f}_d$ will converge to f_d asymptotically, and this estimation can be used to design the novel control law.

4.4.2 The novel sliding control law

Considering the above disturbance observer, the updated control law is the following equation (4.36):

$$u = \frac{1}{b_0}\left[-a_0x_1 + cx_2 + \frac{d^2}{dt^2}r + a_0r + l_0 + \varepsilon sat\left(S\right) + \eta S - b_0\hat{f}_d\right] \tag{4.36}$$

The differential of $\hat{f}_d$ can be gotten by combining (4.32) with (4.34) and (4.36):

$$\dot{\hat{f}}_d = \dot{\hat{h}} - K_0 \dot{x}_2 = K_o \left(-a_0 x_1 - b_0 u + \frac{d^2 r}{dt^2} + a_0 r + l_0 - b_0 \hat{h} + b_0 K_o x_2 \right) - K_0 \dot{x}_2$$

$$= -K_o \left(c x_2 + \dot{x}_2 + \varepsilon sat(S) + \eta S \right) \quad (4.37)$$

The estimated f_d can be calculated from equation (4.37).

Employing the positive definite Lyapunov function candidate:

$$V = V_1 + V_2, \quad V_1 = \frac{1}{2} \tilde{f}^2, \quad V_2 = \frac{1}{2} S^2$$

$$\dot{V}_1 = \tilde{f}_d \cdot \dot{\tilde{f}}_d = \tilde{f}_d \left(\dot{\hat{f}}_d - \dot{f}_d \right) = \tilde{f}_d \cdot \dot{\hat{f}}_d$$

$$= \tilde{f}_d \left(\dot{\hat{h}} - K_o \dot{x}_2 \right) = \tilde{f}_d \left(-b_0 K_o \tilde{h} \right) = -b_0 K_o \tilde{f}_d^{\,2} \leq 0 \quad (4.38)$$

$$\dot{V}_2 = S\dot{S} = S\left(c x_2 + \dot{x}_2 \right) = S\left(-\varepsilon sat(S) - \eta S - b_0 \tilde{f}_d \right)$$

As the above analysis, the system behavior is not determined within the small vicinity, and the saturation function can be replaced by sign function, therefore:

$$\dot{V}_2 = -\varepsilon |S| - \eta S^2 - b_0 \tilde{f}_d S \leq -\eta S^2 - \left(\varepsilon - \left| b_0 \tilde{f}_d \right| \right) |S| \leq 0 \quad (4.39)$$

Under the assumption of $\left| b_0 \tilde{f}_d \right| \leq \varepsilon$.

Hence, $\dot{V} \leq 0$, and the system is stable.

Compare to the previous control law, the new one can lower the ε apparently through replacing $\left| b_0 f_d \right|$ by $\left| b_0 \tilde{f}_d \right|$. This modification can ameliorate the system dynamic performance.

4.5 Simulation results

The proposed system is simulated by using Matlab Simulink. A constant value disturbance and a sinusoidal variation value disturbance are both injected into the simulation, and the disturbance will not be triggered until the simulation time comes to 1 second. Figure 4.6 depicts comparison simulation results of voltage response curves between SMC without disturbance observer and SMC with disturbance observer, the SMC without disturbance observer is on condition that r=5V, c=20, ε=2300, η=15, Δ =0.01, f_d=1, and the SMC with disturbance observer is on condition that r=5V, c=20, ε=0.5, η=15, Δ =0.01, K_o=0.5, f_d=1. Figure 4.9 also shows the comparison voltage response curves simulation results between SMC without disturbance observer and SMC with disturbance observer. The only difference seen from figure 4.6 is that the disturbance is f_d=sin(2*π*t). Figure 4.7 and figure 4.10 depict comparison simulation results of control law between SMC without disturbance observer and SMC with disturbance observer when the disturbance is f_d=1 and f_d=sin(2*π*t) respectively. Figure 4.8 and figure 4.11 show the estimated disturbances according to f_d=1 and f_d=sin(2*π*t) separately.

The frequency adopted in sinusoidal disturbance is to estimate the robustness of the proposed controller against continuous variation disturbance. The bandwidth of the mechanical motion system is only in the order of ten Hz, this low bandwidth reveals that the system itself is a low pass filter, if the disturbance frequency is much higher than the bandwidth of the mechanical motion system, then the disturbance will be filtered by the motion system. Hence, in the simulation, the value of the disturbance frequency will be chosen in a reasonable range, which is close to the bandwidth of the mechanical motion system. As a result, the disturbance with this frequency will disturb the mechanical motion system, and it will be an appropriate test for the proposed controller.

The fixed sample time is T=0.003s.

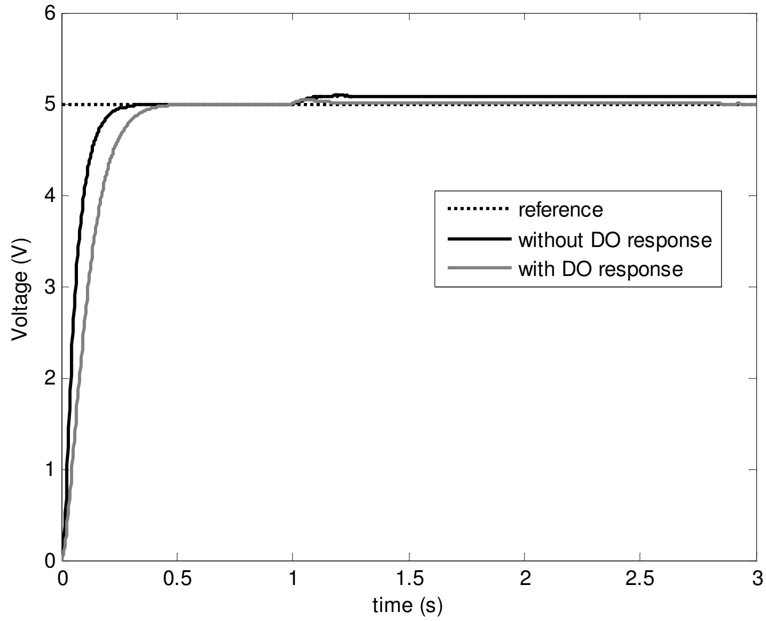

Fig. 4.6 Voltage response curve (f_d=1)

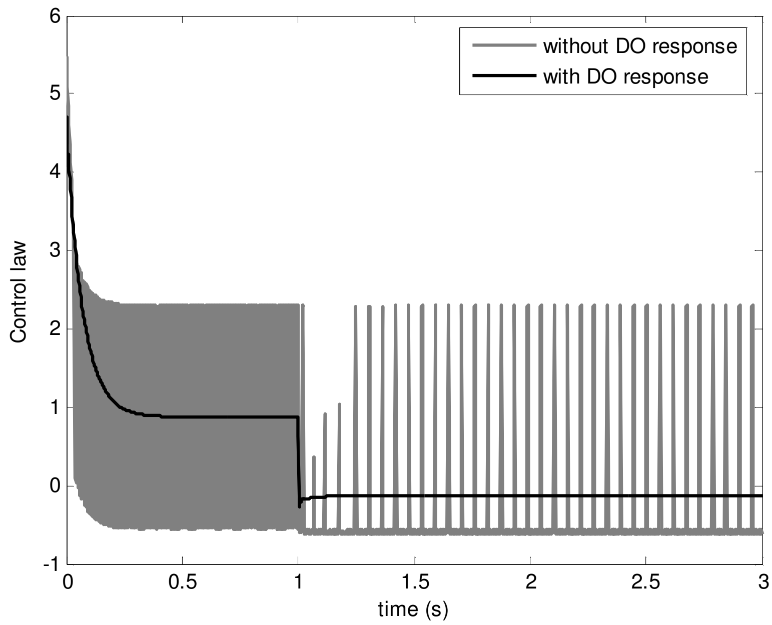

Fig. 4.7 Control law (f_d=1)

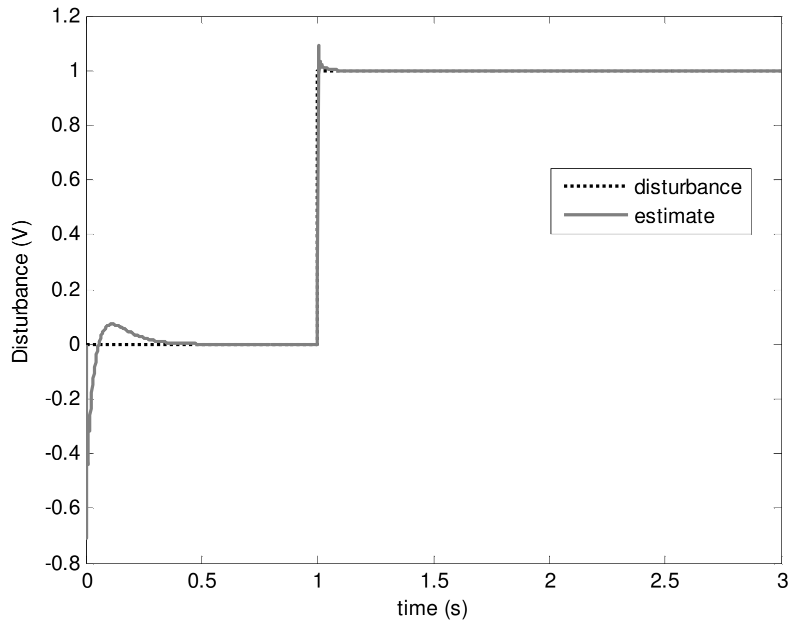

Fig. 4.8 Estimated disturbance curve with the disturbance observer (f_d=1)

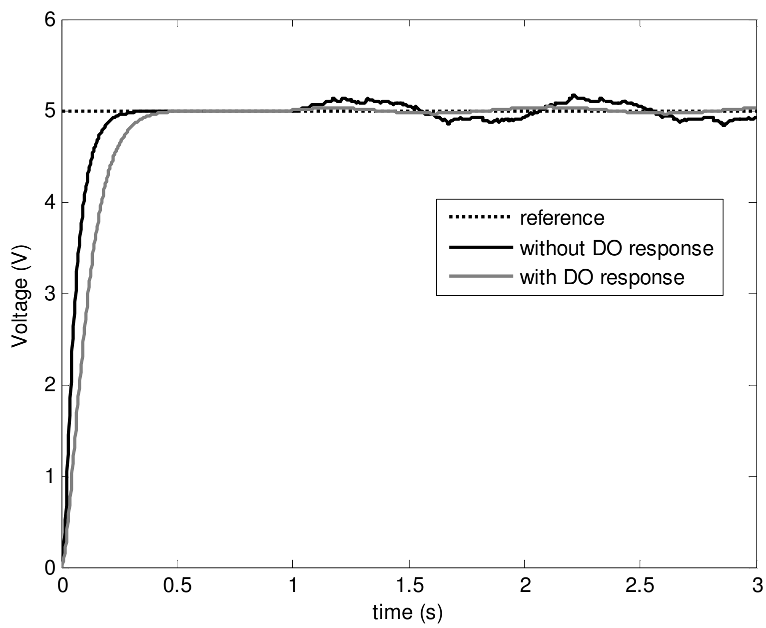

Fig. 4.9 Voltage response curve (f_d= sin(2*π*t))

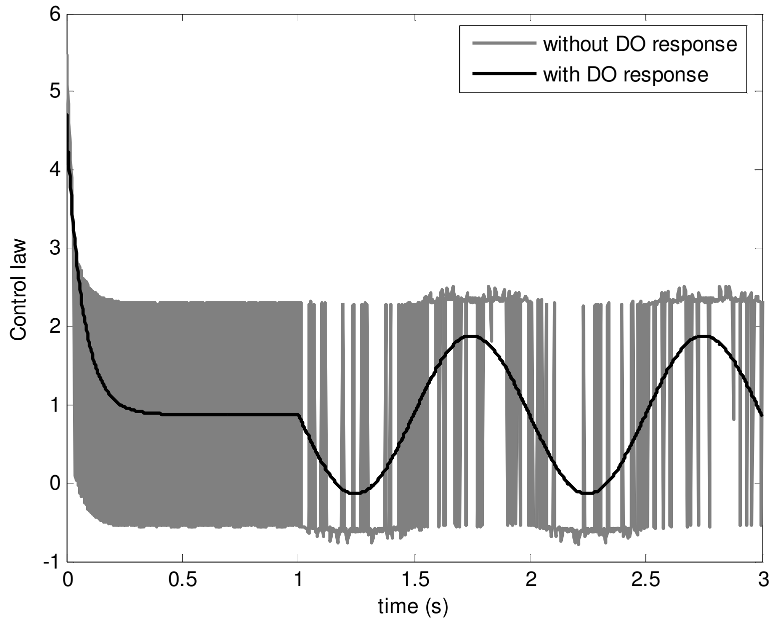

Fig. 4.10 Control law (f_d= sin(2*π*t))

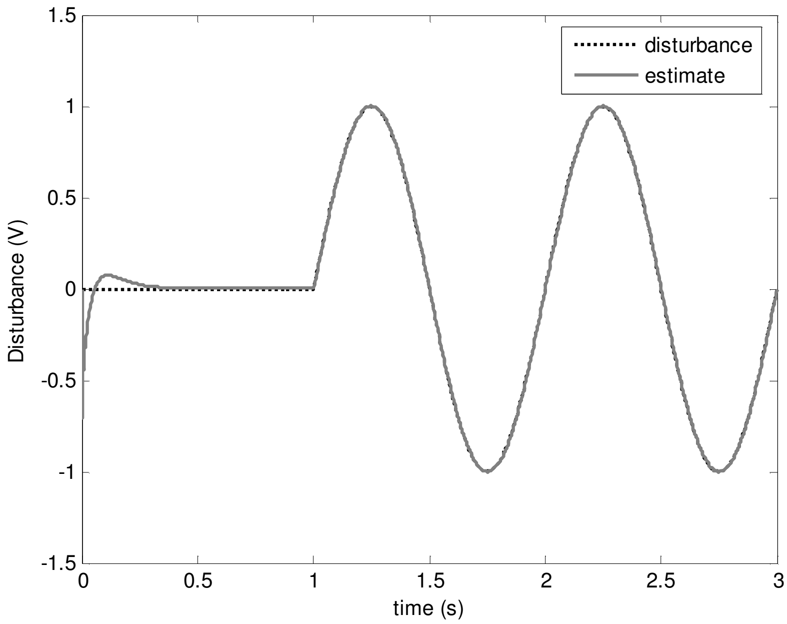

Fig. 4.11 Estimated disturbance curve with the disturbance observer

(f_d= sin(2*π*t))

As shown in figure 4.6, without the disturbance observer, there is a static error between the response and the reference voltage when the constant value disturbance is added into the system. When the disturbance observer is added into the system, there is almost no static error. Besides, figure 4.7 also shows that there is a small magnitude high oscillation in the control law curve without the disturbance observer, the reason is that the dynamic switching is too fast for the high gain ε; while the control law curve is smooth with the disturbance observer. The result of figure 4.8 shows that the estimated disturbance matches the reference disturbance after a short duration. The findings of these figures show that the system performances have improved considerably when the disturbance observer is used. The same conclusions can be drawn from the results of figure 4.9, figure 4.10 and figure 4.11 when the disturbance is a sinusoidal variation value, and the results verify the robustness of the proposed controller even when the disturbance is a continuous variable. These results are identical to the control algorithms of the above section.

4.6 Experimental results

Experiments are also carried out to verify the control algorithms. The control algorithms are constructed under the Matlab/Simulink environment. The real-time implementation of the magnetic levitation system is executed with the Real-time Workshop (RTW) of Matlab. A data capture and processing card is plugged into a Peripheral Component Interconnect (PCI) bus of the host AMD Athlon XP 1223MHz Computer. The card has 16 digital I/O channels and 12 bit A/D converter card. The specifications of the experimental setup are listed in Table 4.2 below:

Size (Length×Width×Height)	350mm × 178mm × 376mm
Winding Turns	2450
Winding Inductance	135mH
Winding Dimension (Diameter×Height)	20 mm×94mm
LED Light Source	+12V， 1W
Sampling Frequency (AD)	30kHz
Power Input	AC220V 50HZ 3A
Data Acquisition Card	16 double-ended analogue input channels, 2 single-ended analogue output channels
	16 digital input/output channels
	12-bit A/D converter, sampling rate up to 100kS/s

Table 4.2 Specifications of experimental setup for the SISO magnetic levitation system

After the magnetic levitation system is switched on and the control software Matlab/Simulink is running, the controlled steel ball is put into the electromagnetic field in about 2 second. When the steel ball is levitated stably, another steel ball of 0.05kg, used as the disturbance, is added to the electromagnetic field in around 17 second.

The disturbance used in the control experiments is to estimate the robustness of the proposed controller. The choice of magnitude of disturbance shall consider the real condition. In real industrial application, the values of disturbance should be in a reasonable range, the disturbance could not too big compare with the controlled system itself, and otherwise it will be meaningless for the system control. For the SISO magnetic levitation system, the mass of the disturbance ball is about 40% of the controlled levitation ball in the control experiments; this magnitude choice is appropriate to valid the effectiveness of the proposed controller.

The experimental results are shown in figure 4.12-4.15.

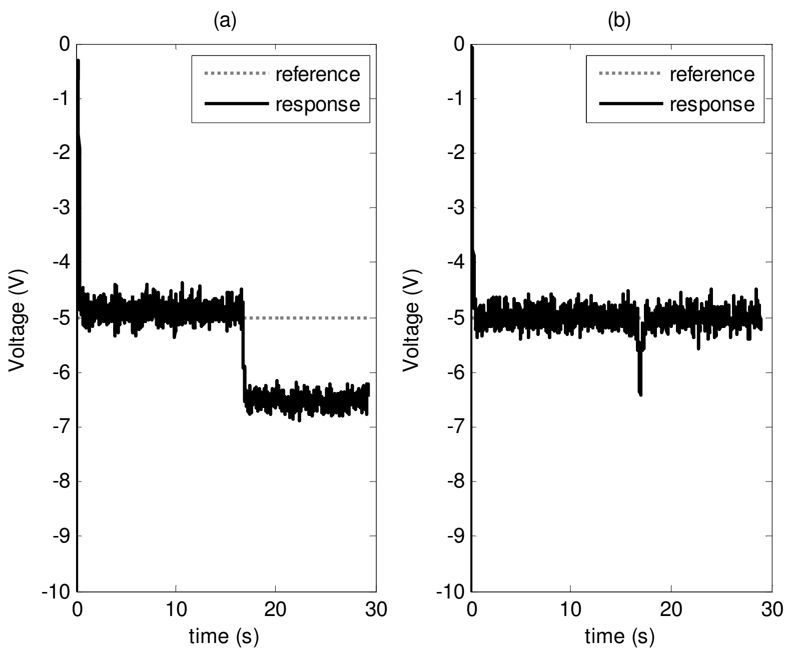

Fig. 4.12 Voltage response curve (r=-5V)

(a) SMC without DO (b) SMC with DO

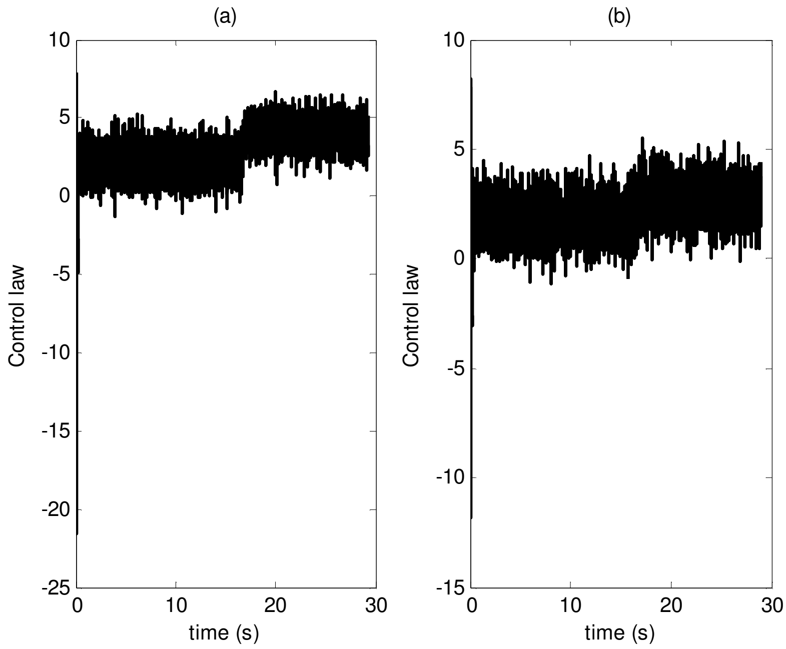

Fig. 4.13 Control law (r=-5V)

(a) SMC without DO (b) SMC with DO

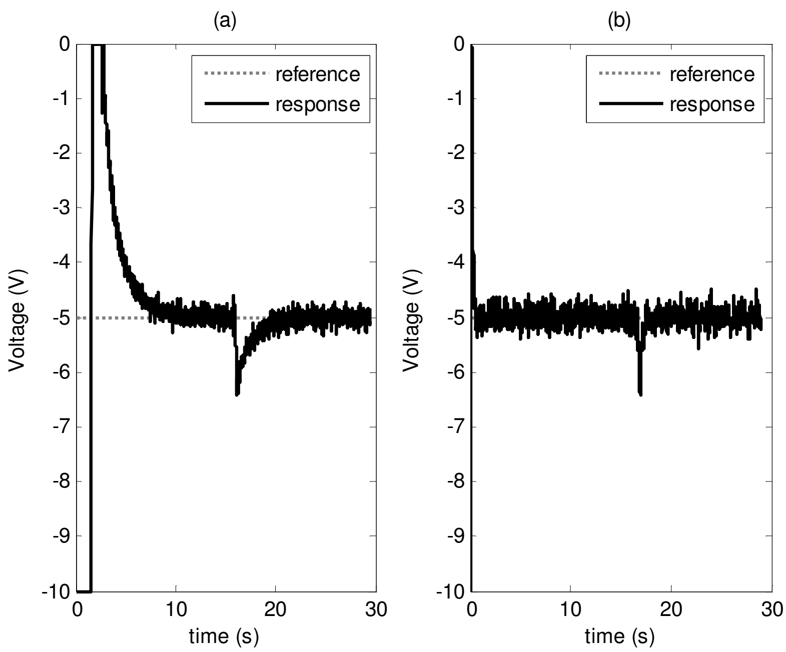

Fig. 4.14 Voltage response curve (r=-5V)

(a) PID (b) SMC with DO

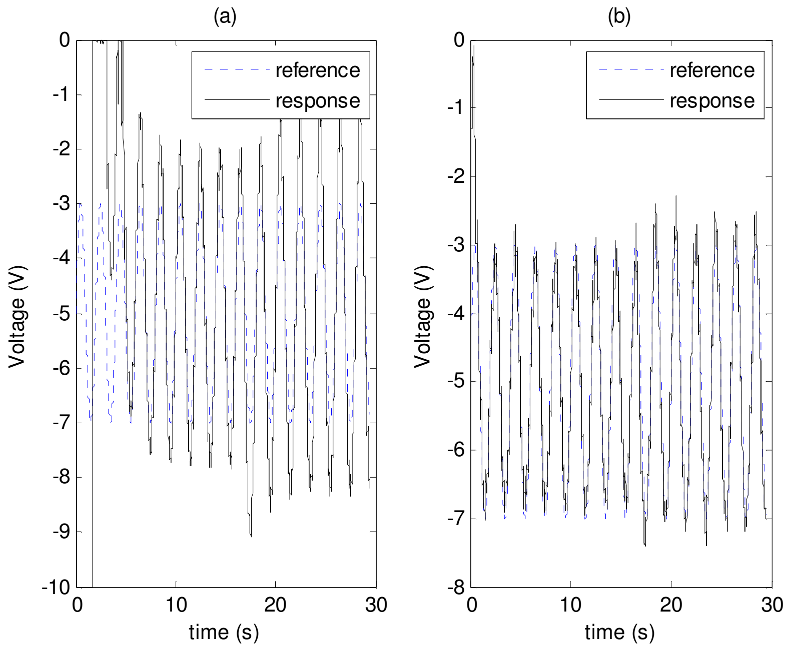

Fig. 4.15 Voltage response curve (r={-5+2*sin(π*t)}V)

(a) PID (b) SMC with DO

Figure 4.12(a) and figure 4.13(a) represent experimental results of the SMC without disturbance observer under the condition that u_{in}=-5V, c=60, ε=100, η=18, $\varDelta$=0.01. Figure 4.12(b) and figure 4.13(b) represent experimental results of the SMC with disturbance observer when the corresponding parameters are: u_{in}=-5V, c=8, ε=0.05, η=5, K_o =0.04, $\varDelta$=0.01. The fixed sample time for both cases are T=0.003s.

Furthermore, the magnetic levitation system performance of SMC with disturbance observer and that of the traditional Proportional-Integral-Differential (PID) control are compared when the input voltage is both a constant value and a sinusoidal variation value.

Figure 4.14(a) shows experimental result of the traditional PID control with u_{in}=-5. The proportional gain, integral gain and derivative gain are K_p=1.4, K_i=0.0018,

K_d=12. The PID gains are selected by trial and error in order to get the satisfying system performance. It is hard to calculate the PID gains for a nonlinear magnetic levitation system. Figure 4.14(b) represents experimental result of the SMC with disturbance observer when the corresponding parameters are: u_{in}=-5V, c=8, ε=0.05, η=5, K_o =0.04, Δ=0.01. Figure 4.15(a) shows experimental result of the traditional PID control when the input voltage is a sinusoidal variation value u_{in}=-5+2*sin(π*t), and the PID gains are the same as those in figure 4.14(a) (when u_{in}=-5). Figure 4.15(b) shows experimental result of the SMC with disturbance observer when the input voltage is also sinusoidal variation value u_{in}=-5+2*sin(π*t), and system parameters are the same as those in figure 4.14(b) (when u_{in}=-5).

As shown in figure 4.12(a), before applying the disturbance observer, the system can reach a different steady state rapidly when the disturbance steel ball is added to the system, the output voltage deviates from the command. After employing the disturbance observer, the response voltage can track the command quickly when there is disturbance in the system. There is no steady error regardless of disturbance when the disturbance observer is used. Figure 4.13 shows that the control laws switch very fast on the two control conditions, the possible reason being that the LED light is sensitive to the environment, this uncertainty will result in the continuous change of output voltage, and the magnetic levitation system is a high nonlinear system, the control law is correlative to the output voltage.

To draw a comparison between figure 4.14(a) and figure 4.14(b) when the command voltage is a constant r=-5V, it is can be seen that the system can be stable without steady error either the proposed sliding mode controller with disturbance observer or the PID controller, and the system dynamic characteristic of the sliding mode controller with disturbance observer is marginally better than that of the PID controller. When the command value is modified to a sinusoidal variation range r=-5+2*sin(π*t), the comparison results are impressed from figure 4.15(a) and figure 4.15(b). When using the PID controller, although the response voltage tries to follow the command, there is obvious delay in the trace, and the system performance is deteriorated when the disturbance ball is put into the system. In contrast, when applying the sliding mode controller with disturbance observer, the response voltage curve can track the command very well, and the system performance keeps well regardless of disturbance. It can be concluded that the system performance of the SMC with disturbance observer is much better than that of the PID controller, and the SMC with disturbance observer is highly robust against the disturbance.

The experimental results show that the magnetic levitation system can be stable with either the sliding mode controller without disturbance observer or with disturbance observer, and the steady error because of the disturbance in the controller without disturbance observer is eliminated in the controller with disturbance observer, which validate the effectiveness of the proposed SMC with disturbance observer. In addition, experimental results reveal that performance of the SMC with disturbance observer is superior to that of the traditional PID controller.

4.7 Summary

In this chapter, an SISO magnetic levitation system based on SMC is investigated. The model of the magnetic levitation system is constructed, and a sliding mode controller is proposed for this system. The stability and system characteristics of the controller are both analyzed. Although the system in this sliding mode controller is stable regardless of disturbance, static error exists when there is disturbance. The static error can be reduced by high system gains, but the dynamic characteristic becomes worse.

After that, an effective disturbance observer for SMC is designed to withdraw the effects of disturbances. When the unknown disturbance is added to the system, a simple but effective observer is employed to estimate the disturbance. Consequently, the system state trajectory performances are significantly improved, and the system is robust against external disturbances. Both the simulation results and experimental results agree with the control algorithms and prove the feasibility of the proposed controllers. Furthermore, the SMC with disturbance observer is compared with the traditional PID controller, and the experimental results show that the SMC with disturbance observer has a much better performance in a nonlinear magnetic levitation system, especially when there is large the command signal variation.

Chapter 5

Decoupled control for MIMO magnetic levitation system with SRA

In chapter 4, the controller design for an SISO magnetic levitation system has been explored and verified. In this chapter, the controller for the proposed MIMO magnetic levitation system with switched reluctance actuator will be discussed and proposed. However, owing to the multiple degrees of freedom, the model of MIMO magnetic levitation system is more complicated than that of SISO magnetic levitation system. The severe coupling behaviors between the three coils result in the difficulty to extend the analysis of the SISO magnetic levitation system to the MIMO magnetic levitation system. Therefore, the controller design for the MIMO magnetic levitation system is much more complicated. If the MIMO magnetic levitation system can be decoupled to several SISO subsystems, the SMC mentioned in above chapter will be used for these SISO magnetic levitation systems, and the levitation position control of the MIMO system can be implemented.

5.1 Review of controller design for MIMO magnetic levitation system

Magnetic levitation systems are well known for the nonlinear dynamic characteristics and open loop instability. In addition, the MIMO magnetic levitation system using switched reluctance actuators has the addition difficulty of coupling elements due to the interaction effect of different electromagnetic forces. Therefore, the position control for this MIMO magnetic levitation system presents a challenging problem. Multivariable controller for MIMO magnetic levitation systems is possible, but the stability of the system could be easily affected by parameter uncertainties and disturbances due to the complexity of the controller.

From the viewpoint of decoupling control, a more simple control method is to employ torsion springs to introduce flexibility in levitation platform [39], therefore the mechanical structure of the MIMO system is separated into several single output systems, and levitation of each magnet can be controlled independently. This method is feasible, but it defeats the purpose of completely contactless between moving surfaces. An alternative controller design scheme is on the basis of the tight association between a magnet and its nearest transducer, each magnet is individually controlled by using the nearest transducer as feedback signals [40]. This method dose not consider the cross coupling, and it is hard to have good tracking performance. Additionally, it can not guarantee robust stability against disturbances. The MIMO magnetic levitation system has at least 3 degrees-of-freedom (DOF), vertical motion, roll rotation and pitch rotation. The concept of independent control of each DOF for the MIMO magnetic levitation system is mentioned in [41]. However, the detailed decoupling transformation is not addressed. In [42], multiphase permanent magnets are used to the generate suspension forces, and a *dq* frame is employed to decouple the forces, then three DOF of levitation are controlled individually.

On the control side, the conventional Proportional- Integral -Derivative (PID) controller [43]-[45] and its transformation, the Proportional-Integral (PI) controller [46] or the Proportional- Derivative (PD) controller [47]-[48] are used in magnetic levitation systems due to its simplicity and usefulness. The lead-lag compensator [42], [49] is also an alternative for magnetic levitation systems, and the electrical voltage or current is typically used as the control signal. Sliding Mode Control (SMC) is applied widely in electro-mechanical systems, and it is efficient to control complicated high-order dynamic plants operating under uncertainty conditions [33]. This merit makes SMC be one of the effective candidates for the magnetic levitation system, and SMC is performed better than PID control in the nonlinear magnetic levitation systems [50].

5.2 Decouple of the MIMO magnetic levitation system

According to the two-time scale method mentioned in chapter 3, the electrical model is fast subsystem and current control is applied by the circuit driving system. A look-up table is used to depict the relationship between electromagnetic force, current and air-gap, which is analytically calculated in chapter 2. Therefore, the mechanical motion model of the proposed MIMO magnetic levitation system should be considered.

The mechanical motion model is conducted in chapter 3, as shown in equation (3.16)-(3.19). Equation (3.16) is the mechanical motion equation of the MIMO magnetic levitation system. Equation (3.17) is the expression of the resultant levitation force and rotation torques of the MIMO magnetic levitation system. All these force and torques are linear function of the three levitation forces produced by the three levitation coils. Equation (3.19) is the expression of the levitation displacement and Euler angles of the MIMO magnetic levitation system. All these displacement and angles are linear function of the three levitation positions of the three levitation points.

$$\begin{cases} F_z = M\ddot{z} \\ T_x = I_{xx}\ddot{\phi} \\ T_y = I_{yy}\ddot{\theta} \end{cases} \tag{3.16}$$

$$\begin{cases} F_z = f_1 + f_2 + f_3 - Mg \\ T_x = (f_2 - f_3) l_x \\ T_y = (f_2 + f_3) l_{y2} - f_1 l_{y1} \end{cases} \tag{3.17}$$

$$\begin{cases} l_x = \dfrac{a}{4} \\ l_{y1} = \dfrac{\sqrt{3}a}{6} \\ l_{y2} = \dfrac{\sqrt{3}a}{12} \end{cases} \tag{3.18}$$

$$\begin{cases} z = (z_1 + z_2 + z_3)/3 \\ \phi = (z_1 - z_3)/a \\ \theta = (2z_2 - z_1 - z_3)/(\sqrt{3}a) \end{cases} \tag{3.19}$$

Substitute equations (3.17) - (3.19) into (3.16) give

$$\begin{cases} \ddot{z}_1 + \ddot{z}_2 + \ddot{z}_3 = \dfrac{3}{M}\left(f_1 + f_2 + f_3\right) - 3g \\ \ddot{z}_1 - \ddot{z}_3 = \dfrac{a^2}{4I_{xx}}\left(f_2 - f_3\right) \\ 2\ddot{z}_2 - \ddot{z}_1 - \ddot{z}_3 = \dfrac{a^2}{4I_{yy}}\left(f_2 + f_3 - 2f_1\right) \end{cases} \tag{5.1}$$

Equation (5.1) reveals the coupling behavior of the MIMO magnetic levitation system, i.e. each levitation force is not only relative to position of the corresponding coil, but is function of the three positions. Therefore, a reliable and feasible control method needs to decouple this system.

The three positions can be measured by position sensors, and they give the feedback signals of the MIMO system. From equation (5.1), it can be seen that the three positions and the three levitation forces are linear function. Hence, each position can be expressed as the function of the three levitation forces by using mathematics transformation. If intermediate variables are adopted to replace the linear function of the three levitation force in each position equation, the overall coupling MIMO system will be changed to three SISO systems. Each SISO system can be controlled individually. The three levitation forces can be expressed as functions of the three intermediate variables by using inverse matrix transform.

Equations (5.2) can be conducted from equation (5.1) as

$$\begin{cases} \ddot{z}_1 = \left(\dfrac{1}{M} + \dfrac{a^2}{12I_{yy}}\right) f_1 + \left(\dfrac{1}{M} + \dfrac{a^2}{8I_{xx}} - \dfrac{a^2}{24I_{yy}}\right) f_2 + \left(\dfrac{1}{M} - \dfrac{a^2}{8I_{xx}} - \dfrac{a^2}{24I_{yy}}\right) f_3 - g \\ \ddot{z}_2 = \left(\dfrac{1}{M} - \dfrac{a^2}{6I_{yy}}\right) f_1 + \left(\dfrac{1}{M} + \dfrac{a^2}{12I_{yy}}\right) f_2 + \left(\dfrac{1}{M} + \dfrac{a^2}{12I_{yy}}\right) f_3 - g \\ \ddot{z}_3 = \left(\dfrac{1}{M} + \dfrac{a^2}{12I_{yy}}\right) f_1 + \left(\dfrac{1}{M} - \dfrac{a^2}{8I_{xx}} - \dfrac{a^2}{24I_{yy}}\right) f_2 + \left(\dfrac{1}{M} + \dfrac{a^2}{8I_{xx}} - \dfrac{a^2}{24I_{yy}}\right) f_3 - g \end{cases} \tag{5.2}$$

Where the system parameters can be written as constant matrix

$$A = \begin{bmatrix} a_{11} & a_{12} & a_{13} \\ a_{21} & a_{22} & a_{23} \\ a_{31} & a_{32} & a_{33} \end{bmatrix} = \begin{bmatrix} \dfrac{1}{M} + \dfrac{a^2}{12I_{yy}} & \dfrac{1}{M} + \dfrac{a^2}{8I_{xx}} - \dfrac{a^2}{24I_{yy}} & \dfrac{1}{M} - \dfrac{a^2}{8I_{xx}} - \dfrac{a^2}{24I_{yy}} \\ \dfrac{1}{M} - \dfrac{a^2}{6I_{yy}} & \dfrac{1}{M} + \dfrac{a^2}{12I_{yy}} & \dfrac{1}{M} + \dfrac{a^2}{12I_{yy}} \\ \dfrac{1}{M} + \dfrac{a^2}{12I_{yy}} & \dfrac{1}{M} - \dfrac{a^2}{8I_{xx}} - \dfrac{a^2}{24I_{yy}} & \dfrac{1}{M} + \dfrac{a^2}{8I_{xx}} - \dfrac{a^2}{24I_{yy}} \end{bmatrix} \tag{5.3}$$

Adopting intermediate variables h_j so as to decouple the MIMO system as follows

$$\begin{cases} \ddot{z}_1 = h_1 - g \\ \ddot{z}_2 = h_2 - g \\ \ddot{z}_3 = h_3 - g \end{cases} \tag{5.4}$$

Where intermediate variables h_1, h_2 and h_3 are

$$\begin{cases} h_1 = a_{11} f_1 + a_{12} f_2 + a_{13} f_3 \\ h_2 = a_{21} f_1 + a_{22} f_2 + a_{23} f_3 \\ h_3 = a_{31} f_1 + a_{32} f_2 + a_{33} f_3 \end{cases} \tag{5.5}$$

Accordingly, the electromagnetic forces f_j are linear function of h_j

$$\begin{bmatrix} f_1 \\ f_2 \\ f_3 \end{bmatrix} = A^{-1} \begin{bmatrix} h_1 \\ h_2 \\ h_3 \end{bmatrix} = \begin{bmatrix} a_{11} & a_{12} & a_{13} \\ a_{21} & a_{22} & a_{23} \\ a_{31} & a_{32} & a_{33} \end{bmatrix}^{-1} \begin{bmatrix} h_1 \\ h_2 \\ h_3 \end{bmatrix} = \begin{bmatrix} b_{11} & b_{12} & b_{13} \\ b_{21} & b_{22} & b_{23} \\ b_{31} & b_{32} & b_{33} \end{bmatrix} \begin{bmatrix} h_1 \\ h_2 \\ h_3 \end{bmatrix} = B \begin{bmatrix} h_1 \\ h_2 \\ h_3 \end{bmatrix} \tag{5.6}$$

Where the constant matrix B is

$$B=\begin{bmatrix} b_{11} & b_{12} & b_{13} \\ b_{21} & b_{22} & b_{23} \\ b_{31} & b_{32} & b_{33} \end{bmatrix}=\begin{bmatrix} \frac{M}{9}+\frac{4I_{yy}}{3a^2} & \frac{M}{9}-\frac{8I_{yy}}{3a^2} & \frac{M}{9}+\frac{4I_{yy}}{3a^2} \\ \frac{M}{9}-\frac{2I_{yy}}{3a^2}+\frac{2I_{xx}}{a^2} & \frac{M}{9}+\frac{4I_{yy}}{3a^2} & \frac{M}{9}-\frac{2I_{yy}}{3a^2}-\frac{2I_{xx}}{a^2} \\ \frac{M}{9}-\frac{2I_{yy}}{3a^2}-\frac{2I_{xx}}{a^2} & \frac{M}{9}+\frac{4I_{yy}}{3a^2} & \frac{M}{9}-\frac{2I_{yy}}{3a^2}+\frac{2I_{xx}}{a^2} \end{bmatrix} \tag{5.7}$$

The module of matrix A is $|A|=\frac{3a^4}{16MI_{xx}I_{yy}}\neq 0$, this means that the matrix B always exits and it is nonsingular.

It can be seen from equation (5.4) and (5.6) that the MIMO levitation system is decoupled to three independent mathematical equations, and each equation can be used as an SISO system modeling. This decoupling leads to the simplification of controller design.

Figure 5.1 shows the simplified control algorithm block diagram. Three input distances r_j are given and the three corresponding output positions z_j are measured by sensors. The three system inputs h_j are obtained from each position controller and the system model is described by equation (5.4). The three levitation forces f_j can be gotten from the three system inputs h_j by using equation (5.6)-(5.7). Using a look-up table method, the reference currents for each coil are decided. Current controllers will guarantee the required currents of the three coils.

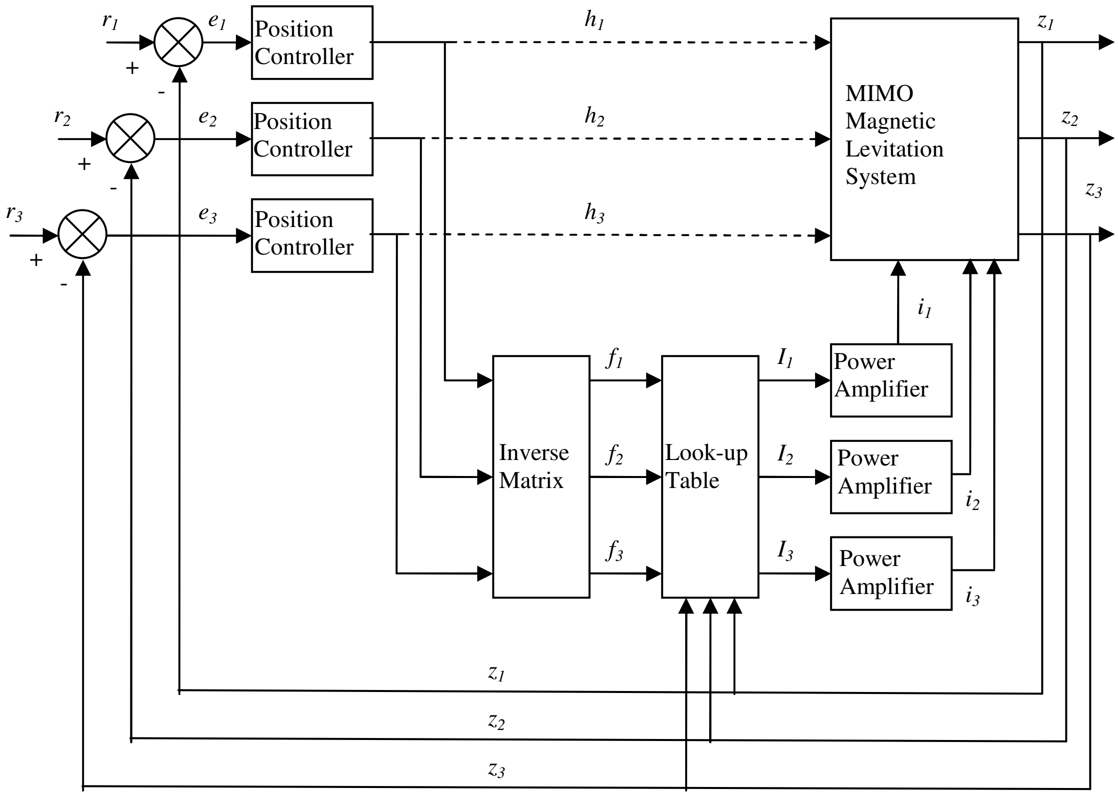

Fig. 5.1 The control block diagram for the MIMO magnetic levitation system

5.3 Sliding mode control for decoupled model

The decoupled mechanical motion model shown in the previous section can be rewritten as follows:

$$\ddot{z}_j = h_j - g \tag{5.8}$$

Where j=1, 2, 3 refers to the three levitation coils of the SRA. Then, the SMC method applied in chapter 4 can be employed for the decoupled model.

Using reference position r_j and output position z_j, the position error $e_j = r_j - z_j$ is adopted as the state variation, suppose $x_{1j}=e_j$, the system state-space equations are as follows:

$$\begin{cases} \dfrac{dx_{1j}(t)}{dt} = x_{2j}(t) \\ \dfrac{dx_{2j}(t)}{dt} = -u_j(t) + F_j(t) \end{cases} \tag{5.9}$$

Where $u_j=h_j$, $F_j = \ddot{r}_j + g - f_{dj}$, f_{dj} denotes the corresponding external disturbance.

The sliding surface is given by

$$S_j = cx_{1j} + x_{2j} \tag{5.10}$$

Where c>0 is a constant parameter. Therefore, its differential can be rewritten as:

$$\dot{S}_j = c\dot{x}_{1j} + \dot{x}_{2j} \tag{5.11}$$

The sliding control law is designed as follows:

$$u_j = cx_{2j} + \ddot{r}_j + g + \varepsilon sat(S_j) + \eta S_j \tag{5.12}$$

Where ε and η are constant parameters, ε>0, η>0, suppose $\varepsilon > |f_{dj}|$, and $sat(S_j)$ is saturation function:

$$sat(S_j) = \begin{cases} 1, & S_j > \Delta \\ S_j / \Delta, & |S_j| \le \Delta \\ -1, & S_j < -\Delta \end{cases} \tag{5.13}$$

Where Δ denotes a small vicinity of the origin to define the boundary layer, 0< Δ <1.

Employing the positive definite Lyapunov function candidate to analyze stability

$$V_j = \frac{1}{2} S_j^{\ 2} \tag{5.14}$$

Combining equations (5.9) and (5.12):

$$\dot{x}_{2j} = -cx_{2j} - \varepsilon sat(S_j) - \eta S_j - f_{dj} \tag{5.15}$$

Substituting equations (5.9) and (5.15) to (5.11):

$$\dot{S}_j = -\varepsilon sat\left(S_j\right) - \eta S_j - f_{dj} \tag{5.16}$$

Hence,

$$\dot{V}_j = S_j \dot{S}_j = -\varepsilon sat\left(S_j\right) S_j - \eta S_j^{\ 2} - f_{dj} S_j \tag{5.17}$$

Since the system behavior is not determined within the small vicinity, the system will be stable if the phase trajectory can converge into the small vicinity. For this purpose, the saturation function can be replaced by sign function, therefore

$$\begin{aligned} \dot{V}_j &= S_j \dot{S}_j = -\varepsilon \left|S_j\right| - \eta S_j^{\ 2} - f_{dj} S_j \\ &\leq -\varepsilon \left|S_j\right| - \eta S_j^{\ 2} + \left|f_{dj}\right| \left|S_j\right| \\ &\leq -\eta S_j^{\ 2} - \left(\varepsilon - \left|f_{dj}\right|\right) \left|S_j\right| \leq 0 \end{aligned} \tag{5.18}$$

That verifies the system is stable.

5.4 Simulation results

The proposed MIMO magnetic levitation system is simulated by using Matlab Simulink. Figure 5.2 shows the simulation block diagram.

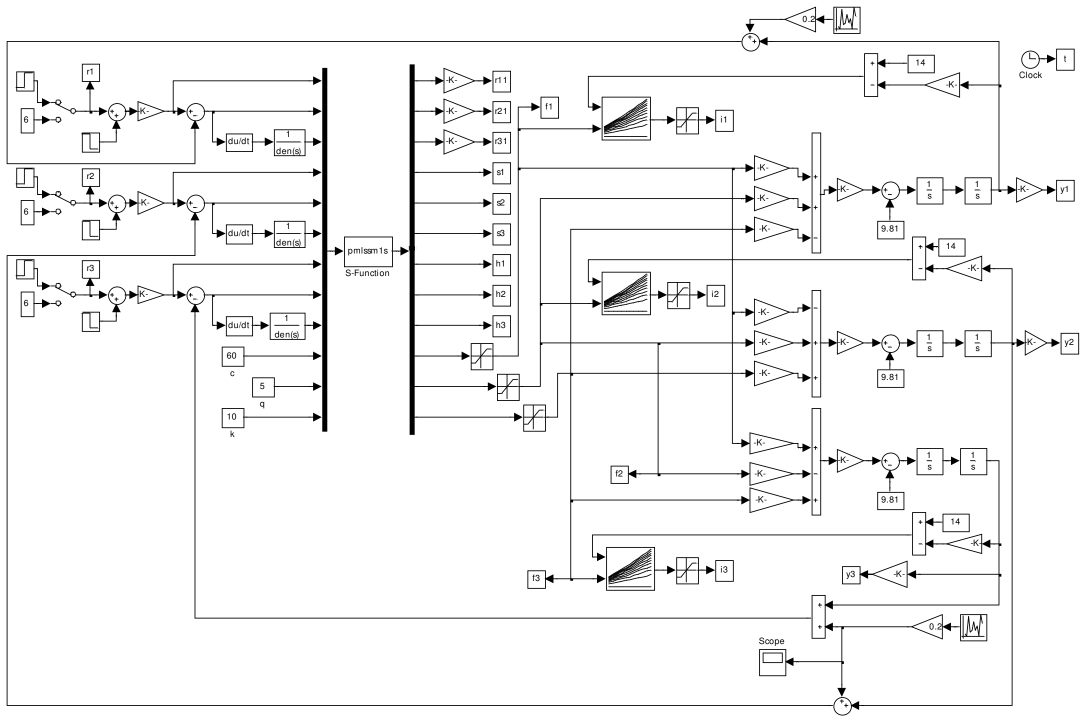

Fig. 5.2 The simulation bock diagram for the MIMO magnetic levitation system

As shown in figure 5.2, the three reference positions r_1=r_2=r_3=6mm, the parameters of the SMC are c=60, ε=5, η=10, Δ=0.01, the acceleration of gravity is g=9.81m/s^2. The fixed sample time is T=0.0005s. The moments of inertia can not calculate accurately because mass and geometrical shape of the levitation plane are irregular distribution according to X and Y axes. The approximate value of moments of inertia is supposed to be I_{xx}=I_{yy}=0.0142Kg·m^2. This approximation will lead to parameter uncertainty in the system.

It can also be seen from figure 5.2 that random disturbance noise signal is added to feedback channels to simulate the feedback signal noise; the magnitude of noise is chosen to be similar to the real conditions.

To analyze the outcomes of system uncertainty and feedback signal noise, some simulations are applied as follows.

1) Assuming no feedback signal noise existing, the comparison results between response with system uncertainty and response without system uncertainty are shown in figure 5.3, and the system uncertainty is presumed that the approximate system parameter is 1.2 times the desired one.

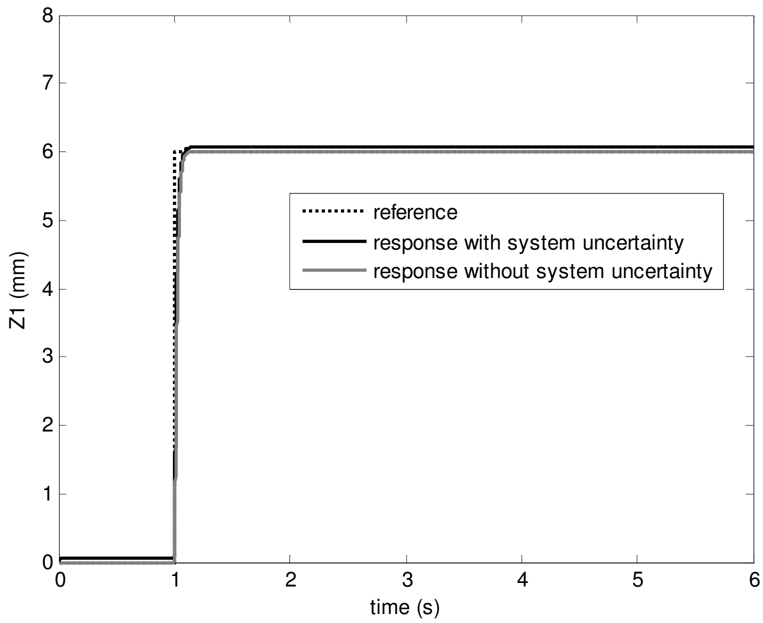

(a)

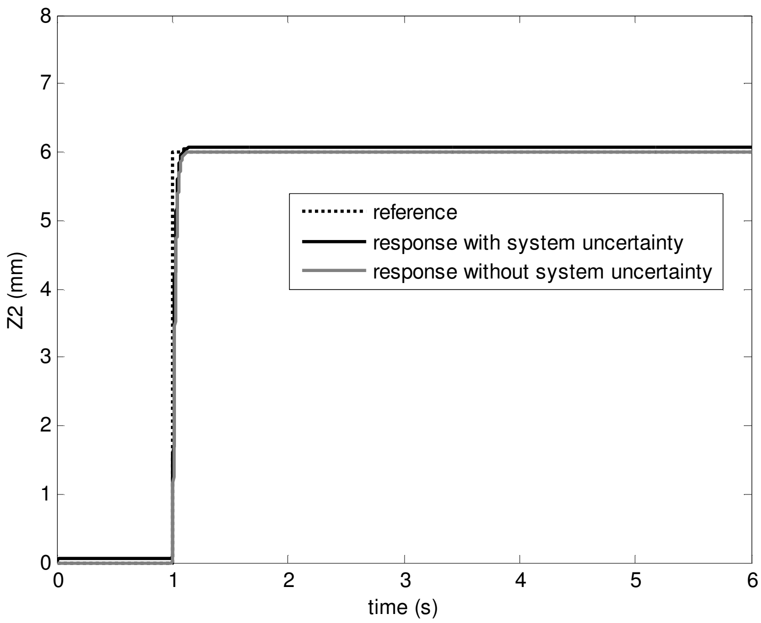

(b)

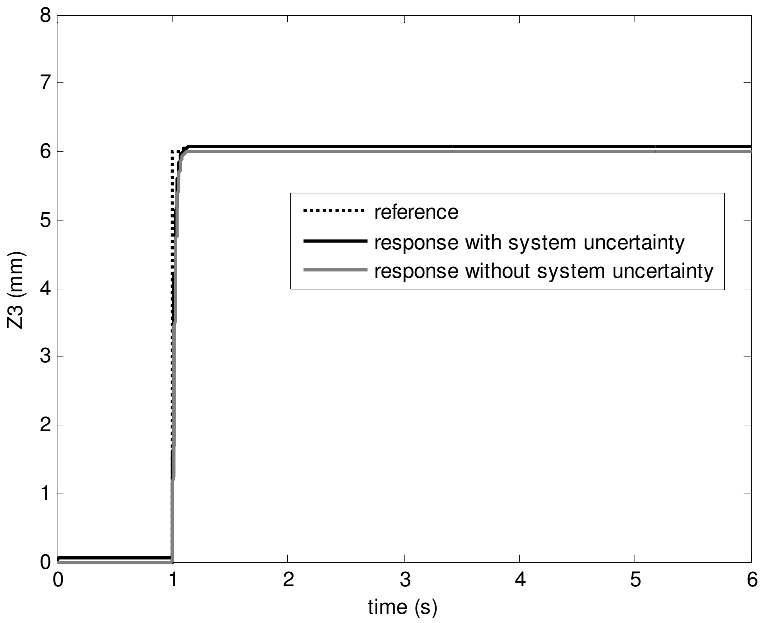

(c)

Fig. 5.3 The comparative results for system uncertainty without feedback noise

As shown in figure 5.3, although there are steady errors between reference and response with system uncertainty, the steady errors are small, and all the responses almost do not have vibration at steady state.

2) Assuming that the system has feedback signal noise, the comparison results between response with system uncertainty and response without system uncertainty are shown in figure 5.4, and the system uncertainty is also presumed that the approximate system parameter is 1.2 times the desired one.

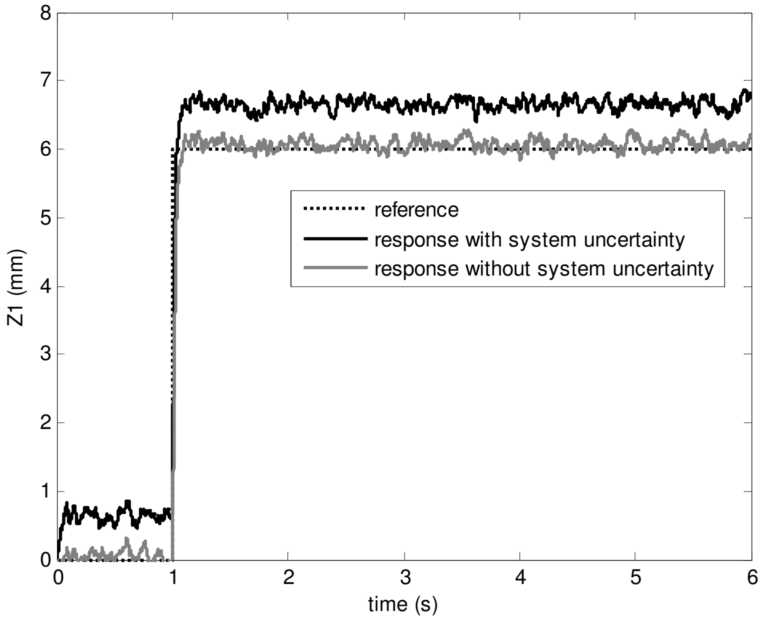

(a)

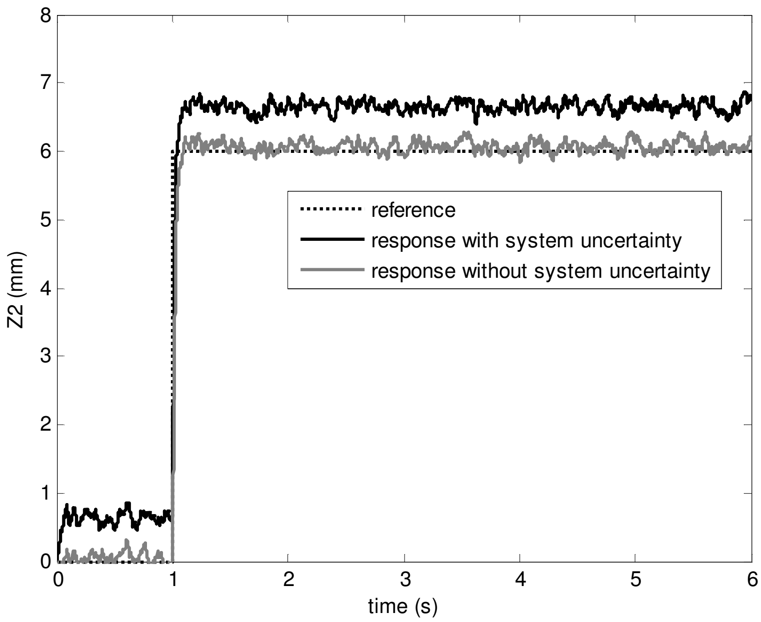

(b)

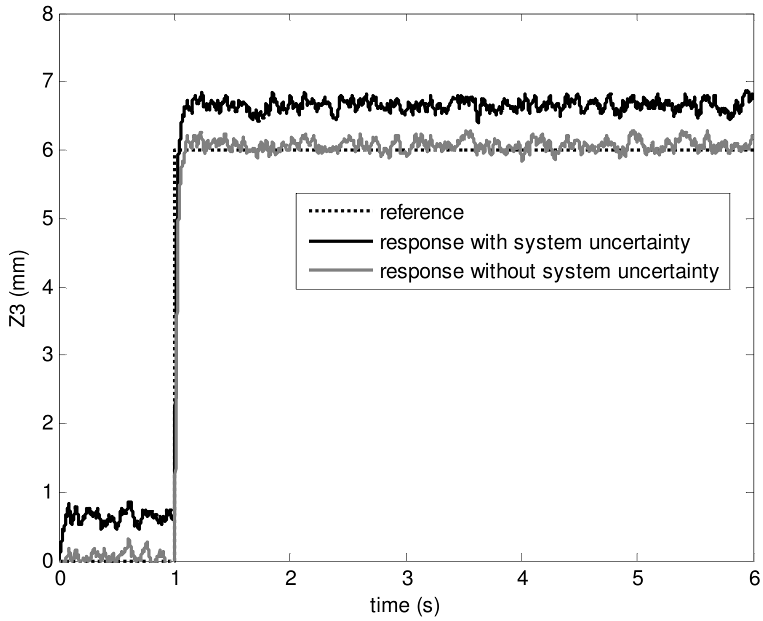

(c)

Fig. 5.4 The comparative results for system uncertainty with feedback noise

As shown in figure 5.4, there are steady errors between reference and response with system uncertainty, and the steady errors in figure 5.4 are much bigger than those in figure 5.3, that means the signal noise could amplify the steady error. On the other hand, the response has vibration at steady state, by comparing the results of figure 5.3 and figure 5.4, it can be concluded that feedback signal noise is one possible reason for vibration.

3) Low pass filter can be used to weaken the bad results of feedback signal noise. Figure 5.5 shows the comparative results between with low pass filter and without low pass filter when there are feedback signal noises within the system.

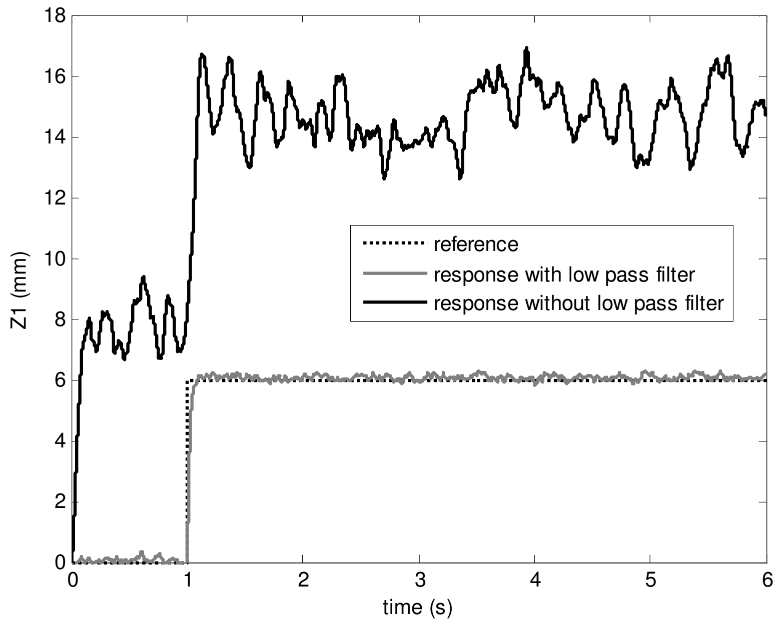
18
16
14
12
10
8
6
4
2
0
Z1 (mm)
0
1
2
3
4
5
6
time (s)
reference
response with low pass filter
response without low pass filter

(a)

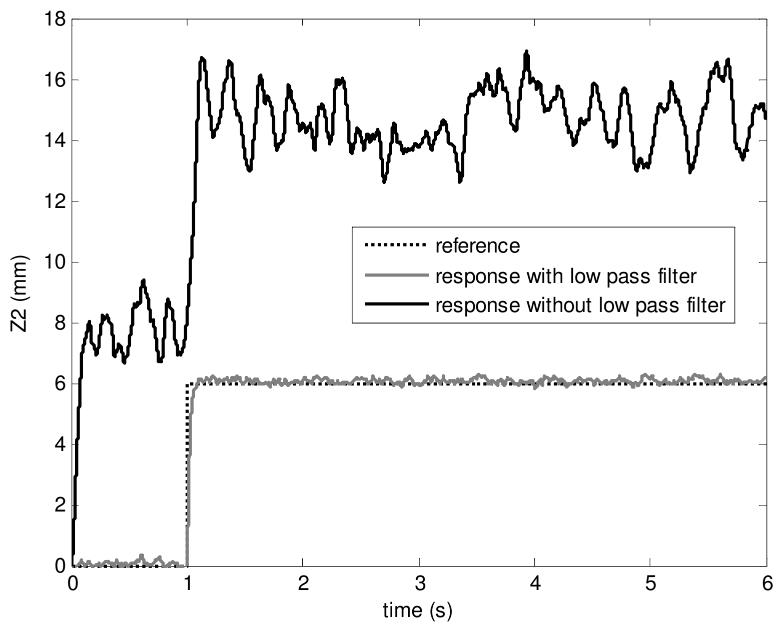
18
16
14
12
10
8
6
4
2
0
Z2 (mm)
0
1
2
3
4
5
6
time (s)
reference
response with low pass filter
response without low pass filter

(b)

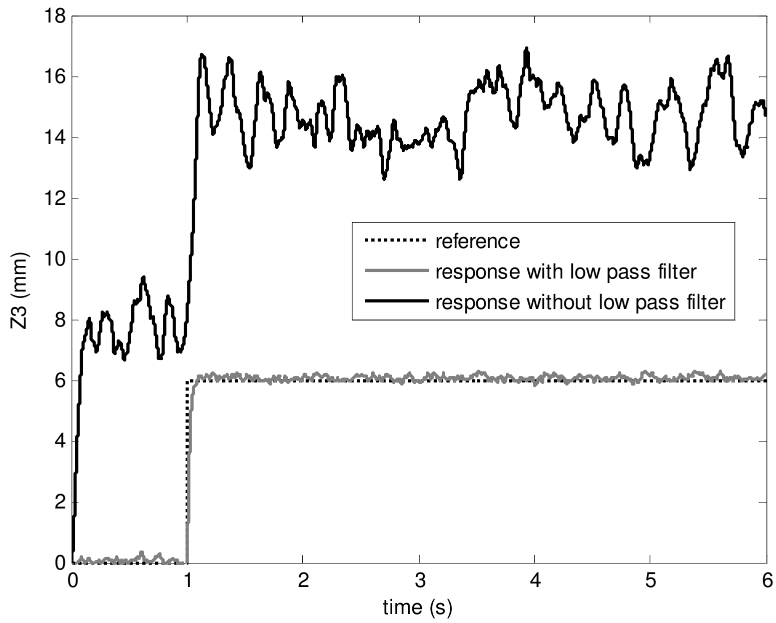

(c)

Fig. 5.5 The comparative results for low pass filter with feedback noise

It can be seen from figure 5.5 that low pass filter can great reduce the amplitude of response position vibration.

From the above analysis, the following features are adopted in the control implementation:

1) A low pass filter is used to curb the influence of the feedback noise.

2) Feed forward position compensation is used to trace the reference position to eliminate the steady state error.

Using the above features, the simulation results are represented in figures 5.6 and 5.7 when the reference positions are 6mm and 3mm separately.

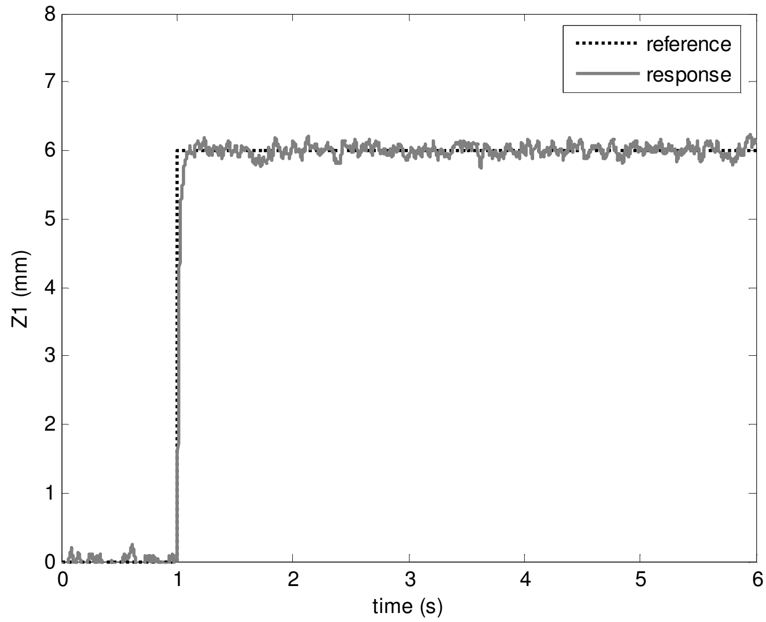
reference
response
Z1 (mm)
time (s)
0
1
2
3
4
5
6
7
8

(a)

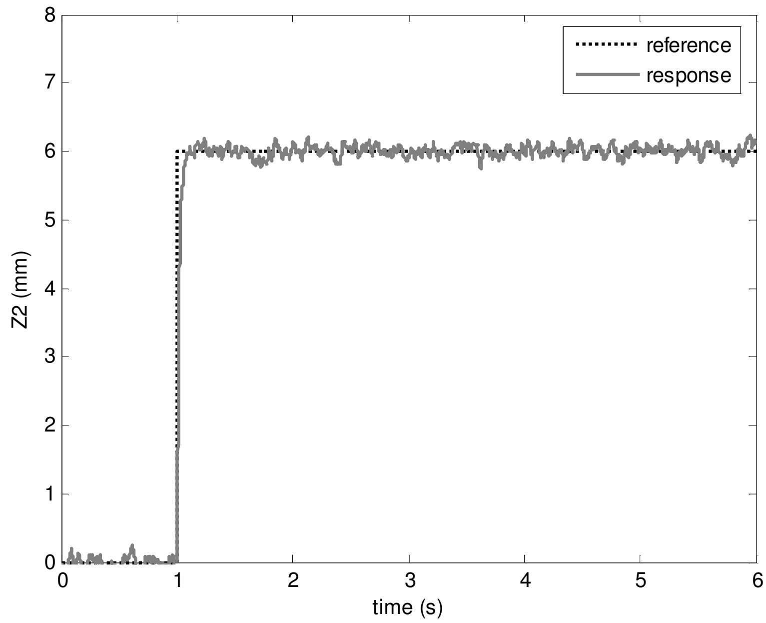
reference
response
Z2 (mm)
time (s)
0
1
2
3
4
5
6
7
8

(b)

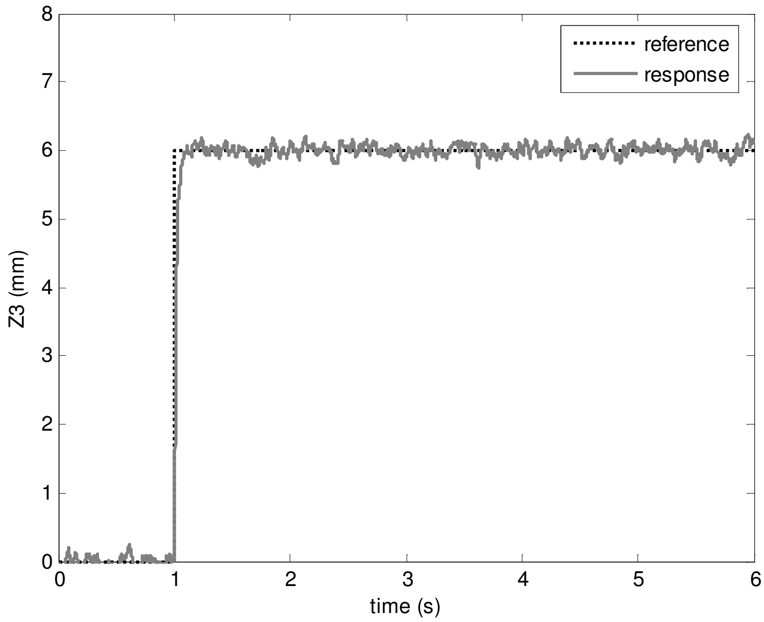

(c)

Fig. 5.6 The position response curves when references r1=r2=r3=6mm

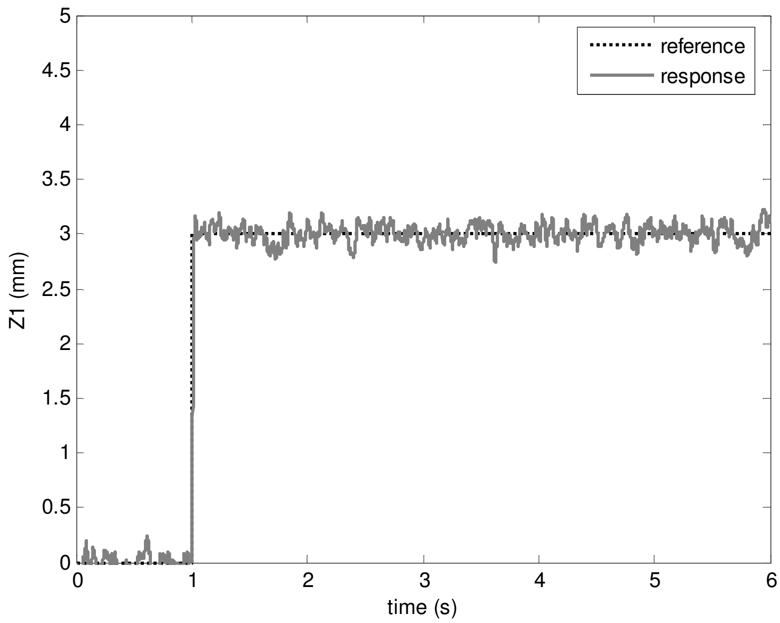

(a)

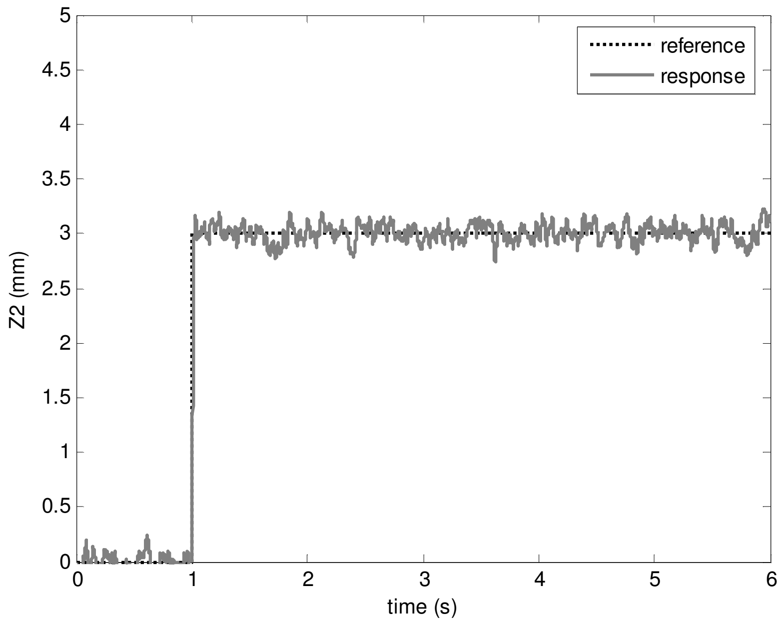

(b)

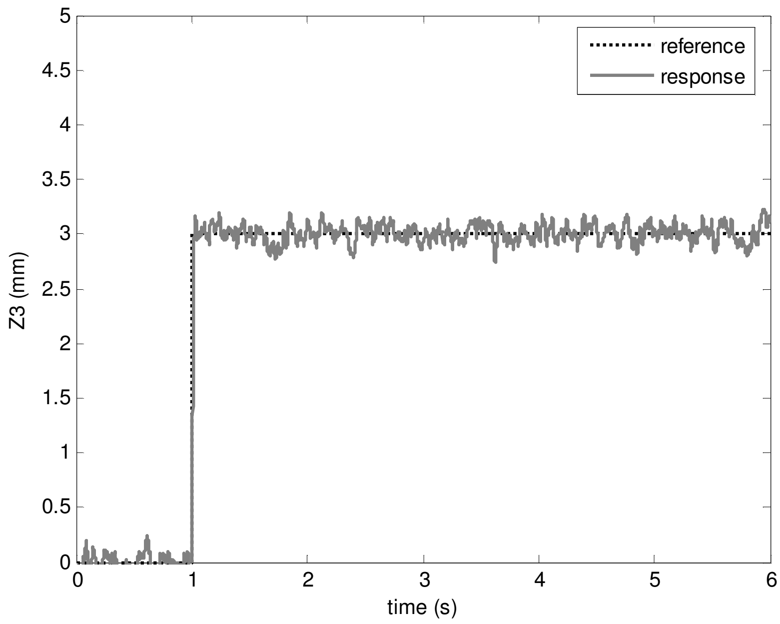

(c)

Fig. 5.7 The position response curves when references r1=r2=r3=3mm

The findings of figure 5.6 and 5.7 reveal that the responses have good dynamic characteristics, they can trace the references quickly and then the responses can follow the references. Due to feedback signal noise, the response curves have vibrations around the reference positions, and steady error from system uncertainty could be removed by using compensations. These results confirm that the levitation plane can be levitated according to the control algorithms approached in this chapter.

5.5 Experimental results

Experiments are also carried out to verify the control algorithms. Figure 5.8 shows the experimental setup of the MIMO magnetic levitation system. Configuration of the total system is shown in figure 5.9. The control algorithms are developed under the Matlab/Simulink environment. The real-time implementation of the MIMO magnetic levitation system is executed with the Real-time Workshop (RTW) of Matlab. A DS1104 dSPACE card is used as the rapid prototyping controller. Real-time Interface (RTI) provides simulink blocks for graphical I/O configuration model; this model can be operated in dSPACE by generating the model code via RTW. Once the real-time model is compiled, it will be downloaded and started automatically. The circuit drives employ three 50A series Pulse Width Modulation (PWM) servo amplifiers to drive the three magnetic levitation actuators. The block diagram of the servo amplifier is shown in figure 5.10 and the specifications of the servo amplifier are listed in Table 5.1.

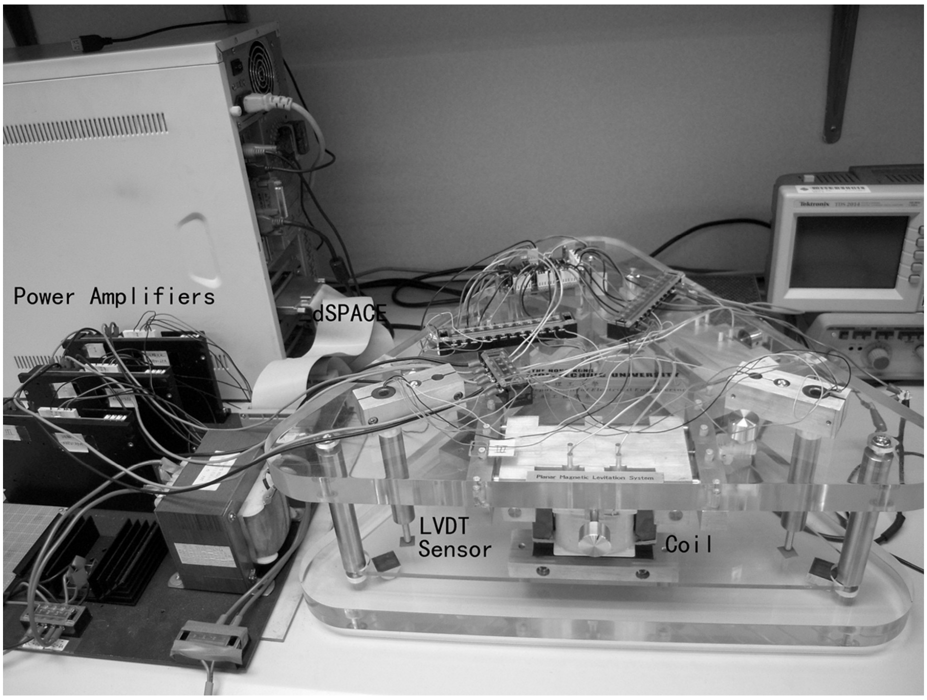

Fig. 5.8 The experimental setup of the MIMO magnetic levitation system

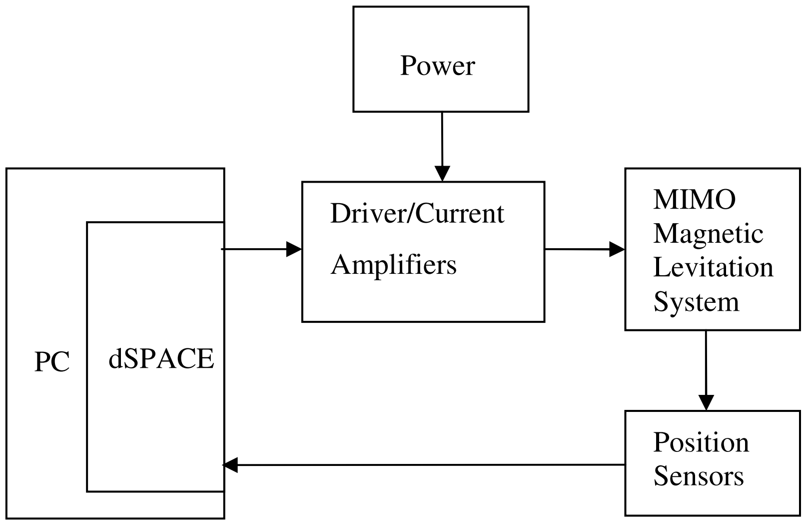

Fig. 5.9 Configuration of the MIMO magnetic levitation system

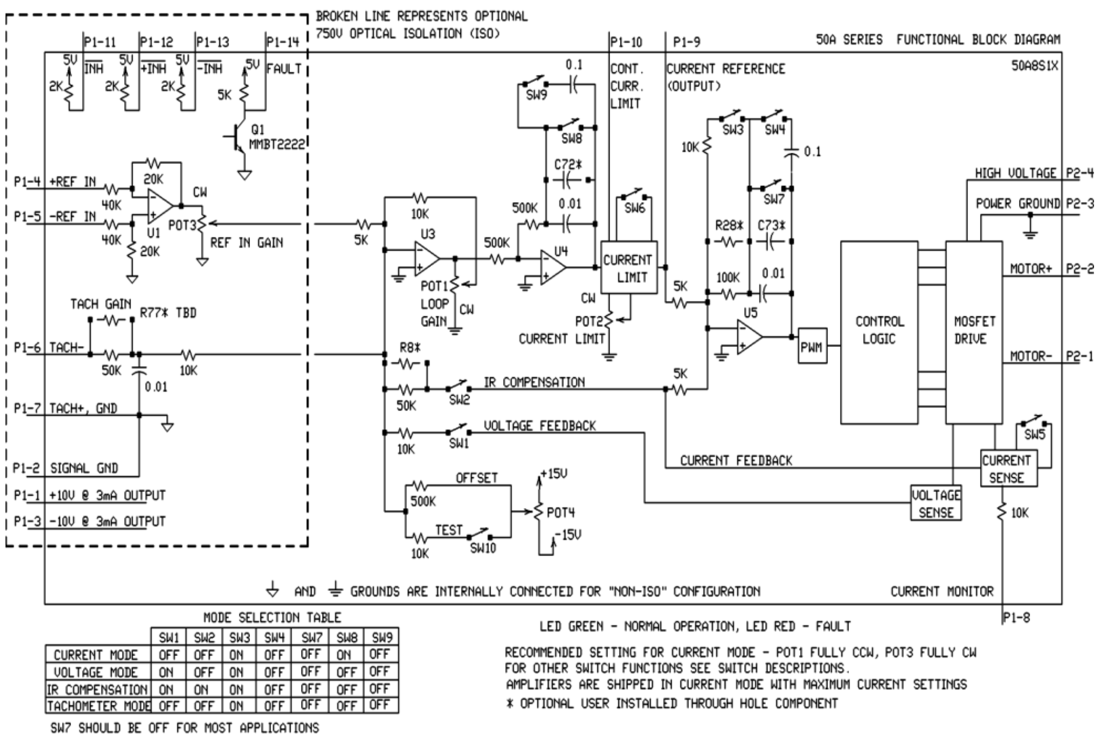

Fig. 5.10 The block diagram of a 50A series PWM servo amplifier

Size (Length×Width×Height)	186.7 x 111.7 x 25.4mm
Weight	0.68kg
DC supply voltage	20 - 80V
Peak current (2 sec. max., internally limited)	$\pm$ 50A
Maximum continuous current (internally limited)	$\pm$ 25A
Switching frequency	22 kHz ± 15%
Temperature range	$0^{o}C$ to $+65^{o}C$
Over voltage shut down (self-reset)	86V
Bandwidth (load dependent)	2.5kHz

Table 5.1 Specifications of the servo amplifier

Three LVDT are adopted to measure the levitation positions of the levitation plane. Table 5.2 shows specifications of the LVDT. The output signal commutation and amplification circuit of each LVDT is shown in figure 5.11, and the parameters of electronic components are listed in table 5.3.

Input voltage	3Vrms
Input frequency	3kHz
Nominal range	±12.5mm
Sensitivity	25mV/V/mm
Temperature range	$-55^{o}C$ to $+105^{o}C$
Vibration tolerance	20g to 2kHz
Shock survival	1kg, 11ms
Core weight	22g

Table 5.2 Specifications of the LVDT

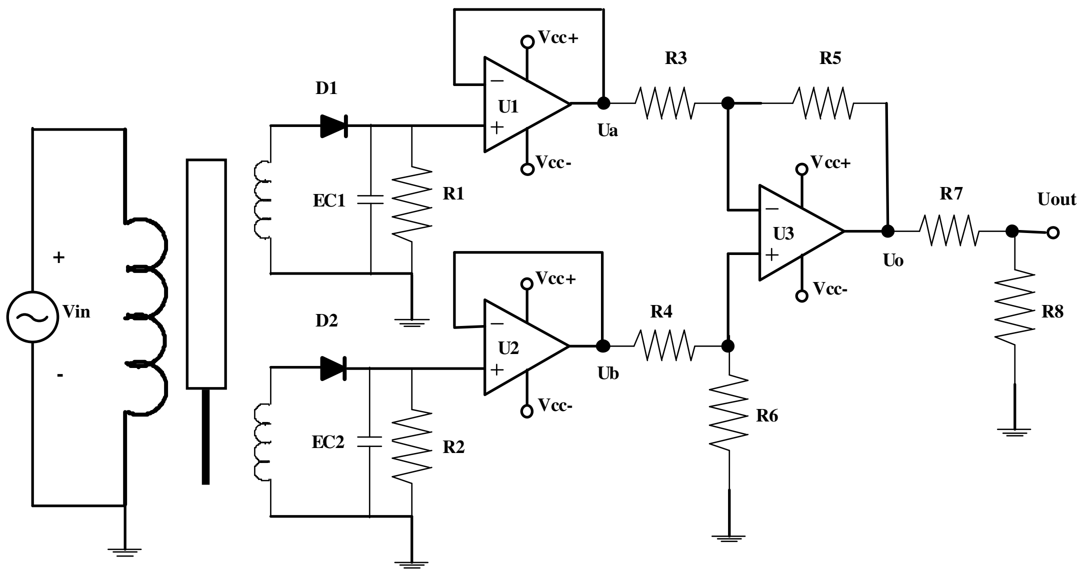

Figure 5.11 Commutation and amplification circuit of the LVDT

D1, D2	Diode
EC1, EC2	Capacitance, 10μF
U1, U2, U3	Operation Amplifier, μ741
R1, R2, R3, R4	Resistor, 10kΩ
R5, R6	Resistor, 100kΩ
R7, R8	Resistor, 20kΩ

Table 5.3 Parameters of electronic components in LVDT circuit

The experimental results are shown in figures 5.12 and 5.13. Figure 5.12 represents experimental results of the position response of the MIMO magnetic levitation system using SMC on condition that r_1=r_2=r_3=6mm, c=26, ε=3.6, η=10, Δ=0.01. The fixed sample time is T=0.0005s. The approximate value of moments of inertia is supposed to be I_{xx}=I_{yy}=0.0142Kg·m^2. The corresponding current curves for the three coils are shown in figure 5.13. The error profiles between reference and response are also given in figure 5.14 to analyze the results. In order to test the controller robustness against levitation plane weight change, an aluminum ingot of

0.13kg is put on the levitation platform, the response curves of position are shown in figure 5.15. The exciting currents are given at around 2s.

The parameters of controller for experiment are different from those for simulation. This is because the simulation is implemented on ideal conditions. Those ideal conditions could not be identical with the real situations completely due to the following reasons:

1) The stator and levitator are both fabricated with laminated silicon steel plates, owing to the skills of manufacture process, the unsmooth surfaces of stators and levitators could create uneven forces between stators and levitators. Due to the nonlinear flux characteristics and coupling behavior of the MIMO magnetic levitation system, the uneven force will worsen the levitation performance. This factor is not considered in the simulation.
2) The simulation results show that the system uncertainties will lead to steady errors between reference and response positions. For the proposed MIMO magnetic levitation system, the moments of inertia can not calculate accurately because mass and geometrical shape of the levitation plane are irregular distribution according to X and Y axes. The approximate value of moments of inertia will lead to parameter uncertainty in the system, and this uncertainty could not be calculated. To weaken the influence of this uncertainty, the parameters of controller need to be adjusted.
3) There are multiple circuit drives for three coils and three LVDT in the MIMO magnetic levitation system. The electromagnetic noise could affect the accuracy of system signals.

Although the above factors could result in the difference of control parameters between simulation and experimental implementation, the simulation is still very useful because it can reveal the system performance according to variations of the control parameters, and it can also capture the relationship among those control parameters. As a result, it is helpful to adjust the control parameters in the experimental implementation.

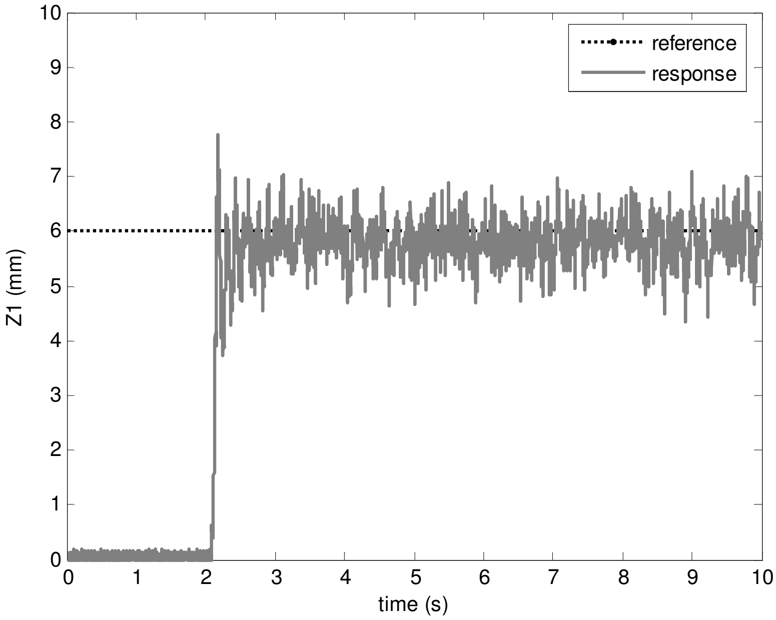

(a)

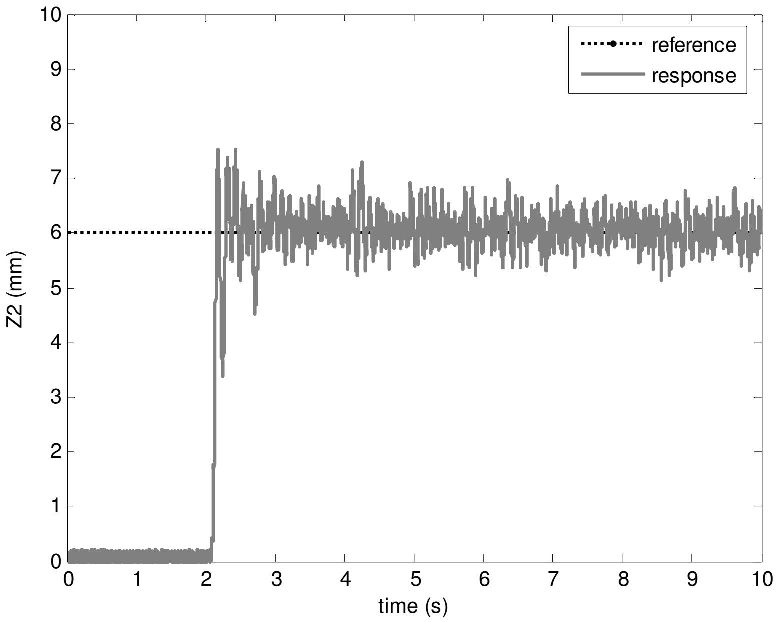

(b)

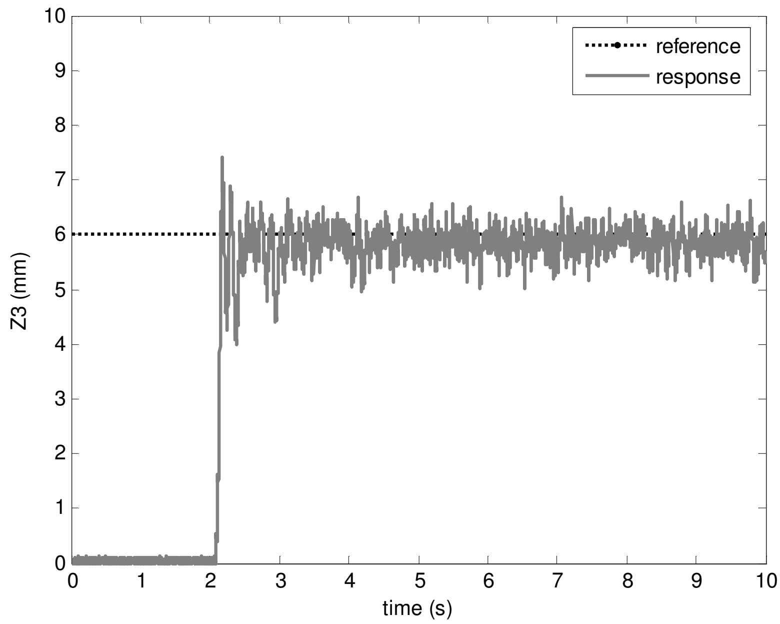

(c)

Fig. 5.12 The experimental position response curves

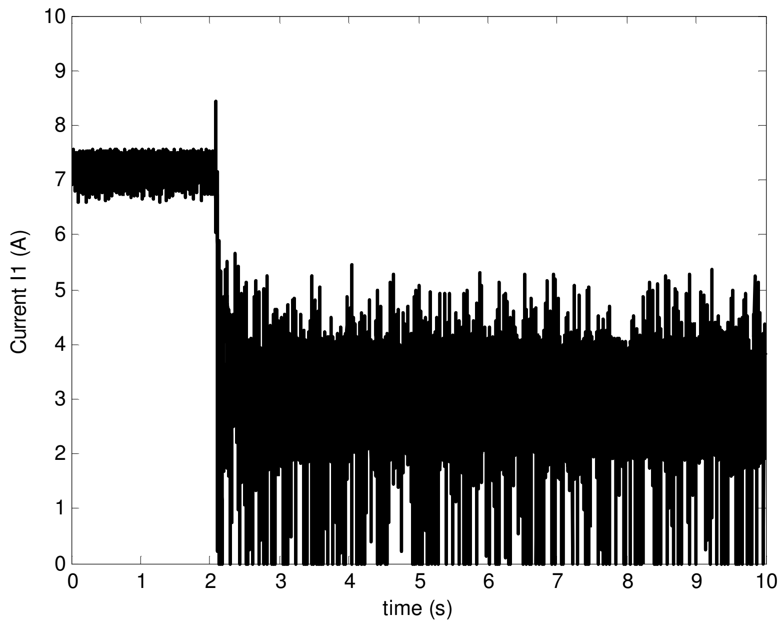

(a)

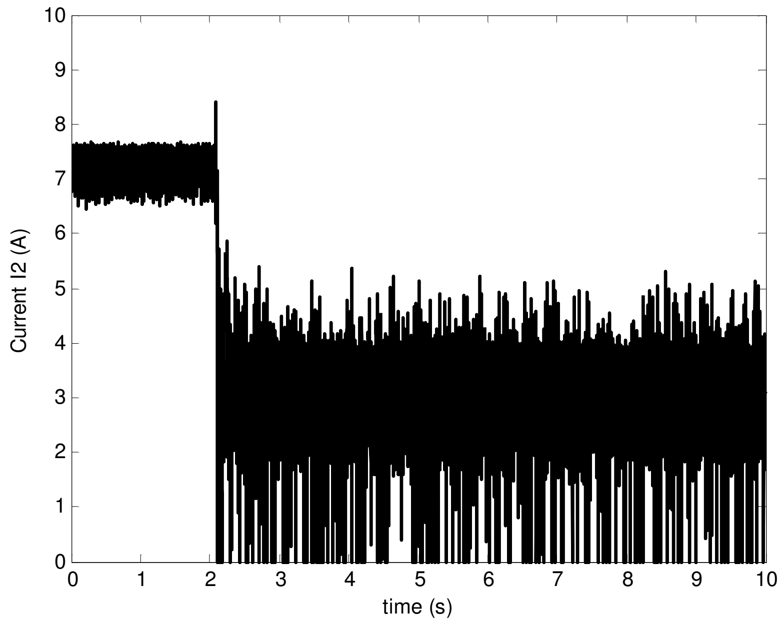

(b)

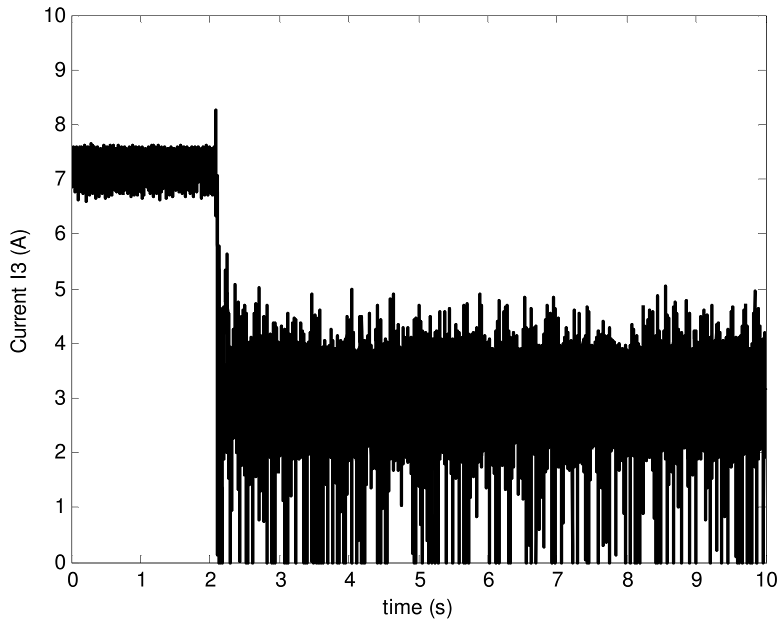

(c)

Fig. 5.13 The experimental current curves

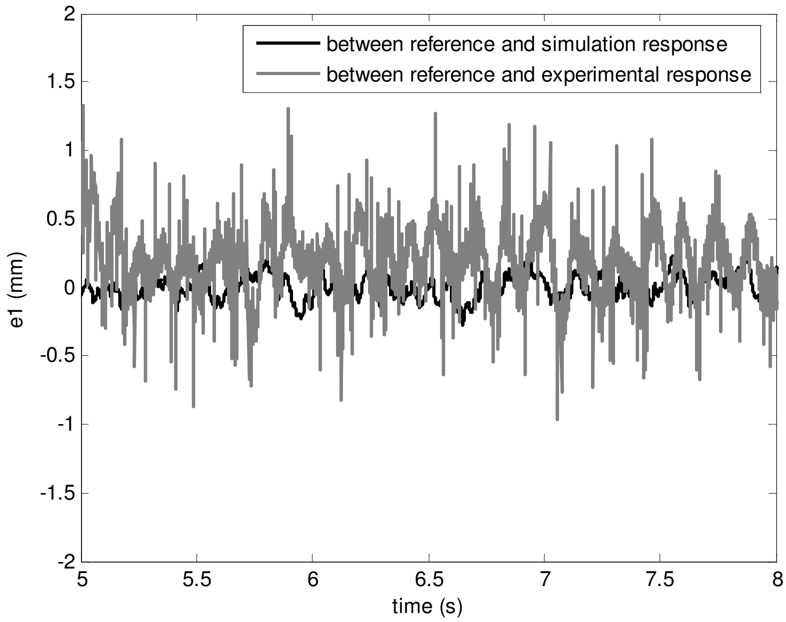

between reference and simulation response
between reference and experimental response
e1 (mm)
time (s)
2
1.5
1
0.5
0
-0.5
-1
-1.5
-2
5
5.5
6
6.5
7
7.5
8

(a)

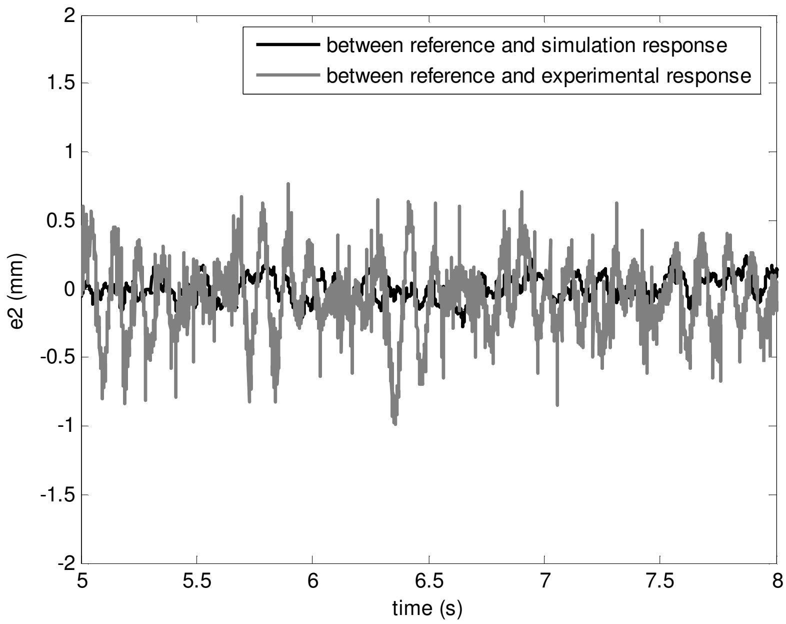

between reference and simulation response
between reference and experimental response
e2 (mm)
time (s)
2
1.5
1
0.5
0
-0.5
-1
-1.5
-2
5
5.5
6
6.5
7
7.5
8

(b)

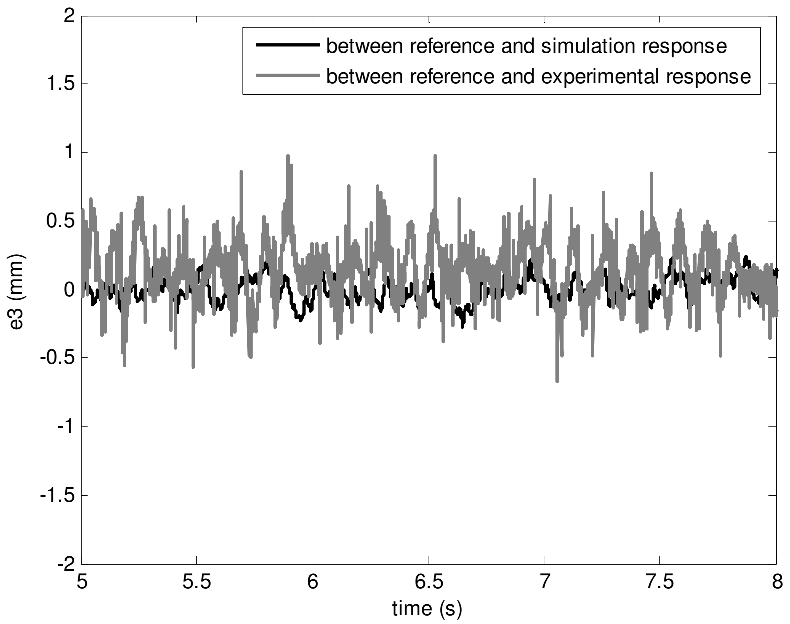

(c)

Fig. 5.14 The error profiles

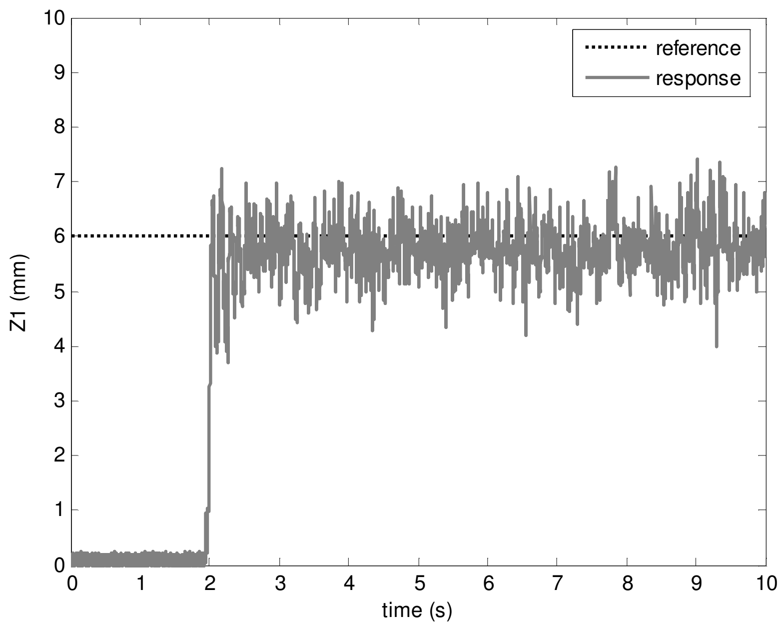

(a)

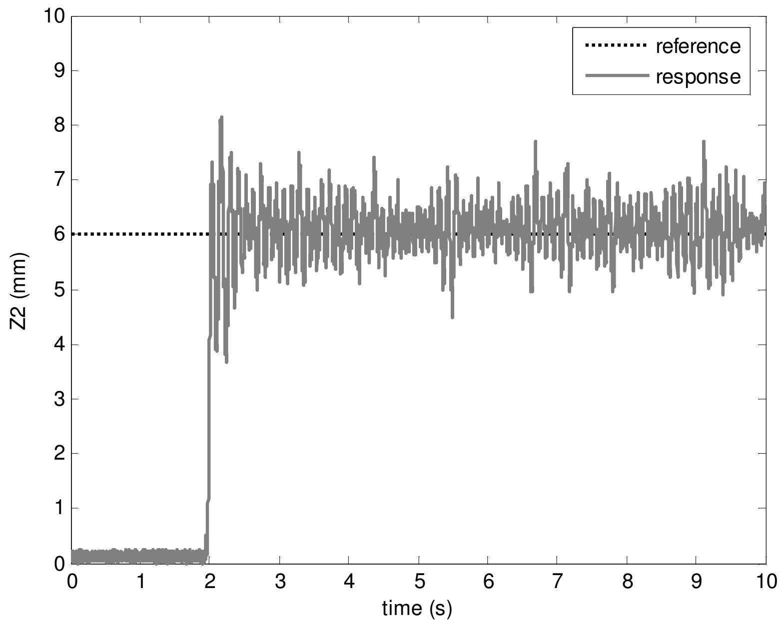

(b)

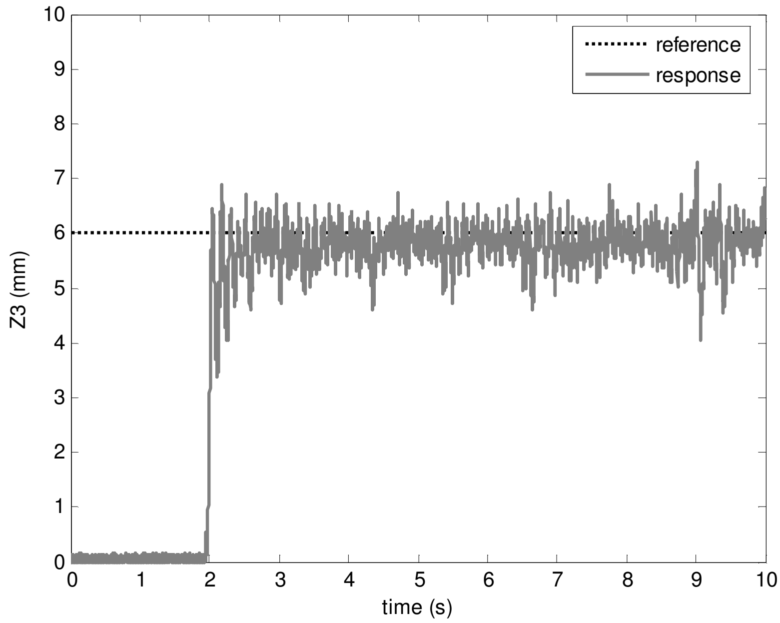

(c)

Fig. 5.15 The position response curves with weight change

The experimental results show that the MIMO magnetic levitation system can be stable. However, similar to simulation results, owing to system uncertainties and feedback signal noise, the response traces around the reference at steady state, it can be seen from figure 5.14 that the steady errors vibration from experimental implementation are almost within ±1mm, and the steady errors from experimental implementation are bigger than those from simulation. As mentioned above, the unsmooth surfaces of stators and levitators could create uneven forces between stators and levitators, and this uneven force will worsen the levitation performance owing to the nonlinear flux characteristics and coupling behavior of the MIMO magnetic levitation system. In addition, the electronics noise may disturb the precision of the output circuit of LVDT and reduce the position resolution of LVDT. Figure 5.12 and 5.15 show that the amplitudes of positions are almost above 0.2mm at the static state, when the coils are not excited at 0-2s. This phenomenon testifies the existing of feedback signal noise. One possible method to decrease those errors is to use high resolution position sensors. The experimental results verify the feasibility of the control algorithm mentioned above, and they also reveal the existing problem of position vibration at steady state.

5.6 Summary

In this chapter, an MIMO magnetic levitation system based on SMC is investigated. On the basis of the modeling of the MIMO magnetic levitation system built in chapter 3, the coupling system is decoupled using mathematical transformation. Following that, the sliding mode controller proposed in Chapter 4 are used for the decoupled subsystems, and the stability of the system is also analyzed. Finally, both the simulation and real-time implementation are used to test the controller design, and the outcomes of simulation and experimental implementation agree with the control algorithms and prove the feasibility of the proposed control methodology. Additional, the results from simulation and experiment also reveal the existing problem of position vibration at steady state.

Chapter 6

Conclusions and suggestions for future research

This thesis is dedicated to research on the proposed MIMO magnetic levitation system with SRA. The structure of the MIMO magnetic levitation system is depicted, the performance of the system is analyzed, the modeling of the system is constructed and the controller is designed for this system. These contents make up every chapter; and review, principle analysis, simulation, real-time implementation and conclusion are elaborated in each chapter.

The main objective of this chapter is to highlight the results and achievements of this thesis and to bring forward some possible issues for future research as well.

6.1 Achievements and contributions

The achievements and contributions of this thesis can be concluded as follows:

1) Structure and performance characteristics analysis of the MIMO magnetic levitation system with SRA

In Chapter 2, an MIMO magnetic levitated switched reluctance actuator system is proposed. The principles of operation of the proposed magnetic levitation system with switched reluctance actuator are reviewed. The usage of magnetic circuit analysis and electromechanical energy conversion principle to analyze the SRA are introduced. To analyze electromagnetic levitation force, both the MCA model and the three-dimensional FEA model are applied. The advantages of MCA and FEA are compared. According to the comparative results, the MCA is further revised to improve the accuracy. The results of improved MCA model are very close to those of FEA model. Corresponding force measurements are also performed and the agreement of both MCA and FEA methods results with the measurement results validate the feasibility of the two simulation models. These results provide useful information for the mechanical structure design of the magnetic levitated switched reluctance actuator.

2) Modeling of magnetic levitation system

Chapter 3 is to present the models of magnetic levitation system. To reveal the characteristics of magnetic levitation system completely, models for both the SISO magnetic levitation system and the MIMO magnetic levitation system are created. On the basis of the Kirchhoff's law, the principles of electromechanical energy conversion and the Newton's law, the electrical model, the electromagnetic force model and the mechanical motion model of the MIMO magnetic levitation system are constructed respectively. Those models show the magnetic levitation system is open loop unstable. On the other hand, the MIMO magnetic levitation system is more complex than the SISO magnetic levitation system because the levitation forces are coupling in the MIMO system. The two-time scale method is implemented to simple the control of the whole driving system. Using this method, the complicated system can be divided into two reduced order subsystems, the fast subsystem for electrical model and the slow subsystem for mechanical motion model. Accordingly, the task of controller design is simplified.

3) Sliding mode control for an SISO magnetic levitation system

In chapter 4, an SISO magnetic levitation system based on SMC is investigated. The model of the magnetic levitation system is extended, and a sliding mode controller is proposed for this system. The stability and system characteristics of the controller are both analyzed. An effective observer for SMC is designed to estimate and compensate the disturbances. In consequence, the system state trajectory performance is significantly improved, and the system is robust against external disturbances. Both the simulation results and experimental results agree with the control algorithms and they prove the feasibility of the proposed controllers. Furthermore, the SMC with DO is compared with the traditional PID controller, and the experimental results show that the SMC with DO has superiority over the PID controller in the magnetic levitation system, especially when the command signal varies within a wide range.

4) Decoupled control methodology for the MIMO magnetic levitation system with SRA

In chapter 5, controller for the proposed MIMO magnetic levitation system is designed. On the basis of the modeling of the MIMO magnetic levitation system built in chapter 3, the coupling system is decoupled by mathematical transform firstly. Then, the total system is divided into three individually controllable subsystems. Following that, the sliding mode controller proposed in Chapter 4 is used for these subsystems. Furthermore, the stability of the system is analyzed. Finally, both the simulation and real-time implementation are conducted to verify the control methodology. And outcomes of simulation and experimental implementation both certify that the levitation plane can be stable and the proposed control algorithm could be used for the MIMO magnetic levitation system based on SRA, at the same time, the results from simulation and experiment also reveal the existing problem of position vibration at steady state.

6.2 Suggestions for future research

Some research work can still be investigated to advance the knowledge of MIMO magnetic levitation system based on switched reluctance actuator.

i) For the SISO magnetic levitation system, the modeling of this system is nonlinear. In this research, the model is linearized at set point using small signal method to simple the controller design. To eliminate the system model inaccuracy from linearization, the nonlinear controller needs to be approached for this model.

ii) For the proposed MIMO magnetic levitation system with switched reluctance actuator, it was found that the response almost vibrates around the reference within ±1mm range; the response results need to be improved further to reduce this vibration. One possible method is to use high resolution sensors.

iii) In this research, the two-time scale method is adopted for the magnetic levitation system. This method separates the overall system into two subsystems and those subsystems will be controlled individually. If this method is not used, a new control algorithm needs to be proposed for the overall system.

iv) For the proposed MIMO magnetic levitation system, it can be used in linear automation transportation system. This could be accomplished by adding linear movement part to the magnetic levitation system by using linear switched reluctance actuator. In this case, the coupling behavior between the levitation subsystem and the linear movement subsystem should be considered.

References

[1] M. Y. Chen, M. J. Wang, and L. C. Fu, “A novel dual-axis repulsive Maglev guiding system with permanent magnet: modeling and controller design”, *IEEE/ASME Trans. on Mechatronics*, vol. 8, no. 1, pp. 77-86, Mar. 2003.

[2] M. Komori, and G. Kamogawa, “Basic study of a magnetically levitated conveyer using superconducting magnetic levitation”, *IEEE Trans. on Applied Superconductivity*, vol. 15, no. 2, pp. 2238-2241, Jun. 2005.

[3] K. Venkataratnam, and A. B. Chattopadhyay, “Analysis of electromagnetic forces in a levitated short rotor LIM I & II”, *IEEE Trans. on Energy Conversion*, vol. 17, no. 1, pp. 95-106, Mar. 2002.

[4] Z. P. Zhang, and C. H. Menq, “Six-axis magnetic levitation and motion control”, *IEEE Trans. on Robotics*, vol. 23, no. 2, pp. 196-205, Apr. 2007.

[5] R. Appunn, B. Schmulling, and K. Hameyer, “Electromagnetic Guiding of Vertical Transportation Vehicles: Experimental Evaluation”, *IEEE Trans. on Industry Electronics*, vol. 57, no. 1, pp. 335-343, Jan. 2010.

[6] Z. Makni, M. Besbes, and C. Marchand, “Multiphysics Design Methodology of Permanent-Magnet Synchronous Motors”, *IEEE Trans. on Vehicular Technology*, vol. 56, no. 4, pp. 1524-1530, Jul. 2007.

[7] C. S. Edrington, M. Krishnamurthy, B. Fahimi, “Bipolar Switched Reluctance Machines: A Novel Solution for Automotive Applications”, *IEEE Trans. on Vehicular Technology*, vol. 54, no. 3, pp. 795-808, May 2005.

[8] X. D. Xue, K. W. E. Cheng, J. K. Lin, Z. Zhang, K. F. Luk, T. W. Ng, and N. C. Cheung, “Optimal Control Method of Motoring Operation for SRM Drives

in Electric Vehicles", *IEEE Trans. on Vehicular Technology*, vol. 59, no. 3, pp. 1191-1204, Mar. 2010.

[9] P. J. Lawrenson, J. M. Stephenson, N.N. Fulton, P.T. Blenkinsop, and J. Corda, "Variable-speed switched reluctance motors", *IEE Proc. B. Electric Power Appl.* vol. 127, no. 4, pp. 253-265, Jul. 1980.

[10] M. B. Khamesee, N. Kato, Y. Nomura, and T. Nakamura, "Design and control of a microrobotic system using magnetic levitation," *IEEE/ASME Trans. on Mechatronics*, vol.17, no.1, pp.1-14, Mar. 2002.

[11] A. Chiba, K. Kiryu, M. A. Rahman, and T. Fukao, "Radial force and speed detection for improved magnetic suspension in bearingless motors," *IEEE Trans. on Industrial Appl.*, vol.42, no.2, pp.415-422, Mar./Apr. 2006.

[12] H. W. Lee, K. C. Kim, and J. Lee, "Review of Maglev Train Technologies," *IEEE Trans. on Magnetics*, vol.42, no.7, pp.1917-1925, Jul. 2006.

[13] H. C. Roters, *Electromagnetic Devices*, 1st ed., New York: Wiley, 1941, pp130-139.

[14] H. D. Chai, "Permeance model and reluctance force between toothed structures", *2nd Annu. Symp. Incremental Motion Contr. Syst. and Device*, University of Illinois, Paper K, May, 1973.

[15] R. Krishnan, *Switched Reluctance Motor Drives: Modeling, Simulation, Analysis, Design, and Applications*, 1st ed., Boca Raton, FL: CRC, 2001, pp. 138-141, 158-160.

[16] U. S. Deshpande, J. J. Cathy, and E. Richter, "High-force density linear switched reluctance machine", *IEEE Trans. on Ind. Applications*, vol. 31, no. 2, pp. 345-351, Mar./Apr. 1995.

[17] N. K. Sheth, and K. R. Rajagopal, “Calculation of flux-linkage characteristics of a switched reluctance motor by flux tube method”, *IEEE Trans. on Magnetics*, vol. 41, no. 10, pp. 4069-4071, Oct. 2005.

[18] W. Meyer, D. Bucherl, and H. G. Herzog, “High speed magnetic network solving”, *IEEE International Electric Machines and Drives Conference 2009*, Miami, Florida, USA, pp. 529-534, May 2009.

[19] T. S. Low, H. Lin, and S. X. Chen, “Analysis and comparison of switched reluctance motors with different physics sizes using a 2D finite element method”, *IEEE Trans. on Magnetics*, vol. 31, no. 6, pp. 3503-3505, Nov. 1995.

[20] A. di Gaeta, L. Glielmo, V. Giglio, and G. Police, “Modeling of an Electromechanical Engine Valve Actuator Based on a Hybrid Analytical--FEM Approach”, *IEEE/ASME Trans. on Mechatronics*, vol. 13, no. 6, pp. 625-637, Dec. 2008.

[21] H. C. Lai, D. Rodger, and P. J. Leonard, “Coupled meshes in 3D problems involving movements”, *IEEE Trans. on Magnetics*, vol. 28, no. 2, pp. 1732-1734, Mar. 1992.

[22] A. Benhama, A.C. Williamson, and A.B.J. Reece, “Force and torque computation from 2-D and 3-D finite element field solutions”, *IEE Proc. Electr. Power Appl.*, vol. 146, no. 1, pp. 25-31, Jan. 1999.

[23] F. Ishibashi, S. Noda, and M. Mochizuki, “Numerical simulation of electromagnetic vibration of small induction motors”, *IEE Proc. Electr. Power Appl.*, vol. 145, no. 6, pp. 528-534, Nov. 1998.

[24] A. Arkkio, M. Antila, K. Pokki, A. Simon, and E. Lantto, “Electromagnetic force on a whirling cage rotor”, *IEE Proc. Electr. Power Appl.*, vol. 147, no. 5, pp. 353-360, Sept. 2000.

[25] M. Popescu, D.M. Ionel, T.J.E. Miller, S.J. Dellinger, and M.I. McGilp, "Improved finite element computations of torque in brushless permanent magnet motors", *IEE Proc. Electr. Power Appl.*, vol. 152, no. 2, pp. 271-276, Mar. 2005.

[26] W. G. Hurley, and W. H. Wolfle, "Electromagnetic design of a magnetic suspension system," *IEEE Trans. on Education*, vol.40, no.2, pp.124-130, May 1997.

[27] A. El Hajjaji, and M. Ouladsine, "Modeling and nonlinear control of magnetic levitation systems," *IEEE Trans. on Industrial Electronics*, vol.48, no.4, pp.831-837, Aug. 2001.

[28] S. J. Joo, and J. H. Seo, "Design and analysis of the nonlinear feedback linearizing control for an electromagnetic suspension system," *IEEE Trans. on Control Systems Technology*, vol.5, no.1, pp.135-144, Jan. 1997.

[29] Z. J. Yang, and M. Tateishi, "Adaptive robust nonlinear control of a magnetic levitation system," *Automatica*, vol.37, pp.1125-1131, 2001.

[30] Z. H. Man, A. P. Paplinski, and H. R. Wu, "A robust MIMO terminal sliding mode control scheme for rigid robotic manipulators," *IEEE Trans. on Automatic Control*, vol.39, no. 12, pp.2464-2469, Dec. 1994.

[31] Y. Fujimoto, and A. Kawamura, "Robust servo-system based on two-degree-of-freedom control with sliding mode," *IEEE Trans. on Industrial Electronics*, vol.42, no.3, pp.272-280, Jun. 1995.

[32] J. H. Park, K. W. Kim, and H. H. Yoo, "Two-stage sliding mode controller for vibration suppression of a flexible pointing system," *Proceedings of the Institution of Mechanical Engineers, Part C: Journal of Mechanical Engineering Science*, vol. 215, no. 2, p155-166, 2001.

[33] V. Utikin, J. Guldner, and J. X. Shi, *Sliding mode control in electromechanical systems*, Taylor & Francis Ltd, 11 New Fetter Lane, London EC4P 4EE, 1999.

[34] C. Fallaha, M. Saad, H. Kanaan, and W. H. Zhu, "Sliding mode nonlinear switching functions for control input transient constraints reduction," *IEEE ISIE 2006*, Montreal, Quebec, Canada, pp.284-288, Jul. 9-12, 2006.

[35] Z. J. Yang, K. Miyazaki, S. Kanae, and K. Wada, "Robust position control of a magnetic levitation system via dynamic surface control technique," *IEEE Trans. on Industrial Electronics*, vol.51, no.1, pp.26-34, Feb. 2004.

[36] D. M. M. Hassan, and A. M. Mohamed, "Variable structure control of a magnetic levitation system," *Proc. of the American Control Conference*, Arlington, VA, pp.3725-3730, 25-27 Jun., 2001.

[37] H. K. Chiang, C. A. Chen, and M. Y Li, "Integral variable-structure grey control for magnetic levitation system," *IEE Proc. on Electric Power Appl.*, vol.153, no.6, pp.809-814, Nov. 2006.

[38] F. J. Lin, L. T. Teng, and P. H. Shieh, "Intelligent sliding-mode control using RBFN for magnetic levitation system," *IEEE Trans. on Industrial Electronics*, vol.54, no.3, Jun. 2007.

[39] M. Kozek, G. Puchhammer, and H. P. Jorgl, "A MISO sliding mode control for a high speed EMS MAGLEV-vehicle using disturbance estimation", *Proceedings of the 3rd IEEE Conference on Control Applications*, vol. 1, pp. 587-592, 1994.

[40] H. C. Wu, and Y. F. Hu, "Study on fuzzy control algorithm for magnetic levitated platform", *International Conference on Measuring Technology and Mechatronics Automation*, vol. 2, pp. 598-601, 2009.

[41] B. V. Jayawant, *Electromagnetic Levitation and Suspension Techniques*, 1st ed., Edward Arnold (Publishers) Ltd, London, 1981, pp. 90-91.

[42] W. J. Kim, D. L. Trumper, and J. H. Lang, "Modeling and vector control of planar magnetic levitator", *IEEE Trans. on Industry Applcations*, vol. 34, no. 6, pp. 1254-1262, Nov./Dec. 1998.

[43] K. S. Jung, and Y. S. Baek, "Study on a novel contact-free planar system using direct drive DC coils and permanent magnets", *IEEE/ASME Trans. on Mechatronics*, vol. 7, no. 2, pp. 35-43, Mar. 2002.

[44] Y. C. Lai, Y. L. Lee, and J. Y. Yen, "Design and servo control of a single-deck planar maglev stage", *IEEE Trans. on Magnetics*, vol. 43, no. 6, pp. 2600-2602, Jun. 2007.

[45] J. W. Jansen, C. M. M. van Lierop, E. A. Lomonova, and A. J. A. Vandenput, "Magnetically levitated planar actuator with moving magnets", *IEEE Trans. on Industry Applications*, vol. 44, no. 4, pp. 1108-1115, Jul./Aug. 2008.

[46] J. H. Park, and Y. S. Baek, "Design and analysis of a maglev planar transportation vehicle", *IEEE Trans. on Magnetics*, vol. 44, no. 7, pp. 1830-1836, Jun. 2008.

[47] Y. Ueda, and H. Ohsaki, "Six-degree-of-freedom motion analysis of a planar actuator with a magnetically levitated mover by six-phase current controls", *IEEE Trans. on Magnetics*, vol. 44, no. 11, pp. 4301-4304, Nov. 2008.

[48] J. de Boeij, E. Lomonova, and J. Duarte, "Contactless planar actuator with manipulator: a motion system without cables and physical contact between the mover and the fixed world", *IEEE Trans. on Industry Applications*, vol. 45, no. 6, pp. 1930-1938, Nov./Dec. 2009.

[49] H. Shakir, and W. J. Kim, "Nanoscale path planning and motion control with maglev positioners", *IEEE/ASME Trans. on Mechatronics*, vol. 11, no. 5, pp. 625-633, Oct. 2006.

[50] Z. G. Sun, N. C. Cheung, S. W. Zhao, and W. C. Gan, "The Application of Disturbance Observer-Based Sliding Mode Control for Magnetic Levitation Systems", *Proceedings of the Institution of Mechanical Engineers Part C: Journal of Mechanical Engineering Science*, vol. 224, no. 8, pp. 1635-1644, Aug. 2010.

[51] T. H. E. Miller, *Switched reluctance motors and their control*, Magna Physics Publishing and Clarendon Press, Oxford, 1993.

[52] V. Gourishankar, and D. H. Kelly, *Electromechanical energy conversion*, 2nd edition, Intext Educational Publishers, New York, 1973.

[53] H. Majmudar, *Electromechanical energy conversion*, Allyn and Bacon Inc., Boston, 1965.

[54] J. C. Prescott, and A. K. El-Kharashi, "A method of measuring self-inductances applicable to large electrical machines", *IEE Proc. Part A: Power Engineering*, vol. 106, no. 26, pp. 169-173, Apr. 1959.

[55] A. D. Cheok, and N. Ertugrul, "Computer-based automated Test Measurement System for determining Magnetization Characteristics of Switched Reluctance Motors", *IEEE Trans. on Instrumentation and Measurement*, vol. 50, no. 3, pp. 690-696, Jun. 2001.

[56] A. Ferrero, and A. Raciti, "A digital method for the determination of the magnetic characteristics of variable reluctance motors", *IEEE Trans. on Instrumentation and Measurement*, vol. 39, no. 4, pp. 604-608, Aug. 1990.

[57] A. Ferrero, A. Raciti, and C. Urzi, “An indirect test method for the characterization of variable reluctance motors”, *IEEE Trans. on Instrumentation and Measurement*, vol. 42, no. 6, pp. 1020-1025, Dec. 1993.

[58] V. K. Sharma, S. S. Murthy, and B. Singh, “An improved method for the determination of saturation characteristics of switched reluctance motors”, *IEEE Trans. on Instrumentation and Measurement*, vol. 48, no. 5, pp. 995-1000, Oct. 1999.

[59] S. C. Wang, W. S. Chen, W. B. Liao, K. Y. Shen, and Y. L. Chen, “A PC-based measurement system for determining magnetic characteristics of switched reluctance motors”, *International Conference on Power System Technology*, vol. 4, pp. 2256-2260, 2002.

[60] R. Gobbi, N. C. Sahoo, and R. Vejian Rajandran, “Rising and falling current methods for measurement of flux-linkage characteristics of switched reluctance motors: a comparative study”, *IEEE International Power and Energy Conference*, pp. 383-387, 2006.

[61] A. D. cheok, and Z. Wang, “DSP-based automated error-reducing flux-linkage measurement method for switched reluctance motors”, *IEEE Trans. on Instrumentation and Measurement*, vol. 56, no. 6, pp. 2245-2253, Dec. 2007.

[62] R. Krishnan, and P. Materu, “Measurement and instrumentation of a switched reluctance motor”, *IEEE Industry Applications Society Annual Meeting*, vol. 1, pp. 116-121, 1989.

[63] W. F. Ray, and F. Erfan, “A new method of flux or inductance measurement for switched reluctance motors”, *5th International Conference on Power Electronics and Variable-Speed Drives*, pp. 137-140, 1994.

[64] S. W. Zhao, N. C. Cheung, W. C. Gan, Z. G. Sun, “A Novel Flux Linkage Measurement Method for Linear Switched Reluctance Motors”, *IEEE Trans. Instrumentation And Measurement*, vol. 58, no. 10, pp. 3569-3575, 2009.

[65] *User Manual, MEGA V6.29*, Applied Electromagnetic Research Centre, University of Bath, Bath, London, U.K., 4th Aug. 2003.

[66] *Tutorial Examples, MEGA V6.29*, Applied Electromagnetic Research Centre, University of Bath, Bath, London, U.K., 4th Aug. 2003.

[67] F. Soares, and P. J. C. Branco, “Simulation of a 6/4 switched reluctance motor”, *IEEE Trans. on Aerospace and Electronic Systems*, vol. 37, no. 3, pp. 989-1009, Jul. 2001.

[68] J. F. Pan, N. C. Cheung, and J. M. Yang, “High-precision position control of a novel planar switched reluctance motor”, *IEEE Trans. on Industrial Electronics*, vol. 52, no. 6, pp. 1644-1652, Dec. 2005.

[69] R. Krishnan, R. Arumugam, and J. F. Lindsay, “Design procedure for switched reluctance motors”, *IEEE Trans. on Industry Applications*, vol. 24, no. 3, pp. 456-461, May/Jun. 1988.

[70] G. S. Buja, and M. I. Valla, “Control characteristics of the SRM motor drives-Part I, operation in the linear region”, *IEEE Trans. on Industrial Electronics*, vol. 38, no. 5, pp. 313-321, Oct. 1991.

[71] G. S. Buja, and M. I. Valla, “Control characteristics of the SRM motor drives-Part II, operation in the saturated region”, *IEEE Trans. on Industrial Electronics*, vol. 41, no. 3, pp. 316-325, Jun. 1994.

[72] T. J. Miller, and M. McGilp, “Nonlinear theory of the switched reluctance motor for rapid computer-aided design”, *IEE Proc. Electric Power Applications*, vol. 137, no. 6, pp. 337-347, Nov. 1990.

[73] M. Stiebler, and K. Liu, "An analytical model of switched reluctance machines", *IEEE Trans. on Energy Conversion*, vol. 14, no. 4, pp. 1100-1107, Dec. 1999.

[74] C. Roux, and M. M. Morcos, "On the use of a simplified model for switched reluctance motors", *IEEE Trans. on Energy Conversion*, vol. 17, no. 3, pp. 400-405, Sept. 2002.

[75] S. Saha, K. Ochiai, T. Kosaka, N. Matsui, and Y. Takeda, "Developing a sensorless approach for switched reluctance motors from a new analytical model", *IEEE Industry Applications Conference*, vol. 1, pp. 525-532, Oct. 1999.

[76] D. N. Essah, Member, and S. D. Sudhoff, "An improved analytical model for the switched reluctance motor", *IEEE Trans. on Energy Conversion*, vol. 18, no. 3, pp. 349-356, Sept. 2003.

[77] D. A Torrey, and J. H. Lang, "Modeling a nonlinear variable-reluctance motor drive", *IEE Proc. Electric Power Applications*, vol. 137, no. 5, pp. 314-326, Sep. 1990.

[78] D. A Torrey, X.-M Niu, and E. J. Unkauf, "Analytical modeling of variable-reluctance machine magnetization characteristics", *IEE Proc. Electric Power Applications*, vol. 142, no. 1, pp. 14-22, Jan. 1995.

[79] S. Mir, I. Husain, and M. E. Elbuluk, "Switched reluctance motor modeling with on-line parameter identification", *IEEE Trans. on Industry Applications*, vol. 34, no. 4, pp. 736-783, Jul./Aug. 1998.

[80] Z. Lin, D. S. Reay, B. W. Williams, and X. He, "Online modeling for switched reluctance motors using B-spline neural networks", *IEEE Trans. on Industrial Electronics*, vol. 54, no. 6, pp. 3317-3322, Dec. 2007.

[81] H. Sahraoui, H.Zeroug, and H. A. Toliyat, "Switched reluctance motor design using neural-network method with static finite-element simulation", *IEEE Trans. on Magnetics*, vol. 43, no. 12, pp. 4089-4095, Dec. 2007.

[82] W. C. Gan, N. C. Cheung, and L. Qiu, "Position control of linear switched reluctance motors for high precision applications", *IEEE Trans. on Industry Applications*, vol. 39, pp. 1350-1362, Sep./Oct. 2003.

[83] D. G. Taylor, "An experimental study on composite control of switched reluctance motors", *IEEE Control System Magazine*, vol. 11, no. 2, pp. 31-36, Feb. 1991.

[84] S. W. Zhao, N. C. Cheung, Y. Lu, W. C. Gan, Z. G. Sun, "Linear Switched Reluctance Motor Based Position Tracking System", *The 13th International Power Electronics and Motion Control Conference(EPE-PEMC 2008)*, pp. 1221-1224, Poznan, Poland, 1-3 Sept. 2008.

[85] S. W. Zhao, N. C. Cheung, W. C. Gan, and J. M. Yang, "An Effective Modeling and Control Strategy for Linear Switched Reluctance Motors," *Proceedings of the Institution of Mechanical Engineers, Part C: Journal of Mechanical Engineering Science*, vol. 222, no. 11, pp. 2111-2121, Nov. 2008.

[86] K. D. Young, V. I. Utkin, and U. Ozguner, "A control engineer's guide to sliding mode control", *IEEE Trans. on Control Systems Technology*, vol. 7, no. 3, pp. 328-342, May 1999.

[87] A. S. I. Zinober, *Deterministic control of uncertain systems*, Peter Peregrinus Press, London, UK, 1990.

[88] H. K. Khalil, *Nonlinear Systems*, Prentice Hall, NJ, USA, 3rd Edition, 2002.

[89] H. H. Woodson, and J. R. Melcher, *Electromechanical dynamics, Part I: discrete systems*, John, Wiley & Suns Inc., New York, 1968.

[90] A. O. Wilma, F. C. Eduardo, and B. V. Jerson, “Digital implementation of a magnetic suspension control system laboratory experiments,” *IEEE Trans. on Education*, vol.42, no.4, pp.315-322, Nov. 1999.

[91] Z. Y. Yang, K. M. P. Gerulf, and H. P. Jorgen, “Model-based control of a nonlinear one dimensional magnetic levitation with a permanent-magnet object,” *Automation and Robotics*, Juan Manuel Ramds Arreguin, I-Tech Education and Publishing, Austria, pp.359-374, 2008.